Paleomagnetism and $^{40}Ar/^{39}Ar$ ages of ignimbrites, Mogollon–Datil volcanic field, southwestern New Mexico

by William C. McIntosh, Laura L. Kedzie, and John F. Sutter

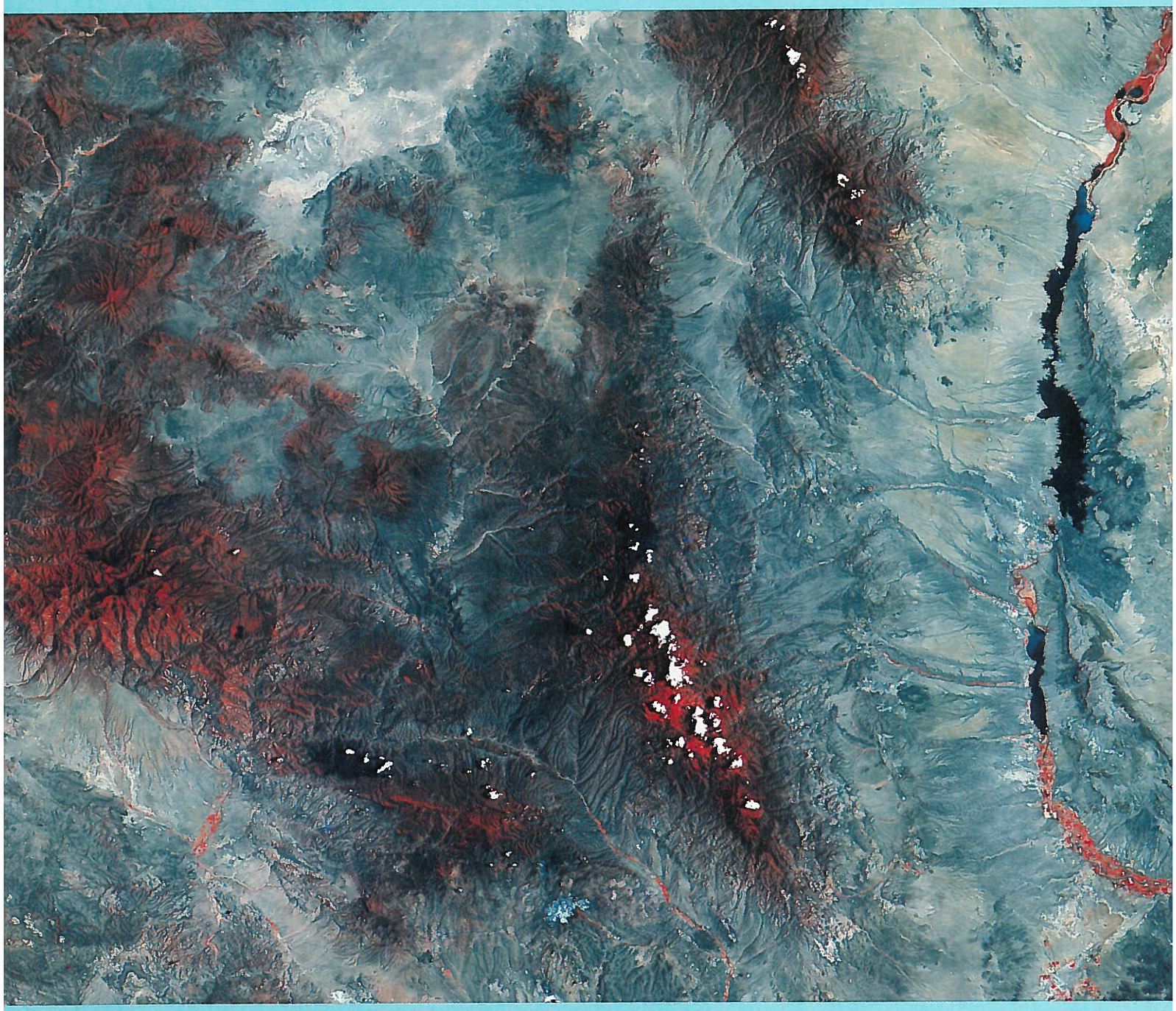

BULLETIN 135 New Mexico Bureau of Mines & Mineral Resources 1991

A DIVISION OF
NEW MEXICO INSTITUTE OF MINING & TECHNOLOGY

Bulletin 135

New Mexico Bureau of Mines & Mineral Resources

A DIVISION OF
NEW MEXICO INSTITUTE OF MINING & TECHNOLOGY

Paleomagnetism and $^{40}Ar/^{39}Ar$ ages of ignimbrites, Mogollon-Datil volcanic field, southwestern New Mexico

William C. McIntosh[1], Laura L. Kedzie[1], and John F. Sutter[1]

[1]*New Mexico Bureau of Mines & Mineral Resources, Socorro, New Mexico 87801*

[2]*U.S. Geological Survey, Reston, Virginia 22092*

SOCORRO 1991

Original Printing

Published by Authority of State of New Mexico, NMSA 1953 Sec. 63-1-4
Printed by University of New Mexico Printing Services, August 1991

Available from New Mexico Bureau of Mines & Mineral Resources, Socorro, NM 87801

Contents

Figures

Tables

Abstract

This report presents $^{40}Ar/^{39}Ar$ sanidine ages and paleomagnetic data for 36 ignimbrites and associated lavas in the Eocene—Oligocene Mogollon—Datil volcanic field of southwestern New Mexico.

$^{40}Ar/^{39}Ar$ age spectra from the ignimbrites yield plateau ages which range from 36.2 to 24.3 Ma and show within-sample and within-unit 10 precision of ±0.5% or better. These ages agree closely with independently established stratigraphic order and indicate that Mogollon—Datil ignimbrite activity was highly episodic, being confined to four brief (<2.6 my.) eruptive intervals separated by 1.5 to 3 m.y. long hiatuses.

Ignimbrite outflow sheets show stable paleomagnetic remanence directions which are uniform over most of their areal extents, including facies ranging from thick, densely welded proximal ignimbrites to unwelded distal fringes as thin as 1.5 m.

Used in concert with lithologic and stratigraphic position data, $^{40}Ar/^{39}Ar$ ages and paleomagnetic directions allow accurate long-range ignimbrite correlations which provide reliable ties between previously established subregional stratigraphic sequences. These correlations have helped to establish an integrated time-stratigraphic framework for the Mogollon—Datil volcanic field.

Introduction

Since the mid-1950's the 40,000 km^2 late Eocene—Oligocene Mogollon—Datil volcanic field (Fig. 1) has been the focus of numerous mapping, stratigraphic, geochemical, petrologic, and isotopic studies, primarily by workers from New Mexico universities, New Mexico Bureau of Mines & Mineral Resources, and the U.S. Geological Survey. Detailed geologic mapping has been successfully used to unravel the stratigraphy in subregions of the field (e.g. Seager et al., 1982; Osburn and Chapin, 1983a, b; Ratté et

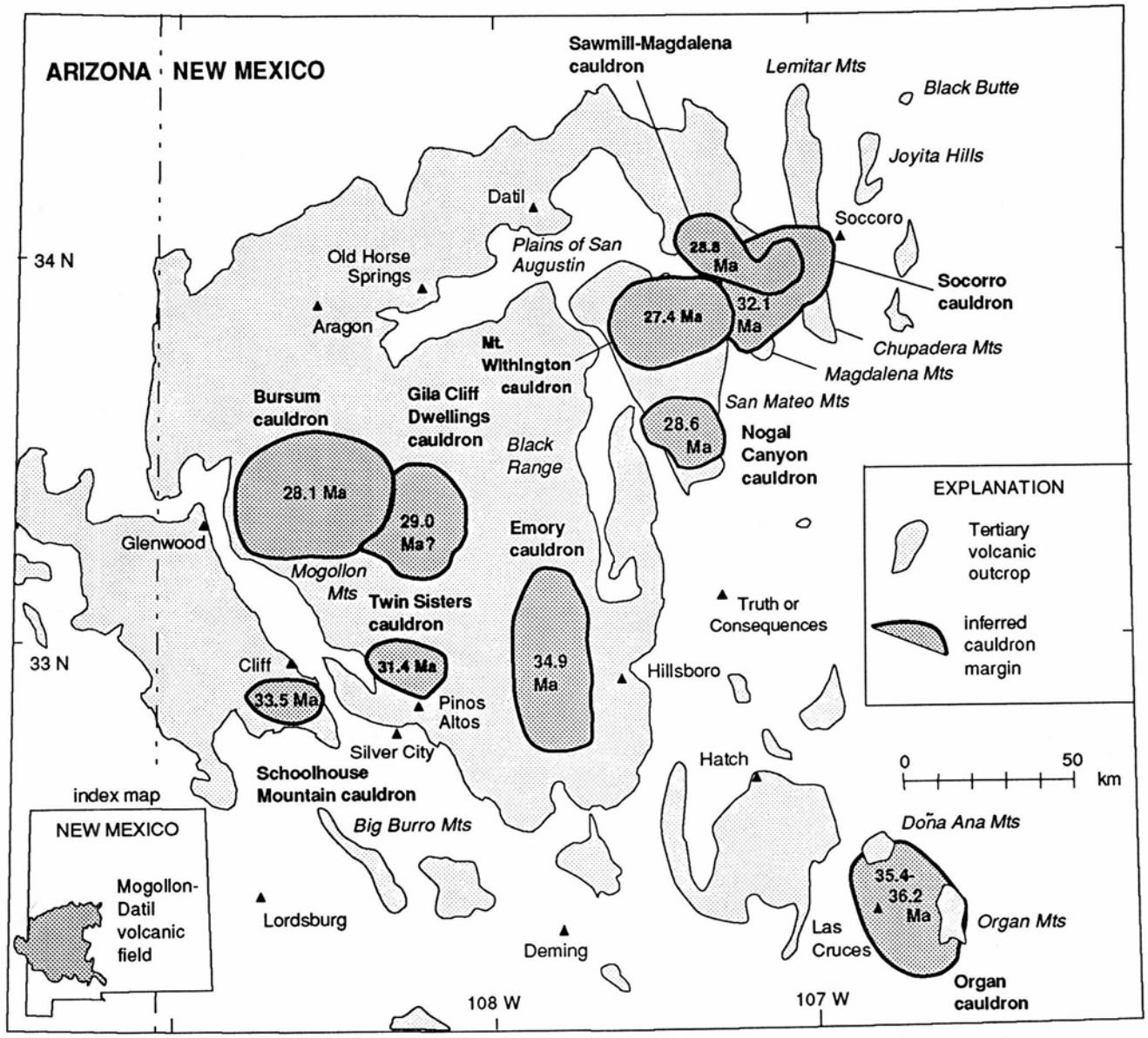

FIGURE 1—Map of the Mogollon–Datil volcanic field showing inferred cauldrons, their ages, and generalized outcrop distribution of late Eocene–Oligocene volcanic rocks.

al., 1984), but synthesis of subregional stratigraphic data has been frustrated by the inability to correlate ignimbrites (ash-flow tuffs) over long distances. Correlations based solely on mapping have been limited by discontinuous basin-and-range outcrop patterns. Lithology and geochemistry, although useful as first-order correlation criteria, have proven unreliable on a regional scale. Many stratigraphically distinct units are lithologically similar, and individual units show lateral, vertical, and sectoral variations in mineralogy, chemistry, welding texture, and phenocryst concentration and size, analogous to variations shown by ignimbrites elsewhere (Bornhorst, 1980; Hildreth and Mahood, 1985). Conventional K—Ar dating techniques have been helpful in some cases, but lack the resolution required by most of the correlation problems (e.g. Marvin et al., 1987).

This report presents results of an ongoing study in which Mogollon—Datil ignimbrite correlation problems have been addressed by a combination of $^{40}Ar/^{39}Ar$ dating and paleomagnetic analysis. This combination of techniques has proven highly successful, yielding ignimbrite correlations which have aided development of an integrated time-stratigraphic framework for the volcanic field (Figs. 2, 3). This report concentrates on data from two separate theses: Kedzie (1984), who performed initial $^{40}Ar/^{39}Ar$ work, and McIntosh (1989), who did paleomagnetic and additional $^{40}Ar/^{39}Ar$ work. The primary aim of this report is to make the complete data sets from these two theses more widely available; discussion of results has deliberately been kept to a minimum. Detailed discussions of the dating and paleomagnetic results and their stratigraphic implications can be found in these two theses and in McIntosh (in press) and McIntosh et al. (1990, in press).

Acknowledgments

This work was a cooperative project of the New Mexico Bureau of Mines & Mineral Resources and the U.S. Geological Survey, with additional financial contributions from the New Mexico Geological Society. We are grateful to the many geologists, including Chuck Chapin, Jim Ratté, Wolf

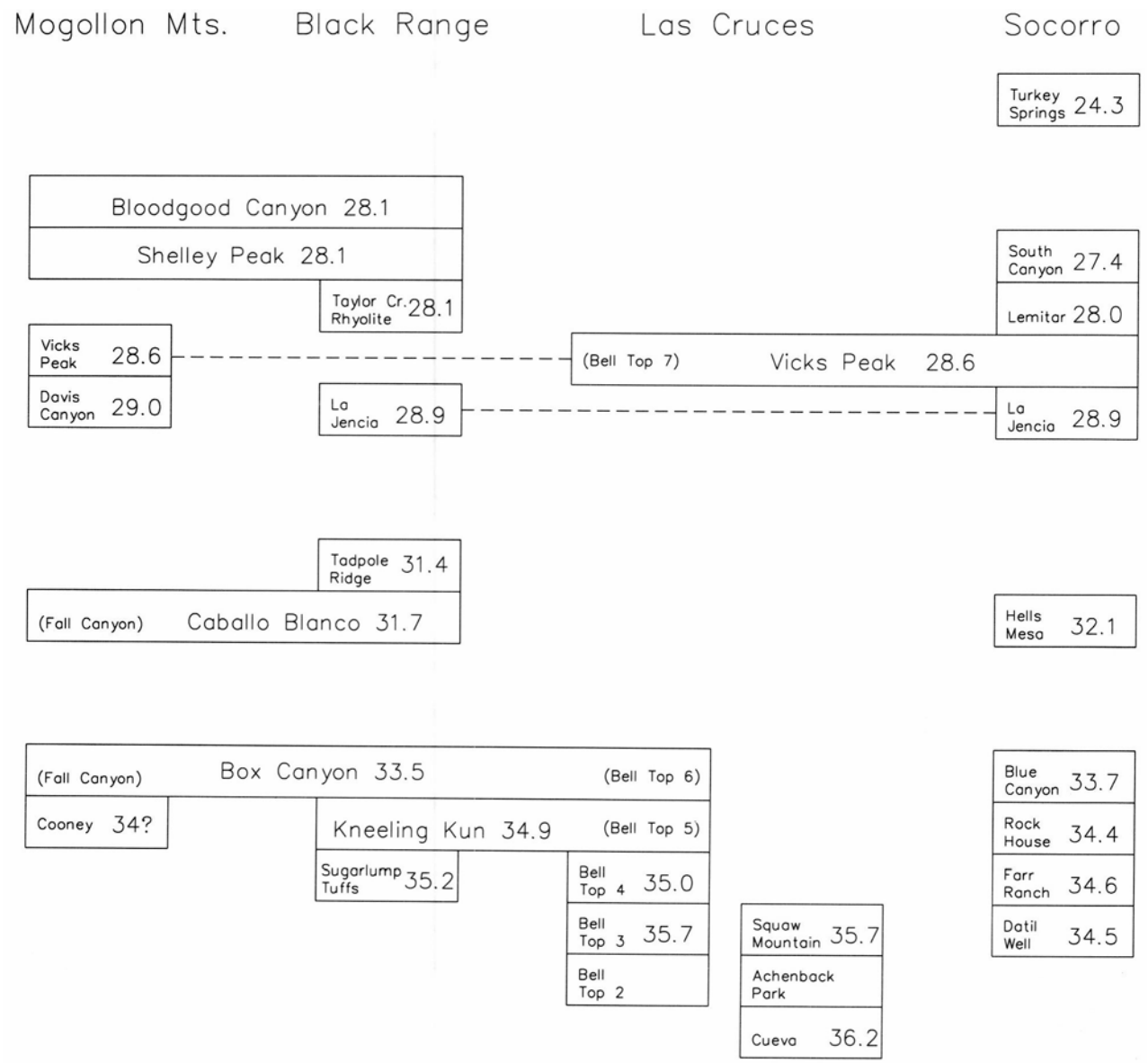

FIGURE 2—Generalized stratigraphic correlation chart for large, regional ignimbrites in the Mogollon–Datil volcanic field, showing $^{40}Ar/^{39}Ar$ ages. Silicic flows and domes of the Taylor Creek Rhyolite are also shown. Parentheses denote other existing names for some of the major ignimbrite outflow sheets.

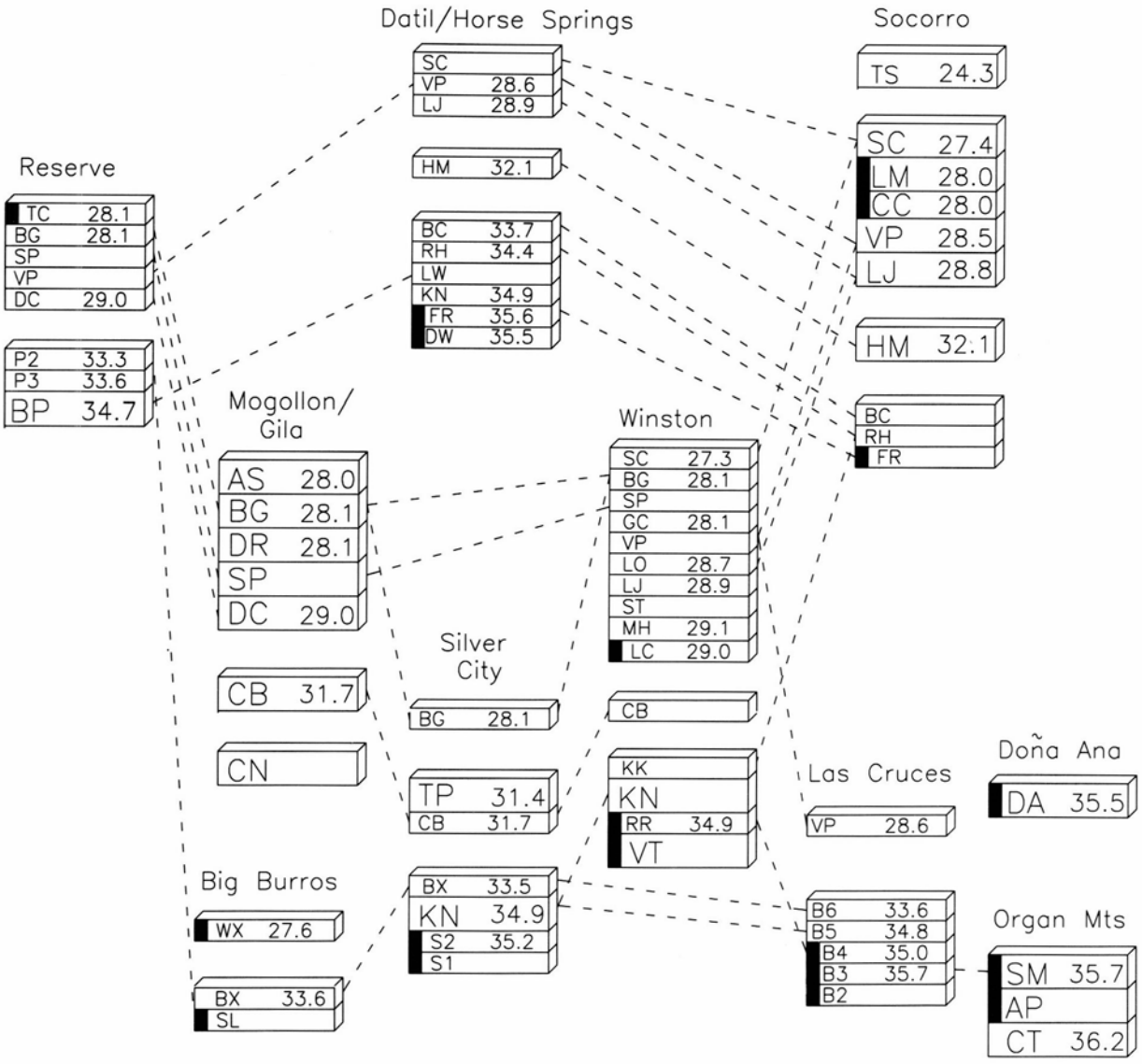

FIGURE 3—Detailed stratigraphic framework for Mogollon–Datil ignimbrites, showing generalized subregional stratigraphic columns in their approximate geographic positions. Each box depicts a locally named ignimbrite; $^{40}Ar/^{39}Ar$ age, and paleomagnetic polarity (black bars = normal). Eruptive hiatuses are shown as gaps in columns and dashed lines are correlations based on $^{40}Ar/^{39}Ar$ and paleomagnetic data. $^{40}Ar/^{39}Ar$ ages refer to local data; some differ slightly from regional unit-mean ages (Table 1). Boxes lacking ages indicate that the unit was not dated in that area, but was correlated using paleomagnetic data, stratigraphic position, and lithology. Unit-name abbreviations: AP=Achenback Park, AS=Apache Springs, B2 to B6=Bell Top tuff members 2 to 6, BC=Blue Canyon, BG=Bloodgood Canyon, BP=Bishop Peak, BX=Box Canyon, CB=Caballo Blanco, CC=Caronita Canyon, CN=Cooney, CT=Cueva Tuff, DA=Doña Ana, DC=Davis Canyon, DM=Diamond Creek, DR=Diablo Range, DW=Datil Well, FR=Farr Ranch, GC=Garcia Camp, HM=Hells Mesa, KK=Koko Well, KN=Kneeling Nun, LC=Little Mineral Creek, LJ=La Jencia, LM=Lemitar, LW=Lebya Well, MH=Mud Hole, P2 and P3=Pueblo Creek tuffs 2 and 3, RH=Rockhouse Canyon, S1=lower Sugarlump, S2=upper Sugarlump, SC=South Canyon, SL=Sugarlump, ST=Stiver Canyon, RR=Rocque Ramos, SM=Squaw Mountain, SP=Shelly Peak, TC=Triangle C Ranch, TP=Tadpole Ridge, TS=Turkey Springs, VP=Vicks Peak, VT=Victoria Tank, WX=Walking X Ranch.

Elston, Philip Kyle, Bob Osburn, John Geissman, Charles Ferguson, Rich Harrison, Steve Cather, Mike Hermann, and Nelia Dunbar, who contributed to field, laboratory, and other aspects of this project. Special thanks go to Mick Kunk of the U.S. Geological Survey for his indispensable assistance in the laboratory.

Geologic setting

The late Eocene-Oligocene Mogollon-Datil volcanic field of southwestern New Mexico is part of a discontinuous belt of mid-Tertiary silicic volcanic fields that extends from the San Juan Mountains in Colorado southward into central Mexico. For the purposes of this report, the Mogollon-Datil field (Fig. 1) is considered to extend as far south as Las Cruces and Lordsburg, New Mexico, and excludes the complex volcanic sequence of Hidalgo County, New Mexico (Elston, 1984).

Mogollon-Datil activity was initiated by eruption of andesites and basaltic andesites from about 40 to 36 Ma, which was followed by episodic bimodal basaltic andesite and silicic activity from 36 to 24 Ma (Fig. 4) (Elston, 1984; Cather et al., 1987; Marvin et al., 1987; McIntosh et al., 1990).

This study concentrates on the Mogollon-Datil silicic sequence which includes domes, flows, intrusives, and numerous ignimbrites. Individual ignimbrites range widely in form, volume, and distribution, from enormous (>1250 km^3), cauldron-derived, densely welded outflow sheets to tiny (<0.1 km^2), unwelded pyroclastic aprons surrounding domes.

From mid-Oligocene to the present time, the Mogollon-Datil volcanic field has experienced inhomogeneously distributed extensional tectonism (Chapin and Seager, 1975). As a result, originally contiguous ignimbrite sheets are now discontinuously exposed in fault-block mountain ranges separated by infilled basins. Structural complexity varies widely from range to range, in extreme cases showing low-angle faulting and steep (45-90°) dips indicative of extension in excess of 100% (Chamberlin, 1983).

Methods

Paleomagnetism

For the paleomagnetic portion of this study, 3055 oriented samples were collected from 404 sites in 25 regional and 54 local ignimbrites. Most sites were field drilled and oriented by sun and magnetic compasses. Oriented hand samples were obtained within designated wilderness areas. The orientation of paleohorizontal was carefully assessed at each site, using attitudes of pumice foliations, welding zonation, and contacts of ignimbrites, as well as bedding in stratigraphically adjacent units. The remanent magnetizations of standard-sized specimens were measured using spinner and cryogenic magnetometers, utilizing both alternating field and thermal demagnetization procedures. A variety of techniques were also used to assess magnetic mineralogy, including reflected light microscopy, thermomagnetic analyses, and isothermal remanent magnetization (IRM) acquisition and demagnetization experiments.

Paleo- and rock-magnetic data show that Mogollon-Datil ignimbrites generally carry uniform, well-defined remanent magnetizations that provide reliable correlation criteria. About 90% of the sites exhibit well-grouped (a_{95}<10°) magnetizations carried by finely dispersed, high-temperature-oxidation assemblages of magnetite, hematite, and maghemite. These magnetizations, interpreted as thermoremanent magnetization (TRM), are readily separated from abundant lightning-induced isothermal components. For the remaining 10% of sites, primarily in altered or poorly welded, lithic-rich tuff, the original TRM's are obscured by

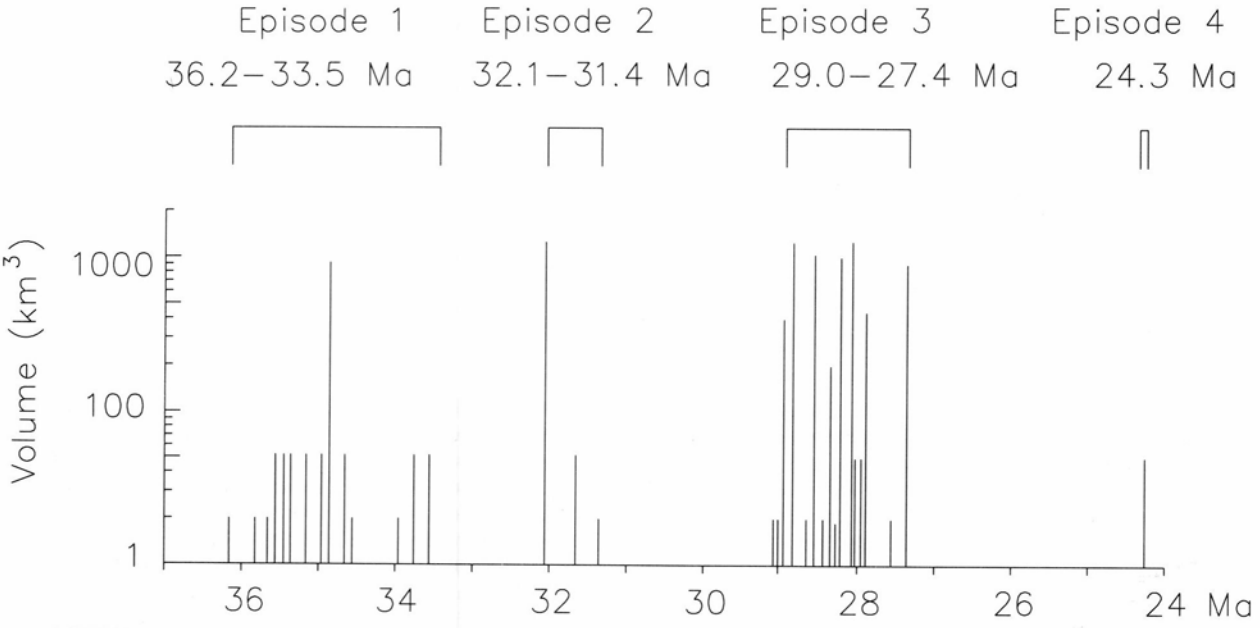

FIGURE 4—Time distribution of well-dated Mogollon–Datil ignimbrites, showing episodic nature of volcanism. Vertical lines each represent a dated ignimbrite, with length proportional to estimated volume from Table 1. Units with no available volume estimate are conservatively shown as 50 km^3 for regional units (maximum known lateral dimension > 40 km) and 20 km^3 for more local units.

chemical remanence (CRM) or randomly directed, lithic-hosted magnetizations.

Within individual ignimbrite outflow sheets, TRM directions are generally laterally and vertically consistent, in both densely welded proximal and poorly welded distal facies. Discordancies in individual site-mean directions primarily reflect uncertainties in structural corrections, particularly in areas of locally strong tectonic extension. Compared to outflow sheet data, the site-mean TRM's of thick (>500 m) intracauldron-facies ignimbrites are poorly grouped, apparently reflecting either secular variation during protracted cooling or large discrepancies between eutaxitic foliations and the syncooling paleohorizontal.

Unit-mean paleomagnetic data from Mogollon—Datil ignimbrites are summarized in Table 1 and Fig. 5. Data from individual sites are presented on a unit by unit basis in Figs. 6 to 31 and in Appendices 2 and 3. Details of paleomagnetic and rock-magnetic methods and results are presented in McIntosh (1989, in press). Previously published paleomagnetic studies of Mogollon—Datil ignimbrites include Strangway et al. (1976), McIntosh (1983), and Diehl et al. (1988).

$^{40}Ar/^{39}Ar$ dating

The $^{40}Ar/^{39}Ar$ dating portion of this study involved analyses of 85 samples from 36 ignimbrites. Sanidine separates (>99% purity) were prepared and irradiated, along with flux monitors of known age (FCT-3, 27.83 Ma, Kunk et al., 1985; corrected for the updated age for Mmhb1, 520.4 Ma, Sampson and Alexander, 1987), in the U.S. Geological Survey TRIGA reactor (Dalrymple et al., 1981). Age spectra were measured at the U.S. Geological Survey $^{40}Ar/^{39}Ar$ dating facility at Reston, Virginia.

A total of 97 $^{40}Ar/^{39}Ar$ age spectra were measured, 94 of which met the plateau age criteria of Fleck et al. (1977); plateau ages were calculated by weighting gas fractions according to the inverse of their variance. Replicate plateau age determinations (n=2 to 6) for eight different samples show within-sample precisions averaging ±0.25%. Plateau ages from multiple (n=3 to 8) samples of individual ignimbrites show within-unit precision (1σ) of ±0.1-0.4% (±0.04-0.13 Ma). In sharp contrast, conventional K—Ar and fission-track ages on the same units generally show relative errors (la) in excess of ±5% (±1.3-2.2 Ma) (Ratté et al., 1984; Marvin et al., 1987).

$^{40}Ar/^{39}Ar$ ages from Mogollon—Datil ignimbrites are summarized in Table 1 and Fig. 4. Plateau ages for individual samples are presented in Table 2 and Figs. 6 to 31. Appendix 1 provides complete data for each age spectrum. Details of $^{40}Ar/^{39}Ar$ methods and results are presented in Kedzie (1984), McIntosh (1989), and McIntosh et al. (1990).

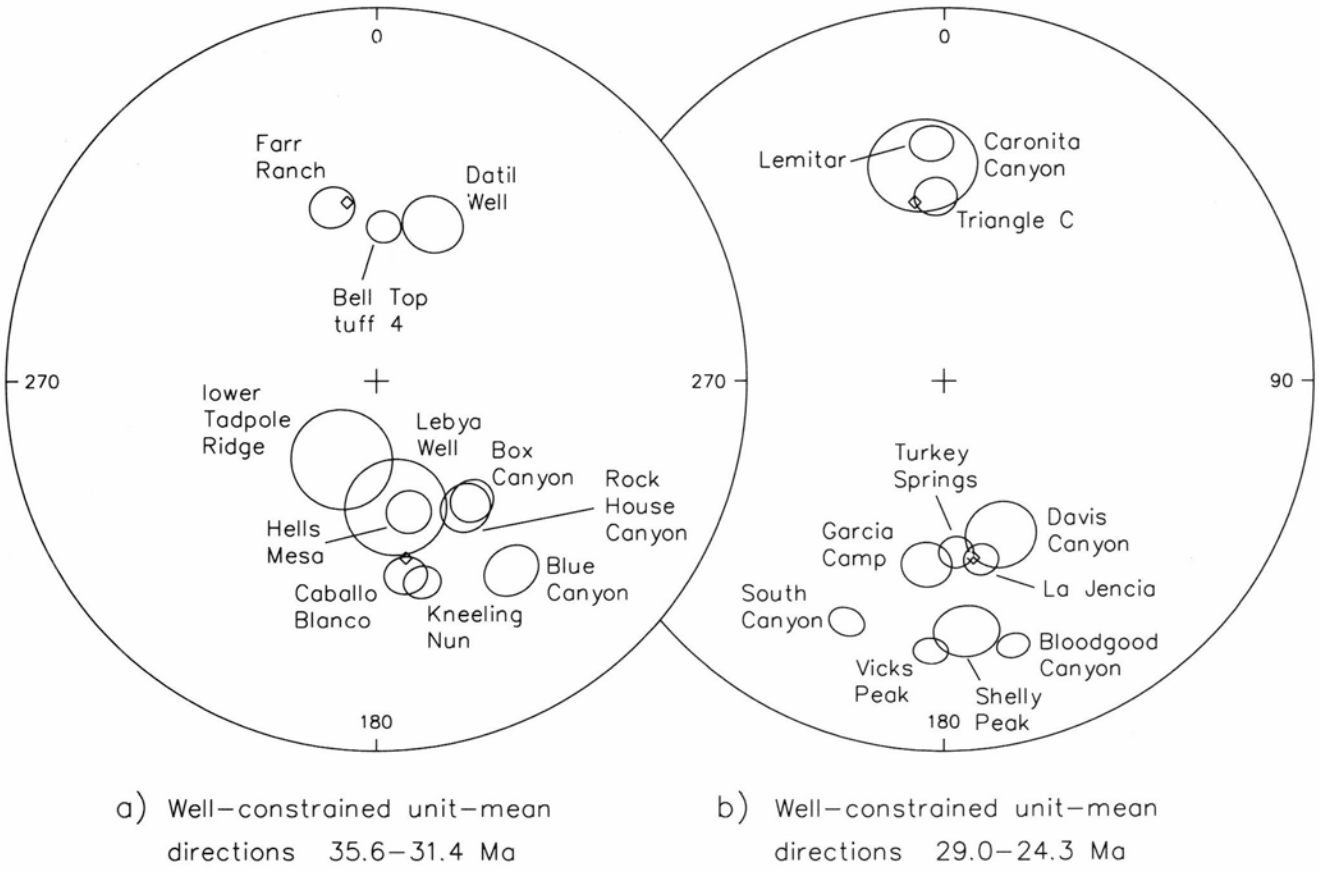

FIGURE 5—Unit-mean paleomagnetic directions (four or more sites per unit) for Mogollon–Datil ignimbrites. Each ellipse represents the cone of 95% confidence (α_{95}) for a unit-mean direction based on four or more sites. All northern hemisphere direction are downward and all southern hemisphere directions are upward. Heavy diamonds represent time-averaged Eocene–Oligocene geomagnetic reference directions (Diehl et al., 1988). Table 1 presents unit-mean paleomagnetic data in tabular form. a) 35.6 to 31.4 Ma units, b) 29.0 to 24.3 Ma units.

TABLE 1—Summary of $^{40}Ar/^{39}Ar$ and paleomagnetic data for Mogollon–Datil ignimbrites.

Stratigraphic unit	ref.	extent (km)	volume (km^3)	$^{40}Ar/^{39}Ar$ age			paleomagnetic remanence					cauldron or source
				n	Ma	σ(Ma)	pol	n/nt	inc	dec	α_{95}	
EPISODE 4												
*Turkey Springs	F86	62		2	24.33	±0.03	R	15 /19	-51.8	175.9	3.6	
EPISODE 3												
*Slash Ranch	R78	22		1	26.10	±0.12	N	2 /3	57.6	166.9	13.0	
South Canyon	OC83	135	700	3	27.36		R	22 /43	-30.7	202.1	3.5	Mt. Withington
*Walking X	H78			1	27.58		N	1 /1	64.0	5.7		
Lemitar	OC83	78	450	2	28.00		N	10 /21	36.6	356.9	4.3	
Caronita Canyon	OC83	40	50	1	27.96		N	4 /5	41.5	354.2	11.0	
*Triangle C Ranch	RA89	58		1	28.05		N	5 /6	49.2	357.3	4.4	Bursum?
Apache Springs	R84	35	1200	1	27.98		R	2 /2	-35.8	166.1	30.6	Bursum
Bloodgood	R84	155	1000	8	28.05		R	22 /23		165.3	3.1	Bursum
Diablo Range	RG75	10		1	28.05		R	1 /1	-24.8	200.3		dome
Shelly Peak	R84	96	100-200		(28.1)			8 /10		174.8	6.4	Gila Cliff Dwellings?
Garcia Camp	D87	25		1	28.10		R	7 /7	-48.8	185.4	5.2	dome
Vicks Peak	OC83	200	1050	3	28.56		R	24 /31	-27.9	182.8	3.3	Nogal Canyon
*Lookout	W82			2	28.69		R	1 /1	-55.4	160.8		dome
La Jencia	OC83	158	1250	4	28.85		R	15 /24		168.2	3.6	Sawmill/Magdalena
Davis Canyon	R84	125	200-400	2	29.01		R	6 /7	-53.5	159.6	7.5	Gila Cliff Dwellings?
*Mud Hole	H90			1	29.09		R	1 /1	-55.9	124.5		dome?
*Stiver Canyon	W82				(29)		R	1 /1	-52.7	172.6		dome?
*Little Mineral	H86			1	29.01		N	1 /1	58.0	3.1		dome
*Monument	K81	25			(29)		N	1 /1	35.2	344.0		
*Pueblo Creek tuff	R89	12			(29)		N	1 /1	51.8	336.9		
EPISODE 2												
upper Tadpole	F76	28		1	31.39		R	3 /3	-23.3	185.2	16.3	Twin Sisters
lower Tadpole	F76	45			(31.4)		R	6 /6	-71.1	203.8	11.0	Twin Sisters
Caballo Blanco	S82	143		5	31.65		R	6 /8	-46.0	171.4	4.4	
Hells Mesa	OC83	152	1200	4	32.06		R	10 /18		166.0	4.8	Socorro
EPISODE 1												
Box Canyon	E57	225	>100	7	33.51		R	12 /17		141.3	4.7	
Blue Canyon	OC83	135		2	33.66		R	6 /9	-37.3	144.4	5.7	
*Table Mountain	E57			1	33.89		R	1 /1	-36.9	181.5		
Cooney	R84	70?			(34)		R	3 /3	-46.7	168.7	28.0	
Rock House	OC83	142		1	34.42		R	8 /11		144.8	5.4	
Mimbres Peak	E75			1	34.57		N	1 /1	58.7	353.0		dome
*Lebya Well	RE89	72		1	34.70		R	4 /4	-61.7	171.2	10.8	
Kneeling Nun	E75	213	>900	4	34.89		R	21 /28		167.1	3.8	Emory
*Stone House	H90				(34.9)		N	3 /3	43.5	323.9	18.3	
Bell Top tuff 4	C76	112		3	34.96		N	5 /5	56.1	2.7	3.6	
upper Sugarlump	S82	50?		1	35.17		N	2 /2	62.3	337.7	8.1	
lower Sugarlump	S82	42?			(35.5)		N	2 /2	44.0	347.3	12.1	
basal Sugarlump	S82				(35.5)		N	1 /1	49.2	271.1		
*Farr Ranch	RE89	143		1	35.57		N	9 /13	50.4	345.5	4.7	
Datil Well	OC83	140		2	35.48		N	5 /5	53.3	19.9	6.4	
Bell Top tuff 3	C76	41		2	35.69		N	2 /2	69.9	329.9	1.6	Organ?

TABLE 1, continued.

Stratigraphic unit	ref.	extent (km)	volume (km^3)	$^{40}Ar/^{39}Ar$ age			paleomagnetic remanence					cauldron or source
				n	Ma	σ(Ma)	pol	n/nt	inc	dec	α_{95}	
Bell Top tuff 2	C76	15			(36)		N	2 /2	39.7	350.0	17.3	
Doña Ana	S76	8		1	35.49		N	2 /2	54.4	155.3	48.5	Doña Ana / Organ
Squaw Mountain	SM88	11		1	35.75		N	2 /2	58.8	178.0	44.5	Organ
Achenback Park	SM88	13			(35.8)		N	3 /3	50.0	177.0	35.6	Organ
*upper Steeple	H90				(36)		R	1 /1	-50.8	158.7		
*lower Steeple	H90				(36)		N	1 /1	-50.8	26.7		
upper Rubio Peak	S82				(36)		R	1 /1	-63.8	152.6		
lower Rubio Peak	S82				(36)		R	1 /1	-40.1	166.5		
Cueva	SM88	13		1	36.20		R	2 /3	-53.4	220.3	67.8	Organ

Explanation: * denotes informal unit name; ages in parentheses are based on stratigraphic constraints; extent is maximum exposed lateral dimension (extents based on uncertain correlations are queried); volume estimates are after McIntosh et al., 1986; n is number of plateau ages used in mean; σ is standard deviation of multiple ages or analytical error of single ages; pol is magnetic polarity; n/nt is number of sites used in unit-mean/total sites; inc, dec, and α_{95} are unit-mean inclination, declination, and cone of 95% confidence (α_{95} omitted for units with results from less than three sites); source cauldrons are shown where known, dome denotes small volume units derived from rhyolitic domes.
References: C76 = Clemons, 1976; D87 = Duffield et al., 1987; E57 = Elston, 1957; E75 = Elston et al., 1975; F76 = Finnell, 1976; F86 = Ferguson, 1986; H78 = Hedlund, 1978; H86 = Harrison, 1986; H90 = Hedlund, 1990; HA90 = Harrison, 1990; K81 = Krier, 1981; OC83 = Osburn and Chapin, 1983b; R78 = Richter, 1978; R84 = Ratté et al., 1984; R89 = Ratté, 1989b; RA89 Ratté, 1989a; RE89 = Ratté et al., 1989; RG75 = Ratté and Gaskill, 1975; S76 = Seager et al., 1976; S82 = Seager et al.,1982; SM88 = Seager and McCurry, 1988; W82 = Woodard, 1982.

TABLE 2—Unit-mean and sample $^{40}Ar/^{39}Ar$ plateau ages and sanidine mineralogy data.

		sanidine mineralogy					total gas	plateau			σ		SEM	
unit	sample	K/Ca	Or	Ab	An	Ex	age (Ma)	$\%^{39}Ar$	n	age (Ma)	Ma	%	Ma	%
Turkey Springs	unit mean	33.2							2	24.33	±0.03	±0.12%		
	137	33.8	56	43	2		24.3	100.0	5	24.35	±0.09	±0.37%		
	217	32.6	54	44	2	E	24.3	100.0	5	24.31	±0.09	±0.37%		
Slash Ranch	472	40.0	49	51	1	U	26.6	69.4	2	26.10	±0.12	±0.46%		
South Canyon	unit mean	29.8							3	27.37	±0.07	±0.26%	±0.04	±0.15
	KJH-22	31.6					27.6	74.0	3	27.40	±0.07	±0.26%		
	77-6-1	19.0	44	54	2		27.4	88.7	4	27.41	±0.07	±0.26%		
	258	38.7	56	43	1	E	27.4	65.7	2	27.28	±0.08	±0.29%		
Walking X Canyon	510	31.4					27.8	100.0	5	27.58	±0.10	±0.36%		
Lemitar	unit mean	27.7							2	28.00	±0.08	±0.29%		
	KTS-1	24.5					28.0	56.5	4	27.94	±0.10	±0.36%		
	KJH-24	30.8					28.1	68.3	5	28.05	±0.07	±0.25%		
Caronita Canyon	167	24.3				E	27.9	67.9	5	27.96	±0.07	±0.25%		
Triangle C Ranch	158:mean	46.2	61	38	1				2	28.05	±0.14	±0.50%		
	158	46.2					28.0	70.5	5	27.95	±0.08	±0.29%		
	158	46.2					28.1	80.2	4	28.15	±0.07	±0.25%		
Apache Springs	487	30.4	50	48	1		28.0	90.7	3	27.98	±0.09	±0.32%		

TABLE 2, continued.

		sanidine mineralogy					total gas	plateau			σ		SEM	
unit	sample	K/Ca	Or	Ab	An	Ex	age (Ma)	%^{39}Ar	n	age (Ma)	Ma	%	Ma	%
Bloodgood Canyon	unit mean	40.4							8	28.05	±0.04	±0.14%	±0.01	±0.05
	94	43.8	48	51	1	E	28.1	100.0	5	28.11	±0.10	±0.36%		
	95	40.9	48	51	1		28.2	97.7	4	28.06	±0.10	±0.36%		
	112	36.0	48	50	2		29.3	100.0	5	28.04	±0.10	±0.36%		
	276	48.8	44	55	1	E	28.1	84.4	4	27.99	±0.12	±0.43%		
	318	40.8	49	50	1	E	28.0	67.4	2	28.05	±0.07	±0.25%		
	430	41.4				E	28.0	71.4	2	28.06	±0.08	±0.29%		
	434: mean	49.2	45	54	1	E			2	28.09	±0.05	±0.18%		
	434	49.4					28.1	90.6	3	28.05	±0.09	±0.32%		
	434	48.9					28.2	98.8	5	28.12	±0.10	±0.36%		
	85G006	22.4	43	55	2		28.1	63.9	2	28.03	±0.08	±0.29%		
Diablo Range	435	34.0	48	51	1	E	28.1	90.6	3	28.05	±0.08	±0.29%		
Shelley Peak	149:mean	25.7	56	42	2	E			2	28.59	±0.11	±0.37%	contaminated	
	149	25.7					28.5	60.2	3	28.67	±0.08	±0.28%		
	149	25.6					28.5	100.0	3	28.52	±0.09	±0.32%		
Garcia Camp	319	25.4	52	46	2	E	28.1	92.1	3	28.10	±0.09	±0.32%		
Taylor Creek	unit mean	26.2							2	28.10	±0.18	±0.66%		
Rhyolite (lava)	116	29.1	45	53	2		28.2	84.7	4	28.23	±0.10	±0.35%		
	85G003	23.2	48	50	2		28.0	91.7	3	27.97	±0.10	±0.36%		
Vicks Peak	unit mean	56.5							3	28.56	±0.06	±0.19%	±0.03	±0.11
	KJH-10	43.2					28.6	73.4	3	28.51	±0.08	±0.28%		
	143	46.1	42	57	1		28.6	63.1	4	28.62	±0.08	±0.28%		
	414	80.3	42	58	0	E	29.0	60.8	2	28.56	±0.08	±0.28%		
	502	52.8	41	57	2		30.4	80.7	3	30.69	±0.11	±0.36%	contaminated	
Lookout Mountain	unit mean	34.4							2	28.69	±0.03	±0.10%		
	433	32.2	45	53	1	E	28.7	97.8	3	28.67	±0.12	±0.42%		
	441	36.6	45	54	1	E	28.8	91.6	3	28.72	±0.11	±0.38%		
La Jencia	unit mean	25.2							4	28.85	±0.04	±0.14%	±0.02	±0.08
	KJH-4	28.8					28.9	71.0	5	28.83	±0.08	±0.28%		
	KJH-5	27.8					28.8	59.8	4	28.81	±0.09	±0.31%		
	146:mean	24.2	44	54	1	E			2	28.90	±0.11	±0.39%		
	146	24.2					29.1	82.3	5	28.98	±0.08	±0.28%		
	146	24.2					28.9	100.0	3	28.82	±0.08	±0.28%		
	111	22.2	45	53	2		28.8	74.9	4	28.86	±0.09	±0.31%		
Davis Canyon	unit mean	36.7							2	29.01	±0.11	±0.35%		
	96	30.1	47	52	2		29.1	100.0	3	29.09	±0.08	±0.28%		
	494	43.3					28.8	59.8	2	28.93	±0.10	±0.35%		
Mud Hole	157	25.7	50	48	2	E	29.1	65.4	2	29.09	±0.11	±0.38%		
Little Mineral Creek	491	19.5	56	42	2		29.0	100.0	5	29.01	±0.10	±0.35%		
upper Tadpole Ridge	496	10.0					31.4	94.8	5	31.39	±0.11	±0.35%		
Caballo Blanco	unit mean	62.8							5	31.65	±0.06	±0.17%	±0.05	±0.15
	200	61.9	64	35	1	E	31.7	95.3	5	31.66	±0.11	±0.35%		
	236	62.4				E	31.7	100.0	5	31.64	±0.11	±0.35%		
	268	63.4	63	36	1	E	31.7	92.7	3	31.71	±0.12	±0.38%		
	478	59.4	66	34	1		31.6	88.2	3	31.56	±0.12	±0.38%		
	525	66.9					31.7	100.0	5	31.67	±0.11	±0.35%		

TABLE 2, continued.

		sanidine mineralogy					total gas	plateau			σ		SEM	
unit	sample	K/Ca	Or	Ab	An	Ex	age (Ma)	%^{39}Ar	n	age (Ma)	Ma	%	Ma	%
Hells Mesa	unit mean	56.7							4	32.06	±0.10	±0.30%	±0.06	±0.17
	KJH26:mean	65.2	64	35	1	E			6	32.06	±0.10	±0.31%	±0.05	±0.15
	KJH-26	62.5					32.2	100.0	8	32.25	±0.08	±0.25%		
	KJH-26	88.6					32.1	87.6	5	32.10	±0.11	±0.34%		
	KJH-26	55.4					32.0	92.1	3	31.99	±0.11	±0.34%		
	KJH-26	61.0					32.0	73.8	3	31.99	±0.11	±0.34%		
	KJH-26	61.3					32.0	72.8	3	32.03	±0.11	±0.35%		
	KJH-26	62.6					32.0	100.0	5	32.01	±0.11	±0.34%		
	KD-1	62.1					32.2	54.2	2	32.11	±0.10	±0.31%		
	KBM-3	45.7					32.3	77.8	3	32.15	±0.11	±0.34%		
	SU-4-77	53.8					31.9	93.5	5	31.93	±0.09	±0.28%		
Box Canyon	unit mean	48.6							7	33.51	±0.13	±0.40%	±0.05	±0.15
	201	52.7	64	35	1	E	33.5	76.4	4	33.52	±0.12	±0.36%		
	207	49.4	66	33	1	E	33.6	87.1	3	33.57	±0.09	±0.27%		
	232	53.7	65	34	1		33.4	78.6	3	33.29	±0.14	±0.42%		
	234	54.9	65	33	1	U	34.6	64.0	2	33.62	±0.10	±0.30%		
	297	52.8	65	34	1	E	33.4	81.5	2	33.36	±0.10	±0.30%		
	505	22.6					33.7	90.8	3	33.65	±0.12	±0.36%		
	508	54.2					33.5	65.1	2	33.55	±0.12	±0.36%		
Blue Canyon	unit mean	29.5							2	33.66	±0.03	±0.09%		
	240	29.3				U	33.7	79.8	4	33.64	±0.11	±0.33%		
	328	29.7	62	36	2	U	33.7	100.0	7	33.68	±0.12	±0.36%		
	81-12-6:mean	27.6	62	36	2				2	33.98	±0.03	±0.08%	contaminated	
	81-12-6	27.6					34.0	84.2	6	34.00	±0.09	±0.27%		
	81-12-6	27.6					34.0	78.0	3	33.96	±0.08	±0.24%		
Table Mountain	296	32.6	61	37	1	E	34.0	70.7	3	33.96	±0.12	±0.35%		
Rock House Canyon	468	32.6	54	45	1	E	34.4	93.8	3	34.42	±0.12	±0.35%		
	239	32.9	61	37	2		34.9	80.3	4	34.88	±0.11	±0.32%	contaminated	
Mimbres Tuff	454	25.9	42	56	2		34.5	100.0	5	34.57	±0.12	±0.35%		
Lebya Well	231	10.9	45	51	4	U	34.8	64.0	2	34.70	±0.10	±0.29%		
Kneeling Nun	unit mean	61.2							4	34.89	±0.05	±0.15%	±0.03	±0.08
	92	63.0				E	35.0	73.0	3	34.90	±0.12	±0.34%		
	202	49.9	64	35	1	E	34.9	100.0	5	34.89	±0.12	±0.34%		
	208	62.0	63	36	1		34.9	86.8	3	34.83	±0.15	±0.43%		
	294	62.4	61	37	1	E	34.9	100.0	5	34.96	±0.12	±0.34%		
	498	61.9					35.0	100.0	5	35.17	±0.12	±0.34%	contaminated	
	110	60.7	66	33	1	E	35.3	67.1	4	35.35	±0.12	±0.34%	contaminated	
	465	68.4				E	45.8			no plateau			contaminated	
Bell Top tuff 4	unit mean	11.4							3	34.96	±0.04	±0.11%	±0.02	±0.07
	206	10.9	38	59	3	E	35.1	82.7	3	35.01	±0.13	±0.37%		
	209	11.1					34.9	100.0	5	34.94	±0.12	±0.34%		
	501	12.2					35.1	63.8	2	34.93	±0.12	±0.34%		
upper Sugarlump	460	23.7	48	50	2		35.2	58.9	2	35.17	±0.12	±0.34%		
Farr Ranch	238	12.8	51	46	4	U	35.6	89.3	5	35.57	±0.13	±0.37%		
Datil Well	unit mean	12.3							2	35.47	±0.07	±0.20%		
	85:mean	12.4	47	50	4				2	35.53	±0.03	±0.08%		
	85	12.4					35.6	81.5	4	35.55	±0.10	±0.28%		

TABLE 2, continued.

unit	sample	sanidine mineralogy K/Ca	Or	Ab	An	Ex	total gas age (Ma)	plateau %^{39}Ar	n	plateau age (Ma)	σ Ma	σ %	SEM Ma	SEM %
	85	12.4					35.6	91.4	4	35.51	±0.10	±0.28%		
	237	14.1	47	50	3		35.4	92.7	4	35.43	±0.13	±0.37%		
	90	10.4	46	51	3		36.4			no plateau			contaminated	
Doña Ana	203	62.8					35.5	100.0	5	35.49	±0.11	±0.31%		
Bell Top tuff 3	205:mean	72.7	47	53	1				2	35.69	±0.02	±0.06%		
	205	71.3					35.7	83.0	4	35.71	±0.12	±0.34%		
	205	73.2					35.7	88.1	3	35.68	±0.14	±0.39%		
Squaw Mountain	529	18.7					36.0	72.3	3	35.75	±0.12	±0.34%		
lower Cueva	483	160.9					36.2	94.9	4	36.20	±0.13	±0.36%		
	482	102.6	42	58	0		35.6			no plateau			altered	

Explanation: K/Ca is molar ratio determined from ^{37}Ar/^{39}Ar measurements; Or, Ab, and An are percent orthoclase, albite, and anorthite end members in sanidine analyzed by microprobe (average of 5-8 analyzed crystals); Ex is degree of exsolution shown by x-ray diffraction: E=cryptoperthitic exsolution, U=unexsolved; %^{39}Ar is % of total ^{39}Ar in age plateau; n is the number of heating steps in age plateau or samples used for mean age; σ is single-spectrum, within sample, or within-unit 1 sigma error; SEM is within-unit standard deviation of the mean; final column also identifies samples apparently contaminated by older feldspar.

Paleomagnetism and ^{40}Ar/^{39}Ar dating as correlation criteria

Paleomagnetism has been used as an ignimbrite correlation criterion for more than two decades (e.g. Dalrymple et al., 1965; Grommé et al. 1972; Best et al., 1973; Reynolds, 1977; Hoblitt et al., 1985; Weiss et al., 1989). Successful paleomagnetic correlation of ignimbrites requires, above all else, that the units in question carry precisely measurable TRM components acquired during rapid post-emplacement cooling. Because of reversals and secular variation of the geomagnetic field, paleomagnetic analysis can potentially distinguish between individual volcanic units differing in age by as little as a few thousand years or less (Grommé et al., 1972; Bogue and Coe, 1981; Holcomb et al., 1986). Because geomagnetic field directions vary non-uniquely through time, paleomagnetism constitutes a negative correlation criterion, i.e. disagreement of TRM directions is negative evidence for correlation, yet agreement is only permissive evidence. The ability to paleomagnetically distinguish among different ignimbrites is favored by large angular differences among their mean TRM directions; these differences must exceed uncertainties introduced by measurement and structural correction errors.

As discussed in previous sections, the requirement of precisely measurable primary TRM is well satisfied by 90% of the studied sites in Mogollon—Datil ignimbrites. The requirement for angular differences among TRM direction depends upon which units are being compared. In cases where the units in question differ in polarity, paleomagnetic correlation is unambiguous. In cases which require comparing TRM directions of units of the same polarity, identification is most successful for units with TRM directions which diverge significantly from the expected time-averaged Oligocene field direction (Table 1, Fig. 5).

Like paleomagnetism, the ^{40}Ar/^{39}Ar dating method has provided a strong criterion for correlating Mogollon—Datil ignimbrites. Where sufficient numbers of sanidine-bearing units have been dated, it has proven possible to reliably distinguish between units differing in age by only 0.5% (about 0.15 Ma).

^{40}Ar/^{39}Ar and paleomagnetic correlation criteria are complementary: ^{40}Ar/^{39}Ar data serve to resolve age difference between paleomagnetically similar units, and paleomagnetism helps distinguish between units that are altered, lack sanidine, or are too close in age to be resolved even by the ^{40}Ar/^{39}Ar method.

Table 3 lists specific ignimbrite correlations problems which have been addressed by ^{40}Ar/^{39}Ar dating and paleomagnetic analysis; it includes both newly demonstrated correlations and previously published correlations which now appear to be incorrect. These correlations are discussed in more detail in the following sections.

Age and distribution of Mogollon—Datil ignimbrites

Mogollon—Datil ignimbrites range in age from 36.2 to 24.3 Ma. Ignimbrite activity was strongly episodic, being confined to four <2.6 m.y. eruptive intervals separated by 1.5 to 3 m.y. hiatuses. The following sections describe these four eruptive intervals, briefly discussing paleomagnetic and ^{40}Ar/^{39}Ar dating results for each regional ignimbrite.

Episode 1 (36.2 to 33.5 Ma)

The 36.2 to 33.5 Ma interval of Mogollon—Datil ignimbrite volcanism is the longest, most complex, and least understood of the volcanic field's four eruptive episodes.

TABLE 3—Ignimbrite correlations aided by $^{40}Ar/^{39}Ar$ and paleomagnetic data.

Ignimbrite	Sites	Evidence		Correlative units and (miscorrelated units)	Reference
		Pmag	Ar		
tuff of Turkey Springs	137,183,185,186,219	X	X	part of Railroad Canyon Tuff	F76
	24,25,215,216	X		(South Canyon Tuff)	D80
South Canyon Tuff	138,187,188,250,251,252	X		part of Railroad Canyon Tuff	F76
	380	X		part of AL Peak Tuff	LB79
	23	X		(Lemitar Tuff)	D80
	258	X	X	tuff in sandstone of Inman Ranch	E82
tuff of Caronita Canyon	543,545	X		(Hells Mesa Tuff)	B80
Bloodgood Canyon Tuff	112,114,332	X	X	part of Railroad Canyon Tuff	F76
Garcia Camp Tuff	113,227,319,333,334,335	X		part of Railroad Canyon Tuff	F76
Vicks Peak Tuff	97,98,502	X		part of tuff of Tularosa Canyon	RS76
	75,190,248	X		part of tuff of Wahoo Canyon	F76
	381	X		part of AL Peak Tuff	LB79
	414	X	X	Bell Top tuff 7	C76
tuff of Lookout Mountain	433		X	Diamond Creek Tuff	A89
La Jencia Tuff	74	X		part of tuff of Wahoo Canyon	F76
Davis Canyon Tuff	96,503	X	X	part of tuff of Tularosa Canyon	RS76
lower Tadpole Ridge Tuff	477,479	X		tuff of Terry Canyon	K81
	156	X		part of Tvt	F82
Caballo Blanco Tuff	525	X	X	part of Fall Canyon Tuff	RG75
	268	X	X	Fall Canyon Tuff	R88
	254	X		tuff in sandstone of Monument Park	W82
Box Canyon Tuff	260,263,304	X		part of Fall Canyon Tuff	RG75
	124,207,415	X	X	Bell Top tuff 6	C76
	505	X	X	tuff of Cherokee Canyon	F87
	233,234	X	X	tuff in Pueblo Creek Formation	R89
	297		X	(Sugarlump Tuff)	E57
	508,511	X	X	(Kneeling Nun Tuff)	H78
Blue Canyon Tuff	354	X		tuff of Shipman Spring	H86
Rockhouse Canyon Tuff	403	X		tuff of Koko Well	HA90
tuff of Lebya Well	231	X		tuff of Bishop Peak	R89
Kneeling Nun Tuff	123,208,416	X	X	Bell Top tuff 5	C76
	294,295	X	X	(Sugarlump Tuff)	E57
Bell Top tuff 4	317,501	X	X	tuff of Rocque Ramos Canyon	H90
tuff of Farr Ranch	313,316	X		tuff of Victora Tank	H90
	308,388,390	X		tuff of Luna Park	F69
	65,66,71	X		(Datil Well Tuff)	OC83
Bell Top tuff 3	122,471	X	X	probable Organ cauldron outflow facies	SM88
Bell Top tuff 2	121,204	X		possible Organ cauldron outlow facies	SM88
Doña Ana Tuff	103,203	X	X	related to Organ cauldron activity	S76

Correlations presented in this table show where other workers have either misidentified (in parentheses) or applied different names to ignimbrites listed in the left-hand column. Evidence column identifies whether correlations are based on paleomagnetic (Pmag) or $^{40}Ar/^{39}Ar$ (Ar) data or both.

References: A89 = Abitz, 1989; B80 = Bowring, 1980; C76 = Clemons, 1976; D80 = Donze, 1980; E57 = Elston, 1957; E82 = Eggleston, 1982; F69 = Farkas, 1969; F76 = Fodor, 1976; F82 = Finnell, 1982; F87 = Finnell, 1987; H78 = Hedlund, 1978; H86 = Hermann, 1986; HA86 = Harrison, 1986; H90 = Harrison, 1990; K81 = Krier, 1981; LB79 = Lopez and Bornhorst, 1979; OC83 = Osburn and Chapin, 1983b; R88 Richter et al., 1988; R89 = Ratté, 1989b ; RG75 = Ratté and Gaskill, 1975; RS76 = Rhodes and Smith, 1976; S76 = Seager et al., 1976; SM88 = Seager and McCurry, 1988; W82 = Woodard, 1982.

Numerous ignimbrites, predominantly low-silica rhyolites, were erupted in this interval; data from 12 regional and 13 subregional to local units are listed in Table 1 and shown in Figs. 6 to 16. Only one ignimbrite, the Kneeling Nun Tuff (Fig. 11, 34.9 Ma, >900 km^3), has been established as a large-volume unit. Several other units extend over large areas (1-10,000 km^2) but are generally only 5 to 50 m thick. The unusually low aspect ratio (Walker et al., 1980) of these ignimbrites probably reflects some combination of subdued pre-eruptive topography and high energy or high mobility of the ash flows.

In spite of the large number of Episode 1 ignimbrites, the Kneeling Nun and Box Canyon Tuffs are the only outflow units for which source cauldrons have been definitely identified (Figs. 11, 16). Cauldron features have also been documented in the Doña Ana and Organ Mountains (Seager et al.,1976; Seager and McCurry, 1988), but identification of correlative outflow sheets is still tentative, as discussed below. The paucity of source cauldrons for Episode 1 ignimbrites is thought to primarily reflect concealment beneath extensional basins or overprinting by younger cauldrons. Alternatively, source cauldrons for these units may be very small features which have not yet been recognized in the course of geologic mapping.

Organ cauldron activity, 36.2 to 35.5 Ma-$^{40}Ar/^{39}Ar$ data indicate that Mogollon-Datil ignimbrite activity initiated with 36.2 to 35.5 Ma cauldron-forming eruptions in the Organ and Doña Ana Mountains (Fig. 6). The presence of intracauldron-facies ignimbrites and cauldron structures in both areas have been documented by detailed mapping (Seager et al., 1976; Seager, 1981). The 9000 m thick stratigraphic sequence within the Organ cauldron consists of three distinct ignimbrites (Cueva, Achenback Park, and Squaw Mountain Tuffs, in ascending order); the entire sequence shows coherent normal geochemical zoning (Seager and McCurry, 1988). The Doña Ana intracauldron sequence includes a >800 m thick multi-cooling-unit ignimbrite termed the Doña Ana Rhyolite Tuff (Seager et al., 1976). Based on published K-Ar data, the age of Organ and Doña Ana cauldron activity has been generally accepted to be about 33 Ma (Seager and McCurry, 1988).

$^{40}Ar/^{39}Ar$ plateau ages from single samples of the Cueva, Squaw Mountain, and Dona Ana Tuffs are respectively 36.2, 35.8, and 35.5 Ma (Table 1), indicating that cauldron activity in this area is older than previously believed. The age difference between the Cueva and Squaw Mountain Tuffs is consistent with their stratigraphic order and the presence of a sedimentary interval above the Cueva Tuff (Seager and McCurry, 1988). The age difference between the Squaw Mountain and Dona Ana Tuffs is not considered significant because only one sanidine sample has been dated per unit, and both showed slightly low radiogenic yields, apparently reflecting minor alteration along cleavages (McIntosh, 1989; McIntosh et al., 1990).

Paleomagnetic data (Fig. 6) indicate reverse polarity for the Cueva Tuff and normal polarity for the Achenback, Squaw Mountain, and Dona Ana Tuffs. Site-mean directions show considerable within-unit scatter (Fig. 6), but such scatter is typical for other thick (>500 m) intracauldron-fades ignimbrites in the Mogollon-Datil volcanic field (McIntosh, 1989, in press) and elsewhere (e.g. Reynolds et al., 1986).

$^{40}Ar/^{39}Ar$ and paleomagnetic data indicate that the Organ and Doña Ana sequences are closely associated in time, and suggest that they are either portions of one (>35 km) large cauldron or parts of the same cauldron complex. Although the data are insufficient to definitely identify outflow fades for this cauldron/cauldron complex, tuffs 2 and 3 of the Bell Top Formation are attractive possibilities, as discussed in the following section.

Small-volume ignimbrites, 35.7 to 35.0 Ma—The least understood stratigraphic interval within Episode 1 is the poorly exposed sequence of several small outflow-facies ignimbrites which predate the eruption of the 34.9 Ma Kneeling Nun Tuff. These units (Figs. 3, 6, 7, 8, 9, 10) are generally thin (5-100 m), tend to be poorly welded, and are commonly intercalated with sedimentary sequences. The number of distinct ignimbrites in this interval is not accurately known due to uncertainties in correlations.

In the southern part of the field the pre-Kneeling Nun interval is represented by tuffs 2, 3, and 4 of the Bell Top Formation (Fig. 6; Clemons, 1976), by ignimbrite members of the Rubio Peak and Sugarlump Formations (Fig. 7; Elston, 1957; Seager et al., 1982), and, probably, by the stratigraphically lowest ignimbrites in the Steeple Rock area (Fig. 7). All these ignimbrites show normal polarity, except for the two locally exposed Rubio Peak tuffs and the upper Steeple Rock unit (Table 1). $^{40}Ar/^{39}Ar$ plateau ages from Bell Top tuffs 3 and 5, and upper Sugarlump Tuff are respectively 35.7, 35.0, and 35.2 Ma (Table 1, Figs. 6, 7).

Paleomagnetic data and $^{40}Ar/^{39}Ar$ ages suggest that some of these units were erupted over the same time interval as the Organ and Doña Ana intracauldron sequences (Fig. 6; Table 1). Tuff 3 of the Bell Top Formation (Clemons, 1976) is the best candidate for a co-eruptive outflow sheet for the Achenback Park/Squaw Mountain sequence because of its similar age (35.7 Ma), normal magnetic polarity, and geographic proximity (Fig. 6). A second possibility is the underlying tuff 2 of the Bell Top Formation (Clemons, 1976), a locally exposed ignimbrite which also shows normal polarity but has not yet been dated.

In addition to cauldron/outflow questions, there are also correlation problems among various outcrops of outflow sheets in the pre-Kneeling Nun interval. Two sites in the upper Sugarlump Tuff (sites 460 and 509 in Fig. 7) yield steep site-mean directions that agree well with site-mean directions from Bell Top tuff 3 (Fig. 6), but $^{40}Ar/^{39}Ar$ ages from the two units differ by 0.4 Ma. Likewise, the site-mean directions of two widely separated lower Sugarlump Tuff sites (Fig. 7) closely resemble TRM direction from Bell Top tuff 2 (Fig. 6), but no $^{40}Ar/^{39}Ar$ data have been obtained from these units.

More confident correlations can be made for tuff 4 of the Bell Top Formation, the youngest pre-Kneeling Nun regional ignimbrite in the southern part of the field (Fig. 10; Clemons, 1976). The maximum known lateral dimension of this unit is 68 km in the Goodsight-Cedar Hills area, and paleomagnetic and $^{40}Ar/^{39}Ar$ data strongly support its correlation with a widespread pre-Kneeling Nun unit exposed in the Winston area (Fig. 10; tuff of Rocque Ramos Canyon, Harrison, 1990) and the Salado Mountains (unnamed crystal tuff of Seager and Mayer, 1988). This correlation yields a maximum known lateral dimension of at least 112 km for Bell Top tuff 4 (Table 1). The 35.0 Ma age and geographic proximity to the Emory cauldron suggest that Bell Top tuff 4 may be a precursor unit related to the 34.9 Ma Kneeling Nun Tuff. The 30 m thick tuff of Stone House Ranch (Fig. 10, Table 1), which is

locally present between Bell Top tuff 4 and Kneeling Nun in the Winston area, may be a similar precursor.

At least two regional pre-Kneeling Nun ignimbrites are also present in the northern part of the volcanic field. Datil Well Tuff (35.5 Ma), a well-exposed unit in the Datil area (Fig. 8), shows a distinctive northwesterly TRM direction which supports correlation with a lithologically similar unit in an isolated outcrop 125 km to the southeast (site 481, Fig. 8). Paleomagnetic data also suggest a regional extent for the tuff of Farr Ranch (Fig. 9). This unit is lithologically identical to the locally underlying Datil Well Tuff and their $^{40}Ar/^{39}Ar$ ages (respectively 35.6 and 35.5 Ma) are statistically indistinguishable. Site-mean TRM directions, however, are quite different (Figs. 8, 9) and indicate that outcrops southeast of Socorro (Fig. 9) which were formerly mapped as Datil Well Tuff (Osburn and Chapin, 1983b) are actually tuff of Farr Ranch. Paleomagnetic data (Fig. 9) are furthermore consistent with correlation of tuff of Farr Ranch with the tuffs of Luna Park and Victoria Tank, two poorly known informally named units exposed 40 to 100 km to the south (Hermann, 1986; Harrison, 1990). Source cauldrons are not known for Datil Well or Farr Ranch outflows sheets, but their distributions suggest vents somewhere in the northern part of the field.

Kneeling Nun Tuff, 34.9 Ma-The 34.9 Ma Kneeling Nun Tuff is the largest and best-studied unit in Episode 1. $^{40}Ar/^{39}Ar$ and paleomagnetic data (Fig. 11) indicate that the outflow sheet extends well beyond its previously mapped extent (Elston et al., 1975). These data (Fig. 11) suggest that the Kneeling Nun outflow sheet correlates with Bell Top tuff 5 (Clemons, 1976), with part of the mapped Sugar-lump Tuff near Faywood (Elston, 1957; Seager et al., 1982), and with a thin, unwelded unit overlying tuff of Farr Ranch in the Horse Springs area (Ratté et al., 1989). These correlations suggest that the volume of the Kneeling Nun Tuff may be considerably larger than the 900 km^3 suggested by Elston et al. (1975).

The Kneeling Nun Tuff is the first of four large-volume, crystal-rich, low-silica rhyolites in the older portion of the Mogollon-Datil sequence. It is difficult or impossible to lithologically distinguish the Kneeling Nun Tuff (34.9 Ma) from Box Canyon Tuff (33.5 Ma), Hells Mesa Tuff (32.1 Ma), or Caballo Blanco Tuff (31.7 Ma). Furthermore, paleomagnetism is only marginally helpful for distinguishing among these four ignimbrites, because they all show unit-mean directions similar to the time-averaged Eocene-Oligocene field (Fig. 5). Fortunately, the age differences among these four units are all sufficiently large to be easily resolved by $^{40}Ar/^{39}Ar$ dating (Table 1).

Small-volume ignimbrites, 34.9 to 33.7 Ma-During the 1.3 m.y. interval following eruption of the Kneeling Nun Tuff, the southern portion of the Mogollon-Datil volcanic field was relatively quiescent. Mimbres Peak rhyolite domes and associated local ignimbrites were erupted in the southern Black Range, at least in part as moat-fill of the Emory cauldron (Elston et al., 1975). The only other ignimbrite erupted in the southern part of the field during this quiescent period is a 34.0 Ma crystal-rich, low-silica unit locally exposed at Table Mountain, south of Faywood, New Mexico (Table 1; herein termed tuff of Table Mountain, but mapped as a member of the Sugarlump Tuff by Elston, 1957, and Seager et al., 1982).

During this interval of quiescence in the southern part of the field, eruptions in the north produced three regional ignimbrites: tuff of Lebya Well (34.7 Ma), Rockhouse Canyon Tuff (34.4 Ma), and Blue Canyon Tuff (33.7 Ma). The tuff of Lebya Well (Fig. 12) was first recognized in the Horse Springs area by its stratigraphic position between 34.9 Ma Kneeling Nun and 34.4 Ma Rockhouse Canyon Tuff (Fig. 4). Although this unit has not been dated in the Horse Springs area, its stratigraphic position and distinctively steep TRM direction suggest correlation with the 34.7 Ma Bishop Peak Tuff exposed 75 km to the west (Fig. 12). Paleomagnetic and $^{40}Ar/^{39}Ar$ data generally confirm the mapped extents of the Rockhouse Canyon and Blue Canyon Tuffs and also suggest correlations with isolated outcrops further south (Figs. 13, 15). Like Datil Well and Farr Ranch, source cauldrons are unknown for the Lebya Well, Rockhouse Canyon, and Blue Canyon outflow sheets, although their distributions indicate vents in the northern part of the field.

The Cooney Tuff, a complex unit embracing several thin ignimbrites separated by sedimentary sequences, may also have been erupted in the 34.9 to 33.7 Ma interval. Published K-Ar data from this unit, exposed near the western edge of the field, suggest an age near 34 Ma, but samples bearing fresh sanidine suitable for $^{40}Ar/^{39}Ar$ dating have not been found. Dispersed site-mean TRM directions are shown by three sites in different members of the Cooney Tuff and from a possibly correlative (Ratté et al., 1984) unit near Clifton, Arizona (Fig. 14). These data suggest that eruption of the Cooney Tuff members may have spanned at least several centuries, which implies that there may be little hope for accurate long-range paleomagnetic correlation of this unit.

Box Canyon Tuff, 33.5 Ma-Box Canyon Tuff, the final ignimbrite erupted in Episode 1, has not been previously identified as a regional unit. This crystal-rich, low-silica unit was first recognized by Elston (1957) from its stratigraphic position between Kneeling Nun and Caballo Blanco Tuffs. $^{40}Ar/^{39}Ar$ plateau ages near 33.5 Ma and somewhat distinctively steep TRM directions (Figs. 5, 16) suggest that Box Canyon Tuff extends over much of the southern and western edges of the volcanic field (Fig. 16). Units now correlated with Box Canyon Tuff include Bell Top tuff 6 (Clemons, 1976), portions of mapped Sugarlump Tuff (Elston, 1957), mapped Kneeling Nun Tuff of Hedlund (1978), tuff of Cherokee Canyon (Finnell, 1987), portions of Fall Canyon Tuff (Ratté et al., 1984; Richter et al., 1988), and a tuff in the Pueblo Creek Formation (Rate, 1989b). The apparent source for the Box Canyon Tuff is the poorly known Schoolhouse Mountain cauldron (Fig. 16; Wahl, 1981), based on its correlation with the tuff of Cherokee Canyon, an intracauldron-facies ignimbrite within the Schoolhouse Mountain cauldron.

Episode 2 (32.1 to 31.4 Ma)

The second brief but intense episode of Mogollon-Datil ignimbrite activity commenced at 32.1 Ma, 1.5 m.y. after the eruption of Box Canyon Tuff. Episode 2 spanned only 0.7 m.y. but produced two major regional units, Hells Mesa and Caballo Blanco Tuffs, and a third thick but more localized unit, the Tadpole Ridge Tuff. All three of these units show reverse magnetic polarity.

Hells Mesa Tuff, 32.1 Ma-The first Episode 2 ignimbrite, the 1250 km^3 Hells Mesa Tuff, erupted at 32.1 Ma from the **Socorro** cauldron (Fig. 17). The Hells Mesa Tuff is the oldest of five large-volume ignimbrites exposed in

the Socorro area, and the extent of its cauldron and outflow sheet have been well established by a series of thesis maps (referenced in Osburn and Chapin, 1983b). The outflow sheet shows a highly asymmetric distribution about the cauldron, extending almost 100 km to the west, but absent to the south and east. Four $^{40}Ar/^{39}Ar$ ages from the northern part of the outflow sheet yield a mean age of 32.06 ±.13 Ma.

Paleomagnetic data from the Hells Mesa Tuff generally support the mapped extent of the outflow sheet and intracauldron fades. Mean directions from 10 of 17 sites are tightly clustered, but the remaining seven sites are anomalous, plotting 15-42° from the unit-mean direction (Fig. 17). Net rotations related to extreme tectonic extension in the Lemitar Mountains, Joyita Hills, and Black Butte are probably responsible for the anomalous declinations at sites 14, 134, 38, and 31, and the latter two sites also show alteration-related chemical remanent magnetizations (CRM's; McIntosh, 1989, in press). Sites 423 and 73 are in a badly disrupted zone adjacent to a major fault, and non-paleohorizontal pumice foliations at the base of the Hells Mesa may explain the anomalous declination of site 387.

The unit-mean direction (D=166, I=-60) of the Hells Mesa Tuff is not a strong correlation criterion, because it is nondistinctive (only 11° from the time-averaged Eocene-Oligocene field direction) and similar to the lithologically indistinguishable Caballo Blanco, Box Canyon, and Kneeling Nun Tuffs (Fig. 5). Tentatively though, paleomagnetic data from sites 312 and 329, together with stratigraphic sequence data, suggest that crystal-rich tuffs exposed in the southern San Mateo Mountains and the area north of Horse Springs represent distal Hells Mesa Tuff (Fig. 17).

Caballo Blanco Tuff, 31.7 Ma-The second Episode 2 ignimbrite, the Caballo Blanco Tuff, was erupted at 31.7 Ma and extends over some 10,000 km² of the southeastern Mogollon-Datil volcanic field. Although this unit was early recognized as a crystal-rich, low-silica ignimbrite overlying the Kneeling Nun in the southern Black Range (Elston, 1957; Elston et al., 1973), accurate assessment of its extent was prevented by inability to distinguish it from Kneeling Nun and Box Canyon Tuffs. $^{40}Ar/^{39}Ar$ data now allow reliable identification of the Caballo Blanco outflow sheet. Five dated samples, ranging from 31.56 to 31.71 Ma and averaging 31.65 ±.06 Ma, suggest that the unit extends 70 km west and 100 km north of its mapped extent in the Black Range and Santa Rita areas (Fig. 18). The Caballo Blanco Tuff correlates with at least part of the mapped Fall Canyon Tuff of Ratté et al. (1984), including the type section (site 525 in Fig. 18). Although the unit-mean TRM direction of Caballo Blanco Tuff is not particularly distinctive (Fig. 18), paleomagnetic data are consistent with a wide distribution for the unit. Site-mean directions are tightly grouped except for two anomalous sites which reflect unremoved CRM or poor attitude control (sites 253 and 181, Fig. 18).

Although no source cauldron has been established for this unit, two possibilities include the southern end of the Emory cauldron (as suggested in Abitz, 1989) and a now obliterated precursor to the Bursum cauldron (suggested by abundant large lithics at site 525).

Tadpole Ridge Tuff, 31.4 Ma-The third and last ignimbrite erupted during Episode 2 is the 31.4 Ma Tadpole Ridge Tuff, a thick, geographically restricted (40 km maximum known lateral dimension) unit exposed north of Pinos Altos, New Mexico (Fig. 19). This mineralogically distinctive ignimbrite (low-silica rhyolite, 10-25% plagioclase and biotite phenocrysts) was mapped as a local unit by Finnell (1976), who recognized distinct upper and lower members. Our observations of abrupt thickness changes, coarse lithic breccias, and a high-angle basal unconformity suggest that much or all of the mapped Tadpole Ridge Tuff is lying within a small cauldron (herein termed the Twin Sisters cauldron) with an east-west margin located immediately north of Pinos Altos (Fig. 19). The northern margin of the proposed Twin Sisters cauldron (inferred it Fig. 19) is buried by younger units.

Paleomagnetic data suggest a time break of at least centuries between eruption of the upper and lower members of the Tadpole Ridge Tuff, although neither paleosols nor significant sedimentary deposits are found along their mutual contact. The lower and upper intracauldron-facies members show, respectively, unusually steep and unusually shallow unit-mean TRM directions (Fig. 19). These directions are 49° apart, suggesting that at least 2000 yrs, elapsed between eruption of the two units, given a typical average secular variation rate of 4.5° per century (Holcomb et al., 1985). Alternatively, these differing TRM directions may have resulted from two closely spaced eruptions which occurred during a rapidly changing field excursion or polarity-transition event.

Paleomagnetic data have also helped to identify an outflow sheet associated with the lower member of the Tadpole Ridge Tuff. Two thin plagioclase-biotite tuffs, a member of Tvt of Finnell (1982) and tuff of Terry Canyon of Krier (1981), are exposed 20 km west and 30 km northeast, respectively, of the mapped extent of Tadpole Ridge Tuff. Correlation of these units with the lower member of the Tadpole Ridge Tuff is strongly supported by their distinctively steep site-mean directions (sites 156, 477, 479; Fig. 19).

Due to low sanidine content (<0.5%), it has proven difficult to obtain an accurate $^{40}Ar/^{39}Ar$ age for the Tadpole Ridge Tuff. An incorrect published age of 35.14 Ma (McIntosh et al., 1986) probably represents extreme xenocrystic contamination by sanidine from the Kneeling Nun Tuff, which is exposed in the nearby cauldron wall (site 498, Fig. 11) and locally forms abundant lithic fragments in the Tadpole Ridge Tuff. The present 31.4 Ma age for the Tadpole Ridge Tuff (upper member) should be considered tentative until more data are obtained. However, this age agrees well with K-Ar data (three dates between 31.6 and 31.9 Ma; Marvin et al., 1987) and is consistent with stratigraphic relationships of the outflow sheet, which is underlain by 31.7 Ma Caballo Blanco Tuff and overlain by 29.0 Ma Davis Canyon Tuff.

Episode 3 (29.0 to 27.4 Ma)

Following a 2.4 m.y. ignimbrite hiatus, the largest pulse of Mogollon-Datil ignimbrite activity began at 29.0 Ma. Within a span of 1.6 m.y., nine major regional ignimbrites and at least 11 subregional to local units were erupted, totalling more than >6000 km³ in volume (Table 1). The major units, primarily high-silica rhyolites, were erupted from two clusters of cauldrons, one located in the Mogollon Mountains near the western edge of the field and the second in the San Mateo and Magdalena Mountains west of Socorro. The distribution and source cauldrons of Episode 3 ignimbrites are relatively well understood.

Subregional stratigraphic sequences of major units around the two cauldron clusters were established by detailed mapping prior to this study (Osburn and Chapin, 1983a; Ratté et al., 1984). $^{40}Ar/^{39}Ar$ and paleomagnetic data have helped to constrain eruptive timing of the Socorro and Mogollon centers, in part by identifying stratigraphic relationships of distal-fades ignimbrites in the overlap area between the two centers. These techniques have also helped to clarify understanding of several more locally distributed units.

Davis Canyon Tuff, 29.0 Ma-The first major regional ignimbrite erupted in Episode 3 is the Davis Canyon Tuff (Fig. 20), which extends over a 10,500 km² area of the southwestern Mogollon-Datil field. Two $^{40}Ar/^{39}Ar$ plateau ages from the northern edge of this crystal-poor, high-silica rhyolitic outflow sheet yield a mean age of 29.0 Ma, and site-mean TRM directions from six sites are well-grouped, supporting the distribution mapped by Ratté et al. (1984). The source cauldron for the Davis Canyon Tuff is not known, although its distribution is consistent with a source in either the Bursum or Gila Cliff Dwellings cauldron areas.

The unit-mean direction of the Davis Canyon Tuff, although near the expected time-averaged reverse field direction, is useful for distinguishing this unit from the lithologically similar Vicks Peak Tuff, which shows lower paleomagnetic inclination (Fig. 22). This distinction is particularly important in the overlap area of the two ignimbrites, where both were formerly mapped as tuff of Tularosa Canyon (Rhodes and Smith, 1976). The Davis Canyon Tuff represents the first of several reverse polarity units erupted between 29.0 and 28.0 Ma (Table 1).

La Jencia Tuff, 28.9 Ma-The La Jencia Tuff is a well-mapped, crystal-poor, high-silica rhyolitic ignimbrite erupted from the Sawmill-Magdalena cauldron west of Socorro (Fig. 21; Osburn and Chapin, 1983a). Early $^{40}Ar/^{39}Ar$ plateau ages of 28.9 Ma (Kedzie, 1984) were instrumental in recognizing the 3.2 m.y. eruptive hiatus between this unit and the underlying 32.1 Ma Hells Mesa Tuff, whereas previous K-Ar data suggested a La Jencia age near 31 Ma (Chapin et al., 1975).

Paleomagnetic site-mean TRM directions are well-grouped in the La Jencia Tuff, and, like the Davis Canyon Tuff, show a unit-mean direction similar to the expected time-averaged reverse polarity field. This TRM direction provides a useful criteria for distinguishing between La Jencia and Vicks Peak Tuffs (Figs. 5, 21, 22). Although the La Jencia and Davis Canyon Tuffs are paleomagnetically indistinguishable, they have not been found to overlap.

Paleomagnetic and $^{40}Ar/^{39}Ar$ data from the La Jencia Tuff support its previous mapped extent, but suggest that the unit extends even further to the southwest, as much as 80 km from its cauldron margin. Identified distal fringes of the La Jencia Tuff include outcrops along the south edge of the Plains of San Agustin (sites 146 and 372, Fig. 21) and in the central Black Range (site 111, Fig. 21).

Vicks Peak Tuff, 28.6 Ma-Vicks Peak Tuff, a crystal-poor, high-silica rhyolitic ignimbrite erupted at 28.6 Ma from the Nogal Canyon cauldron in the southern San Mateo Mountains (Fig. 22), is the most widely distributed ignimbrite in the northern Mogollon-Datil volcanic field. Its 200 km maximum known lateral dimension (Table 1) is exceeded only by Kneeling Nun and Box Canyon Tuffs.

Site-mean TRM directions for this unit are generally well grouped and show a distinctively shallow inclination (D=165°, I=-27°). A few sites show anomalous declinations, primarily due to fault-block rotations in highly extended areas (Fig. 22; McIntosh, 1989, in press). Three $^{40}Ar/^{39}Ar$ age spectra yield a mean age of 28.56 ±.06 Ma. Paleomagnetic and $^{40}Ar/^{39}Ar$ data indicate that tuff 7 of the Bell Top Formation (Clemons, 1976) and the upper part of the tuff of Tularosa Canyon (Rhodes and Smith, 1976) actually represent thin, unwelded distal facies of Vicks Peak Tuff (Fig. 22). This correlation provides a useful common stratigraphic tie among the ignimbrite sequences in the Socorro, Mogollon, and Las Cruces areas (Figs. 2, 3).

Small-volume tuffs of the Black Range, 29.0 to 28.1 Ma-Interlayered with regional ignimbrites in the central Black Range are several local, small-volume ignimbrites apparently produced by persistent rhyolite dome/flow activity between 29.0 and 28.1 Ma (Table 1, Figs. 3, 23, 24). Most of these units are poorly to moderately welded and rich in rhyolite lava lithic fragments; many are directly overlain by rhyolitic lava with similar phenocryst assemblages (Woodard, 1982; Eggleston, 1982).

The eruption of these units apparently spanned a normalto-reverse polarity reversal near 29.0 Ma. The oldest units (tuffs of Monument Canyon and Little Mineral Creek, 29.0 Ma) show normal polarity and are immediately overlain by a sequence of reverse polarity units [Stiver Canyon Tuff, tuff of Mud Hole (29.1 Ma), La Jencia Tuff (28.9 Ma regional unit discussed above), and tuff of Lookout Mountain (28.7 Ma, a.k.a. tuff of Diamond Creek, Woodard, 1982)].

A second pulse of Black Range dome eruptions, termed the Taylor Creek Rhyolite, occurred near 28.1 Ma (Duffield et al., 1987; Dalrymple and Duffield, 1988). These domes and associated ignimbrites all show reverse polarity (Appendix 3; McIntosh, 1989). One subregional dome-derived ignimbrite, the tuff of Garda Camp, was studied in some detail (Fig. 24). Paleomagnetic site-mean directions from the tuff of Garcia Camp are tightly grouped (Fig. 24), indicating that this multi-cooling-unit ignimbrite was erupted over a brief interval of time. A single $^{40}Ar/^{39}Ar$ plateau age of 28.10 Ma was determined, which compares to published mean $^{40}Ar/^{39}Ar$ laser-fusion ages of 28.21 ±.04 Ma for sanidines from tuff of Garcia Camp (Dalrymple and Duffield, 1988). The difference in ages is discussed by McIntosh (1989) and McIntosh et al. (1990).

Shelly Peak Tuff, 28.1 Ma-Shelly Peak Tuff is a distinctive red-colored, plagioclase-biotite, low-silica rhyolitic ignimbrite erupted about 28.1 Ma from somewhere in the Mogollon eruptive center. Paleomagnetic data from this widespread unit are moderately well-grouped in a shallow-inclination southerly direction (Fig. 25), although some of the sites show slightly anomalous directions and demagnetization behavior indicative of CRM components (Fig. 25; McIntosh, 1989, in press). These remanence directions are sufficient to differentiate Shelly Peak Tuff from lithologically similar Tadpole Ridge Tuff (Fig. 19), but are not helpful in distinguishing between Shelly Peak Tuff and paleomagnetically similar Apache Springs Tuff (Fig. 25).

The age of the Shelly Peak Tuff is tightly bracketed at 28.1 Ma by the underlying tuff of Garcia Camp (28.1 Ma) and overlying Bloodgood Canyon Tuff (28.1 Ma). A single $^{40}Ar/^{39}Ar$ plateau age determined for the Shelly Peak Tuff is 28.52 ±.08 Ma; this anomalously old age probably reflects contamination of the sanidine-poor Shelly Peak Tuff by

older lithic or xenocrystic feldspar (McIntosh, 1989; McIntosh et al., 1990).

Bloodgood Canyon Tuff and related units, 28.1 Ma-The 15,000 km^2, 1000 lore Bloodgood Canyon Tuff (Fig. 26) is the most widely exposed ignimbrite in the southern part of the volcanic field (Ratté et al., 1984). Paleomagnetic data from throughout the extent of this high-silica rhyolitic outflow sheet show distinctive shallow-inclination, southeasterly TRM directions. Similarly, $^{40}Ar/^{39}Ar$ plateau ages from seven widely separated samples are nearly identical, ranging from 27.99 to 28.11 Ma and averaging 28.05 ±.04 Ma. These data strongly support the conclusion that the Bloodgood Canyon Tuff is a single large outflow sheet (Ratté et al., 1984) and oppose the interpretation that exposures north of the Bursum cauldron represent a different eruptive unit, termed the Railroad Canyon Tuff (Elston et al., 1973; Rhodes and Smith, 1976; Elston, 1984). Furthermore, the TRM direction of the Bloodgood Canyon Tuff is sufficiently distinctive to reliably distinguish this unit from four other lithologically similar ignimbrites in the northern part of the field (tuff of Triangle C Ranch, Lemitar Tuff, South Canyon Tuff, tuff of Turkey Springs; Figs. 5, 26, 27, 29, 30, 31).

$^{40}Ar/^{39}Ar$ and paleomagnetic data are also consistent with the interpretation that the 1200 km^3 Apache Springs Tuff represents the intracauldron-facies equivalent of the Bloodgood Canyon Tuff (Ratté et al., 1984). The single $^{40}Ar/^{39}Ar$ plateau age (27.98 Ma) is statistically indistinguishable from the mean of seven Bloodgood Canyon Tuff samples, and site-mean TRM directions from two Apache Springs sites are within 10° of the unit-mean direction of the Bloodgood Canyon Tuff (Fig. 26).

In addition to Bloodgood Canyon and Apache Springs Tuffs, two less voluminous associated units were also investigated. The tuff of Diablo Range is the precursor ignimbrite for an extensive sequence of rhyolitic lavas that is stratigraphically between the Shelly Peak and Bloodgood Canyon Tuffs (Fig. 3). Two sites from this unit (475 and 436, Fig. 22) yield reverse polarity and a 28.1 Ma age identical to that of the overlying Bloodgood Canyon Tuff (Table 1).

North of the Bursum cauldron, the Bloodgood Canyon Tuff is overlain by the poorly welded but lithologically similar tuff of Triangle C Ranch (Figs. 3, 27) (Ratté, 1989a). The one $^{40}Ar/^{39}Ar$ plateau age from this unit (28.05 Ma, Table 1) is also identical to the mean Bloodgood Canyon age, but the six site-mean TRM directions are well-grouped in a *normal* polarity direction. Apparently, the tuff of Triangle C Ranch was erupted soon after a polarity reversal that itself occurred soon after eruption of the Bloodgood Canyon Tuff. The Bloodgood Canyon Tuff and tuff of Triangle C Ranch provide a good example of a situation in which the combination of $^{40}Ar/^{39}Ar$ dating and paleomagnetic correlation provides higher resolution than $^{40}Ar/^{39}Ar$ dating alone.

Lemitar Tuff and tuff of Caronita Canyon, 28.0 Ma-The Lemitar Tuff is a well-mapped 28.0 Ma regional ignimbrite in the Socorro area. Although no source cauldron has been identified for this unit, thickness and distribution (Fig. 29) point to a source in the west-central Magdalena Mountains. About half of the sites in this unit show tightly grouped site-mean TRM directions, but the remaining sites are somewhat scattered (Fig. 29). For the most part these anomalous site-mean directions are related to block rotations in the highly extended Lemitar Mountains and Joyita Hills.

The Lemitar Tuff is underlain by the strongly zoned tuff of Caronita Canyon, formerly interpreted as part of the moat-fill sequence emplaced after eruption of the 28.9 Ma La Jencia Tuff (Osburn and Chapin, 1983b). Normal polarity and an $^{40}Ar/^{39}Ar$ age of 28.0 Ma (Table 1, Fig. 28) suggest instead that the tuff of Caronita Canyon was a precursor unit erupted slightly before the Lemitar Tuff.

Tuff of Walking X Canyon, 27.6 Ma-The youngest ignimbrite at the southern edge of the Mogollon-Datil volcanic field is the tuff of Walking X Canyon (Fig. 23; Hedlund, 1978). This 27.6 Ma, normal-polarity ignimbrite probably represents the distal fades of a large ignimbrite erupted from a source south of the Mogollon-Datil field.

South Canyon Tuff, 27.4 Ma-The 27.4 Ma South Canyon Tuff is the youngest major, widespread ignimbrite in the northeastern Mogollon-Datil volcanic field. This well-mapped high-silica rhyolite was erupted from the Mt. Withington cauldron, a "trapdoor" cauldron hinged along its southern edge (Fig. 30). Both outflow and intracauldron fades are well exposed and were extensively sampled (total of 43 sites). $^{40}Ar/^{39}Ar$ plateau ages from samples of both facies range from 27.28 to 27.40 Ma. Site-mean paleomagnetic data from outflow and thinner (<500 m) southern intracauldron fades are well-grouped in an unusual shallow, southwesterly direction that is distinct from all other Mogollon-Datil ignimbrites (Figs. 5, 30b, c). This distinctive TRM direction, together with $^{40}Ar/^{39}Ar$ data, has been used to identify the 1.5 m thick unwelded distal fringe of the South Canyon Tuff outflow sheet in the central Black Range (site 258 in Fig. 30).

Site-mean TRM directions from thicker (500-1500 m) northern intracauldron-fades sections (Fig. 30d) show large between-site scatter ($a_{,,}$=12.7°) and a mean direction (D=187, 1=46) which is offset toward the expected time-averaged field direction (D=170.5, I=-50), relative to the mean direction of the outflow fades (Fig. 30b, Table 1). The preferred explanation for the non-uniform magnetization of the thick intracauldron fades is that it reflects paleosecular variation which occurred during protracted cooling (Reynolds et al., 1986; Wells and Hillhouse, 1989). Alternatively, the scattered site-mean directions might reflect non-horizontality of pumice foliations during initial cooling, or sub-blocking-temperature welding, flowage, or compaction (Rosenbaum, 1986). These possibilities are discussed in detail by McIntosh (1989, in press). In any case, these results support the conclusion that the use of paleomagnetism as a correlation criterion is less effective in thick intracauldron facies than in outflow sheets.

Tuff of Slash Ranch, 26 Ma?-The tuff of Slash Ranch represents a poorly welded, zeolitized, but prominently exposed multi-cooling-unit ignimbrite which lies at or near the top of the Tertiary volcanic section near the center of the volcanic field (Fig. 31). This unit is apparently correlative with the tuff of Jordan Canyon (Fig. 31) and is probably related to eruption of a rhyolitic dome, although no vent has been identified. This unit shows an unusual south and downward TRM direction (Table 1, Fig. 31) which may reflect eruption during a geomagnetic excursion or polarity transition.

A single $^{40}Ar/^{39}Ar$ age of 26.1 Ma has been determined for the tuff of Slash Ranch. This age determination is not considered reliable, however, because of zeolitization and

abundant non-volcanic(?) cross-twinned feldspar crystals. Because of this uncertainty and the limited extent (22 km) of the unit, the tuff of Slash Ranch was not used to define the end of eruptive episode 3.

Episode 4 (24.3 Ma)

Tuff of Turkey Springs, 24.3 Ma—After a 2.9 m.y. hiatus, Mogollon-Datil ignimbrite activity concluded at 24.3 Ma with the eruption of a single, high-silica rhyolitic ignimbrite, the tuff of Turkey Springs (Ferguson, 1986). Prior to paleomagnetic analysis, this moderately extensive outflow sheet (Fig. 32) was not recognized as a stratigraphically distinct unit, but was instead incorrectly mapped as either South Canyon Tuff (bonze, 1980) or Railroad Canyon Tuff (Fodor, 1976).

Paleomagnetically identified tuff of Turkey Springs (Fig. 32) extends over a 50 x 70 km area centered on the northern San Mateo Mountains. All but two of the site-mean directions from this unit cluster tightly about the unit-mean TRM direction (D=176, 1=-52). Although the unit-mean TRM direction is only 4° from the time-averaged Oligocene field, it is distinctly different from the four other lithologically similar ignimbrites with which the tuff of Turkey Springs has been, or might be, confused (Figs. 5, 26, 27, 29, 30). Two of the sites thought to be tuff of Turkey Springs (424 and 364 in Fig. 32) fall almost equidistant from the unit-mean TRM directions of tuff of Turkey Springs and South Canyon Tuff. These anomalous site-mean directions probably reflect errors in assessment of the paleohorizontal (McIntosh, 1989, in press) and serve to emphasize the need to support paleomagnetic correlations with all other available criteria.

Two $^{40}Ar/^{39}Ar$ plateau ages for the tuff of Turkey Springs average 24.33 Ma (Figs. 4, 32, Table 1), 2.9 m.y. younger than any associated underlying ignimbrites. No source has yet been identified for the tuff of Turkey Springs, but the gross distribution of the outflow sheet and an underlying pumice-fall deposit suggest a vent area, perhaps a small cauldron, in the east-central San Mateo Mountains, an area not yet mapped in detail.

Summary

$^{40}Ar/^{39}Ar$ plateau ages and paleomagnetic data from Mogollon-Datil ignimbrites have been utilized to accurately correlate several units over distances of 40 to 200 km, thus providing reliable ties between previously established stratigraphic sequences. Subregional stratigraphic sequences have been assembled to yield an integrated time-stratigraphic framework for the entire volcanic field (Figs. 2, 3). This stratigraphic framework helps to constrain the timing and distribution of Mogollon-Datil ignimbrite activity and furthermore provides significant age constraints for sequences of mafic and silicic lavas and sedimentary rocks for which precise ages have not been, or cannot be, measured.

Mogollon-Datil ignimbrite activity ranged from 36.2 to 24.3 Ma and was highly episodic, being confined to four brief (<2.6 m.y.) eruptive intervals separated by 1.5 to 3 m.y. hiatuses. Cauldron-forming activity originated in the 36.1-35.4 Organ cauldron area and subsequently migrated north and west. Rhyolitic activity was most intense between 29 and 27.3 Ma; this interval is characterized by alternating ignimbrite eruptions from the Mogollon and Socorro cauldron complexes, punctuated by two brief intervals (29.0-28.7 Ma and 28.1 Ma) of extensive rhyolitic dome and flow eruptions in the central Black Range area between the two cauldron complexes.

Figures 6 through 32 start on next page.

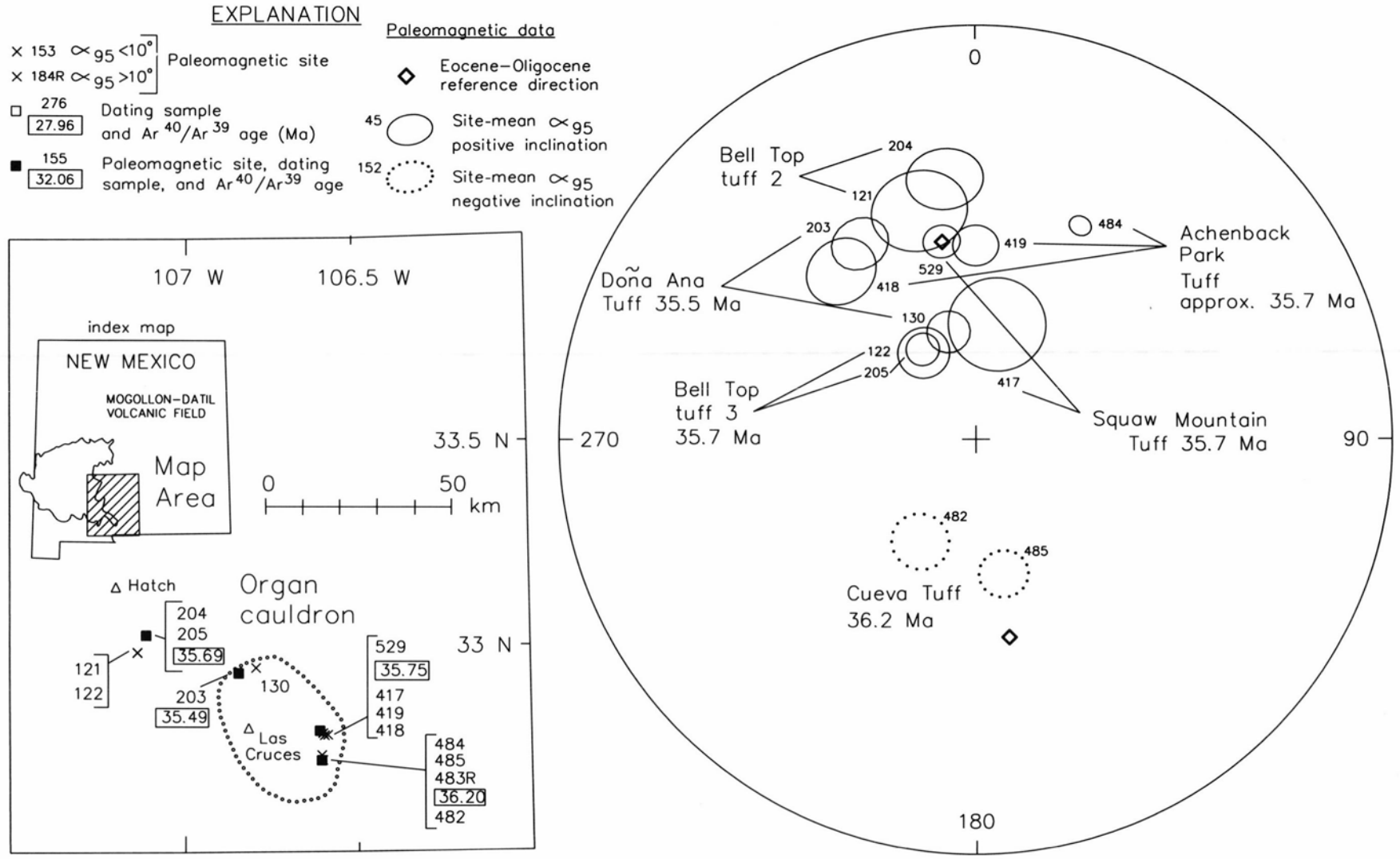

Organ cauldron and related tuffs 36.2–35.5 Ma

FIGURE 6—Organ and Doña Ana intracauldron ignimbrites and possible outflow facies correlatives. Site locations, $^{40}Ar/^{39}Ar$ plateau ages, site-mean paleomagnetic data, and inferred source cauldron margin. In this and following figures, stereographic projections do not show site-mean paleomagnetic directions which were rejected from unit-mean calculations because $\alpha_{95} > 10°$ (site labelled "R" on location map).

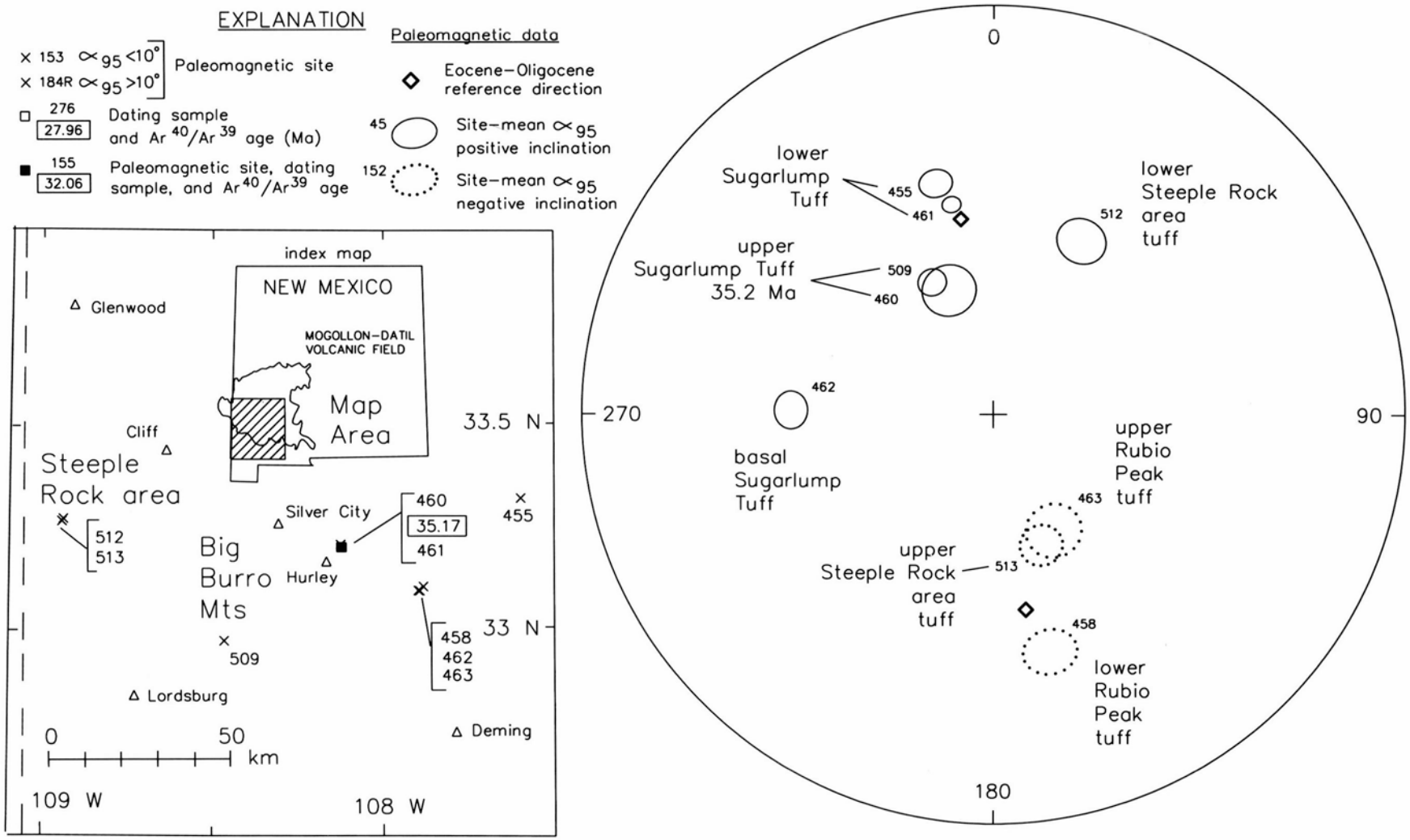

Sugarlump, Rubio Peak, and Steeple Rock area tuffs

FIGURE 7—36 to 35 Ma outflow ignimbrites in the southern Mogollon–Datil volcanic field: site locations, $^{40}Ar/^{39}Ar$ plateau ages, and site-mean paleomagnetic data.

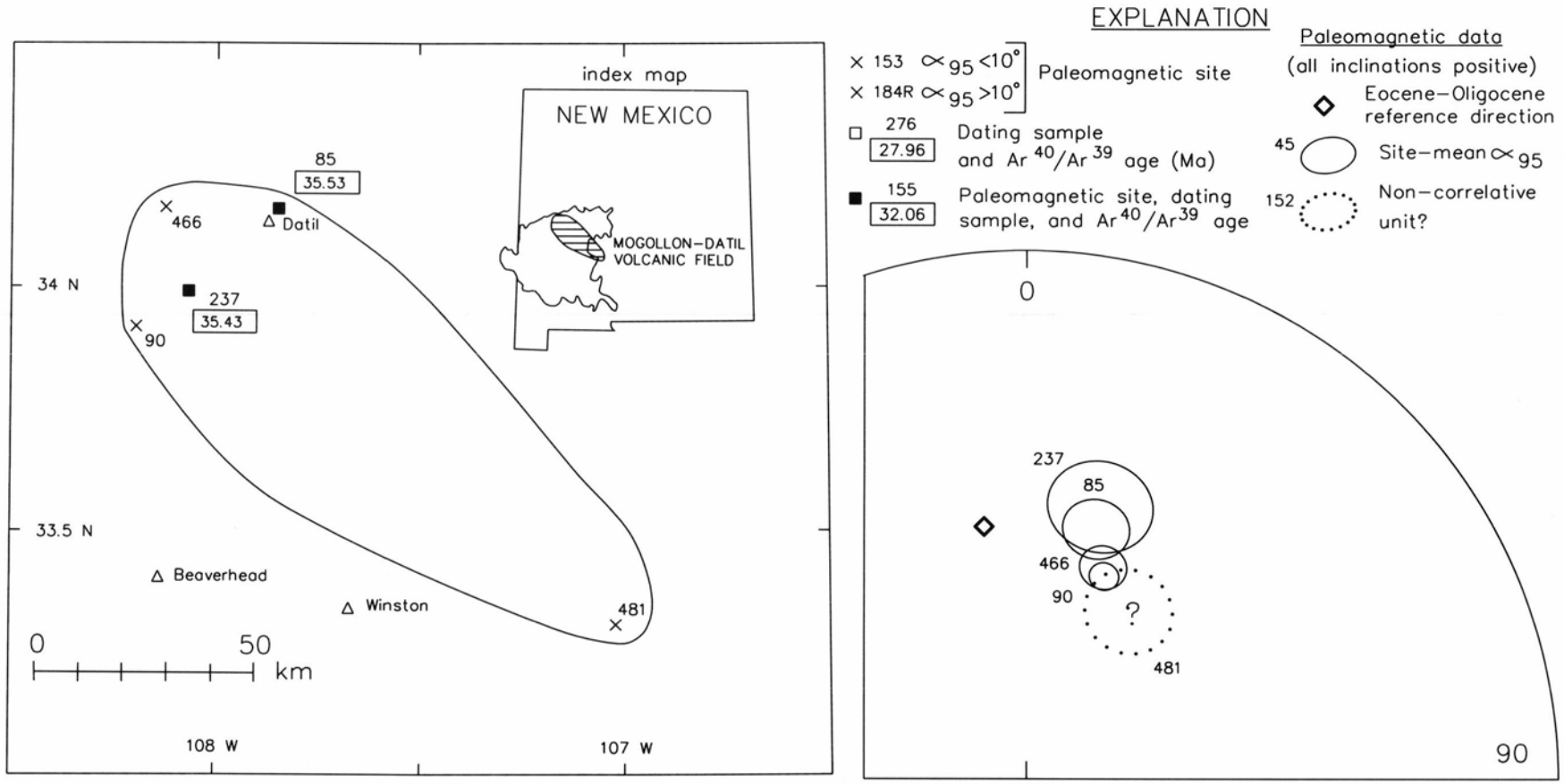

Datil Well Tuff 35.5 Ma

FIGURE 8—Datil Well Tuff. Site locations, areal extent, $^{40}Ar/^{39}Ar$ plateau ages, and site-mean paleomagnetic data. Correlation between Datil Well Tuff and unit at site 481 is tentative.

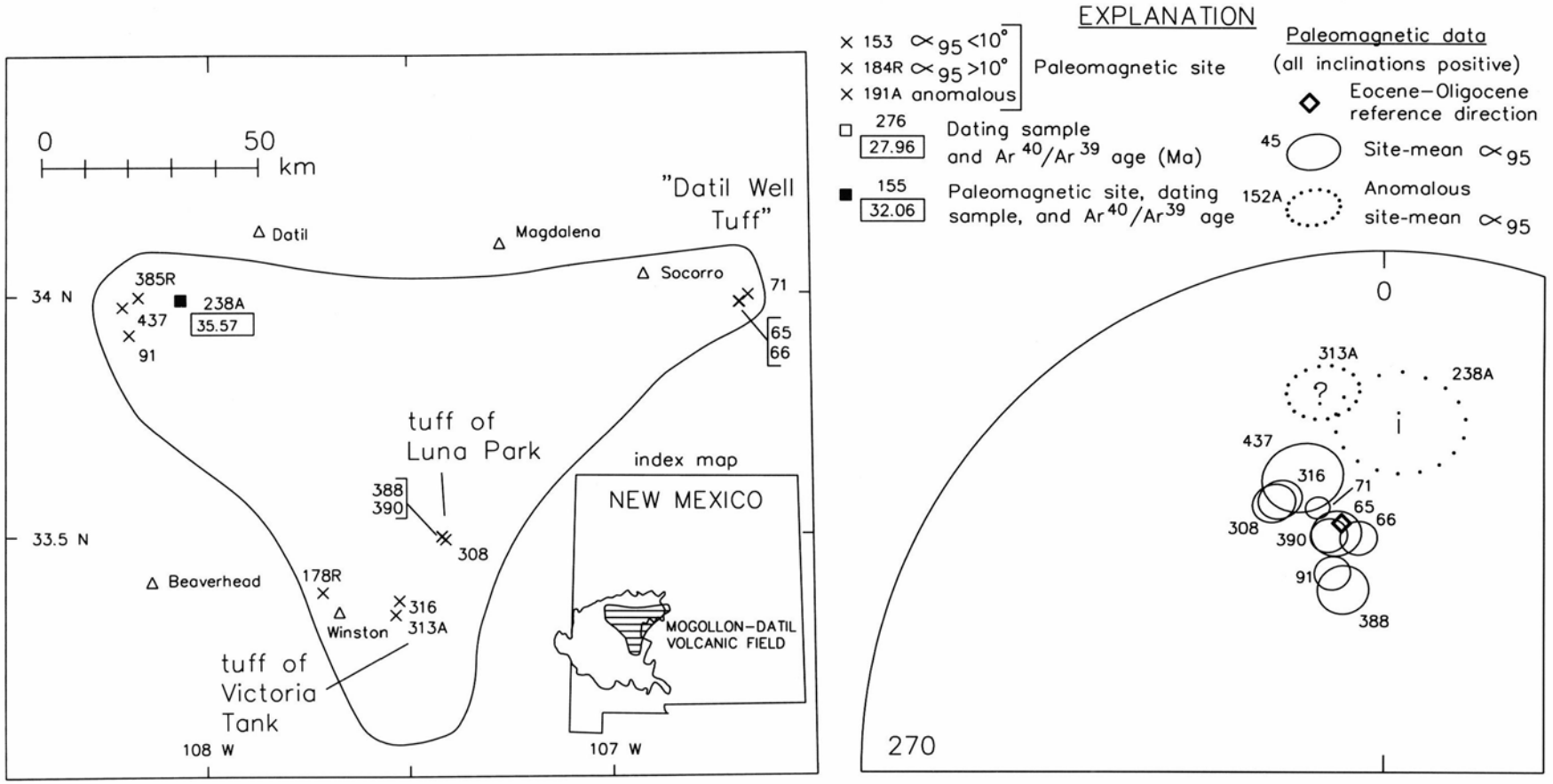

tuff of Farr Ranch 35.6 Ma

FIGURE 9—Tuff of Farr Ranch. Site locations, areal extent, $^{40}Ar/^{39}Ar$ plateau ages, and site-mean paleomagnetic data. Correlations with tuff of Luna Park and tuff of Victoria Tank are based mainly on paleomagnetic data and are considered tentative. Letters suggest reasons for anomalous site-mean directions (dotted ellipses, differing by more than 15° from the unit-mean direction): i=unremoved IRM, ?=possible incorrect unit identification.

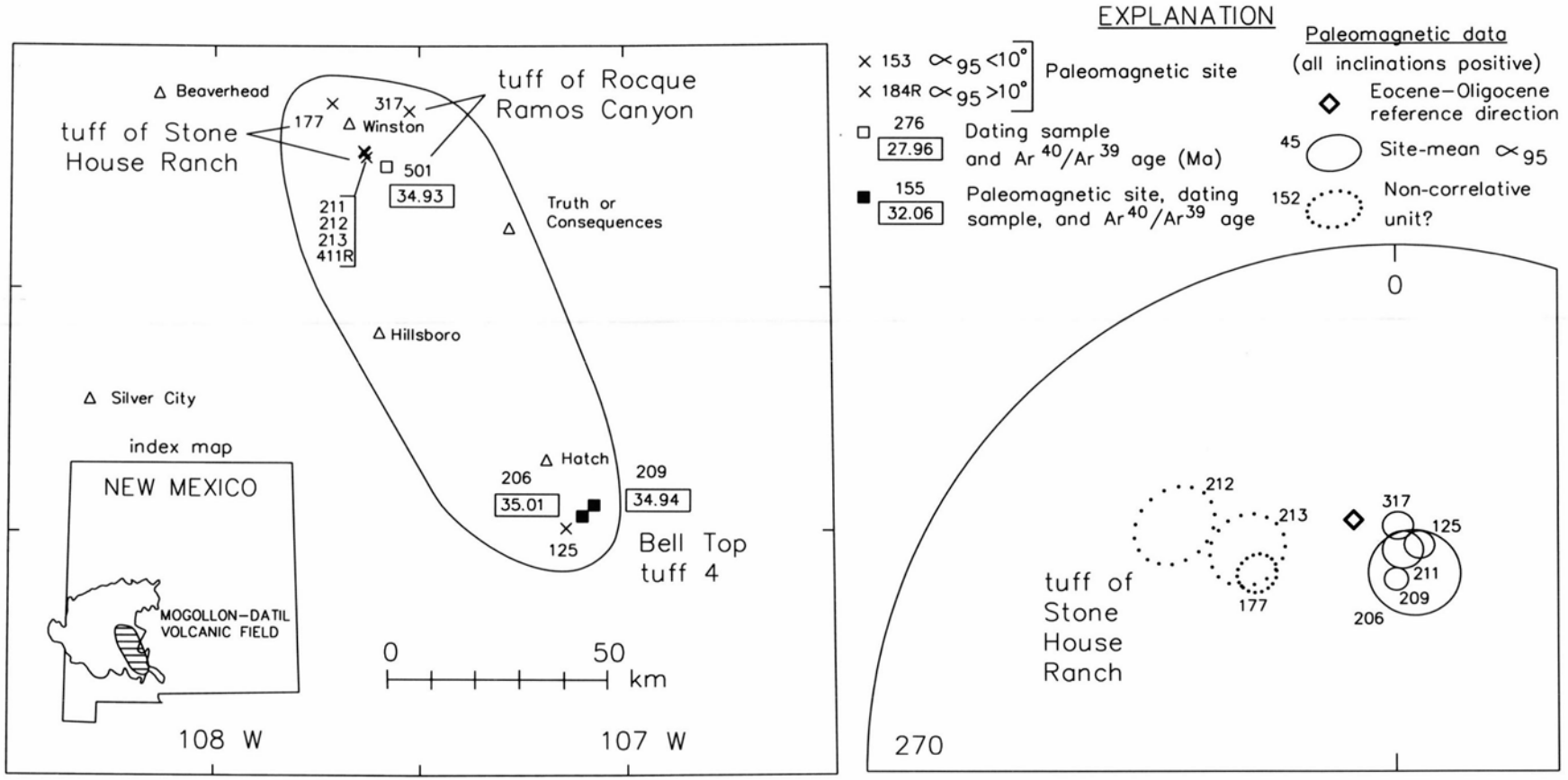

Bell Top tuff 4 34.9 Ma

FIGURE 10—Bell Top tuff 4 and tuff of Stone House Ranch. Site locations, areal extent, $^{40}Ar/^{39}Ar$ plateau ages, and site-mean paleomagnetic data. Correlation of Bell Top tuff 4 with tuff of Rocque Ramos Canyon is well-supported by distinctive site-mean paleomagnetic directions and $^{40}Ar/^{39}Ar$ ages. Paleomagnetic data indicate that these two units do not correlate with the tuff of Stone House Ranch (dotted ellipses).

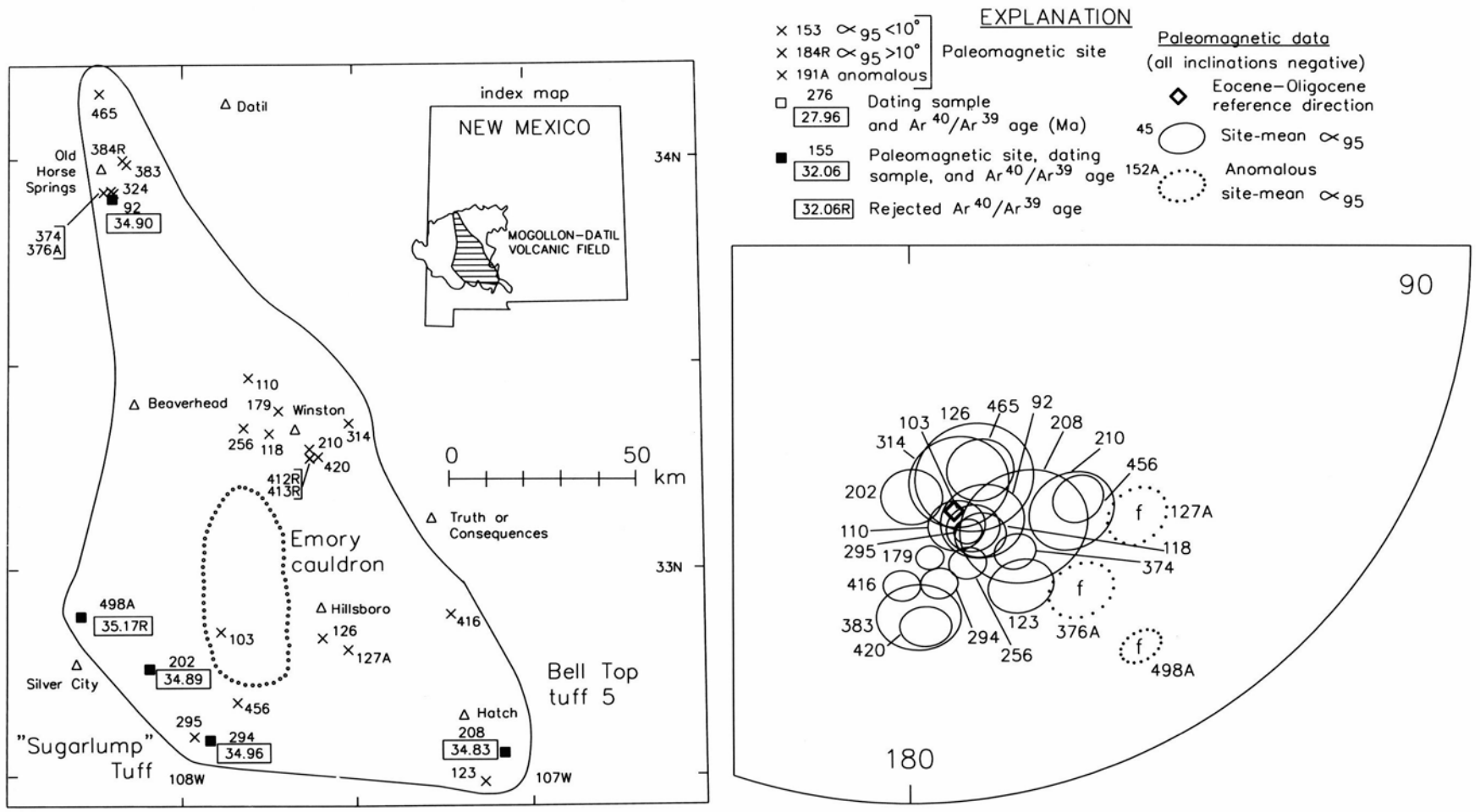

FIGURE 11—Kneeling Nun Tuff. Site locations, areal extent, $^{40}Ar/^{39}Ar$ plateau ages, and site-mean paleomagnetic data. These data indicate that the outflow sheet is more extensive than previously believed and includes Bell Top tuff 5 (Clemons, 1976). The Emory cauldron is well established as the source of the Kneeling Nun Tuff (Elston et al., 1975). Anomalous site-mean directions (dotted ellipses lettered f) probably reflect incorrectly determined paleohorizontal in areas of local structural complexity. Paleomagnetic direction from site 324 is excluded from stereographic projection because $\alpha_{95} > 8.5°$.

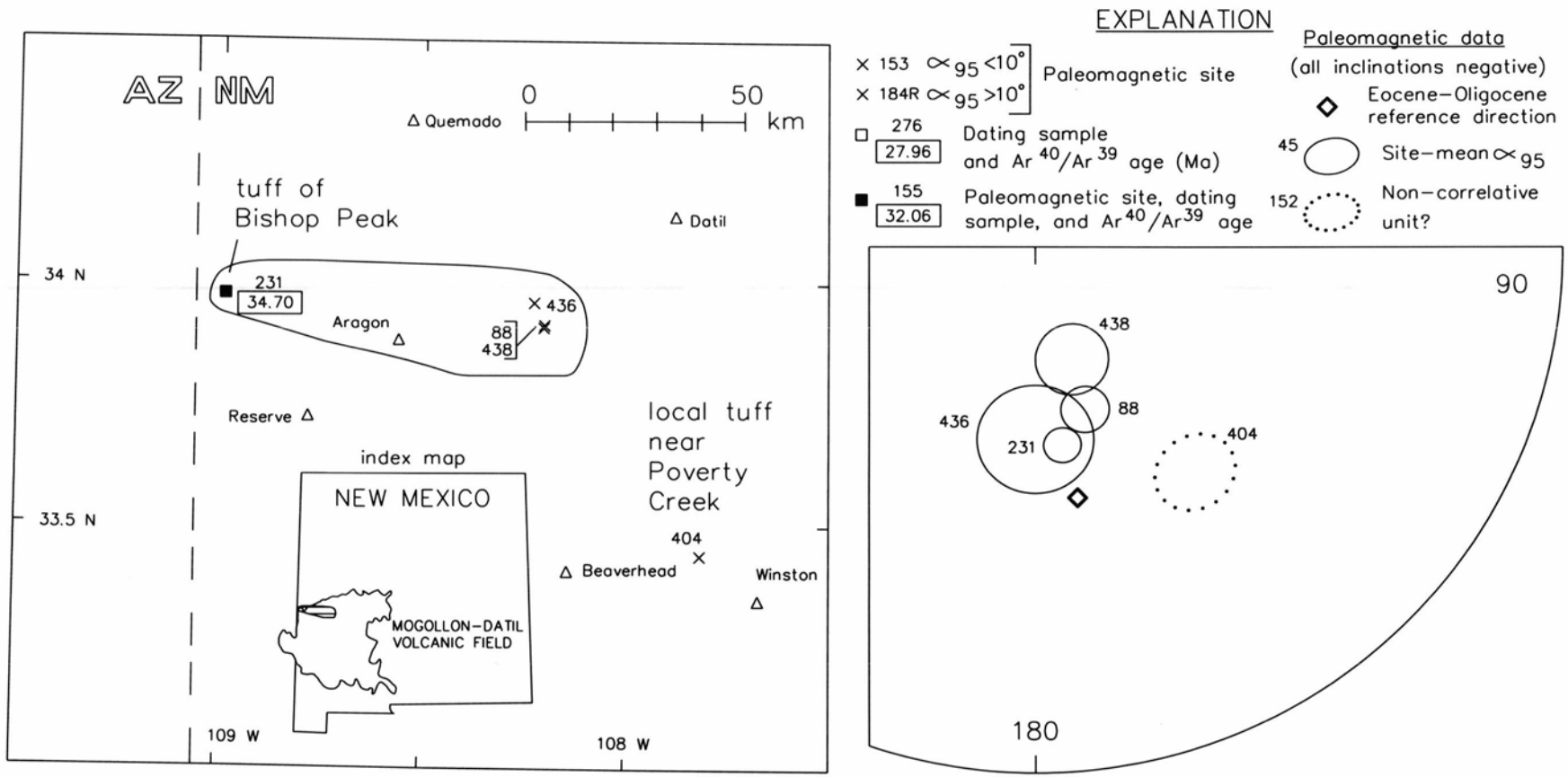

tuff of Lebya Well 34.7 Ma

FIGURE 12—Tuff of Lebya Well. Site locations, areal extent, $^{40}Ar/^{39}Ar$ plateau ages, and site-mean paleomagnetic data. Steep site-mean remanence directions support correlation with 34.70 Ma tuff of Bishop Peak, but oppose correlation with an ignimbrite in the same stratigraphic position which is exposed near Poverty Creek (site 404).

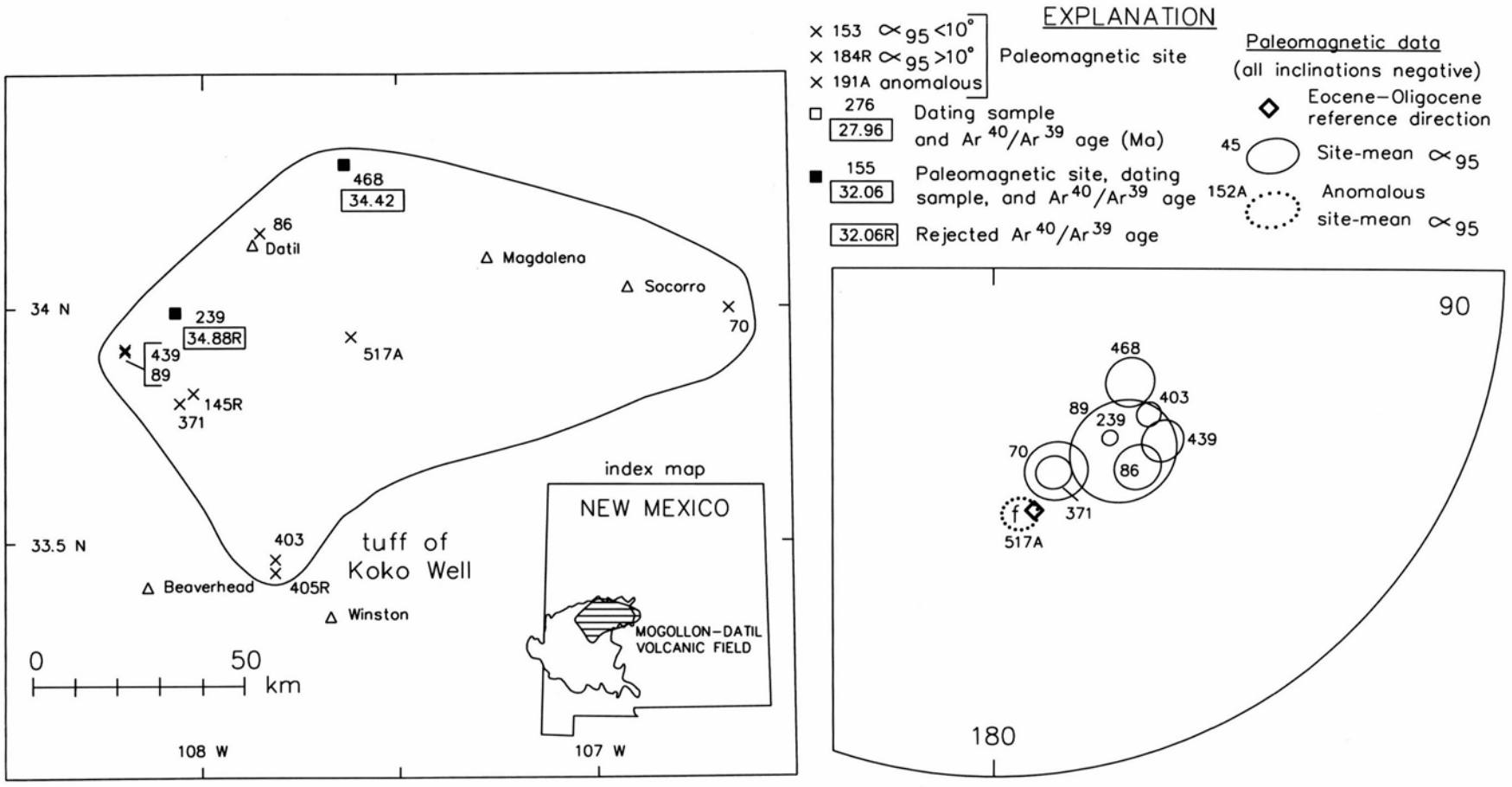

Rock House Canyon Tuff 34.4 Ma

FIGURE 13—Rock House Canyon Tuff. Site locations, areal extent, $^{40}Ar/^{39}Ar$ plateau ages, and site-mean paleomagnetic data. The anomalous direction of site 517 (dotted ellipse lettered f) probably reflects incorrectly determined paleohorizontal in an area of local structural complexity.

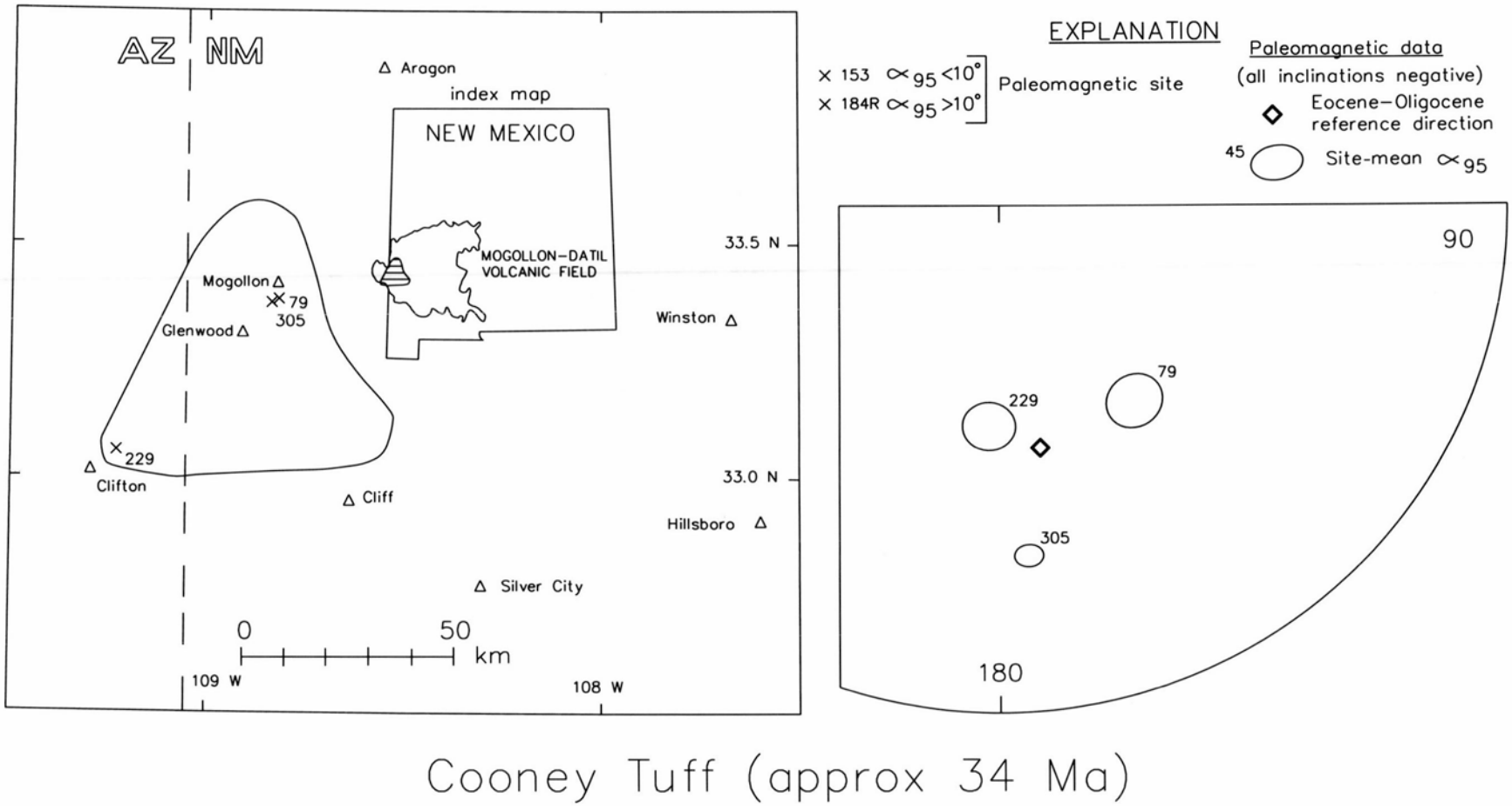

Cooney Tuff (approx 34 Ma)

FIGURE 14—Cooney Tuff. Site locations, areal extent, and site-mean paleomagnetic data. Poorly grouped site-mean directions suggest that eruption of this multi-cooling-unit formation spanned a relatively long time period. No $^{40}Ar/^{39}Ar$ ages have been obtained from this sanidine-poor unit.

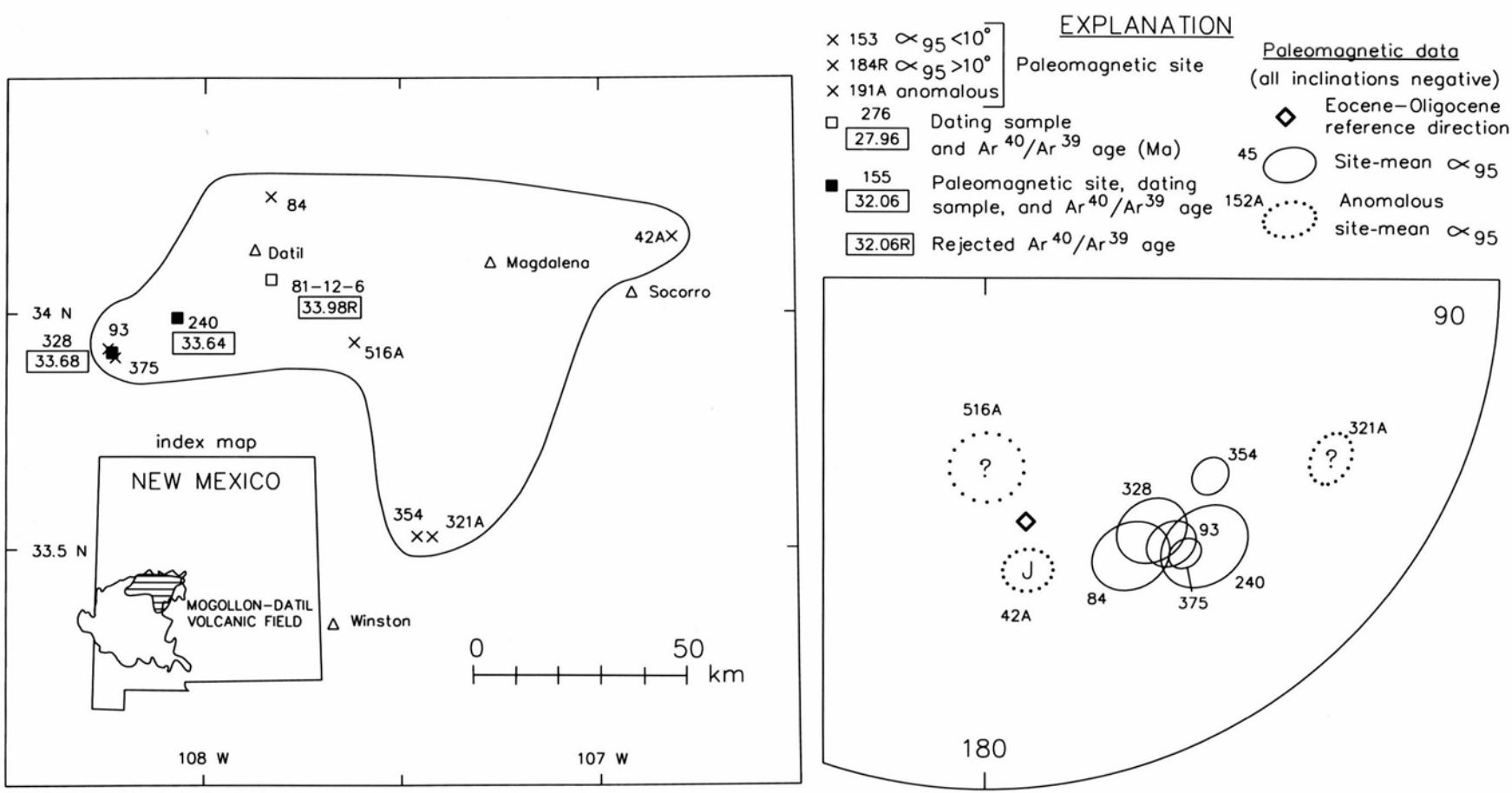

Blue Canyon Tuff 33.7 Ma

FIGURE 15—Blue Canyon Tuff. Site locations, areal extent, $^{40}Ar/^{39}Ar$ plateau ages, and site-mean paleomagnetic data. Letters suggest reasons for anomalous site-mean directions (dotted ellipses, differing by more than 15° from the unit-mean direction): ?=possible incorrect unit identification, J=tectonic rotations in the highly extended Joyita Hills area.

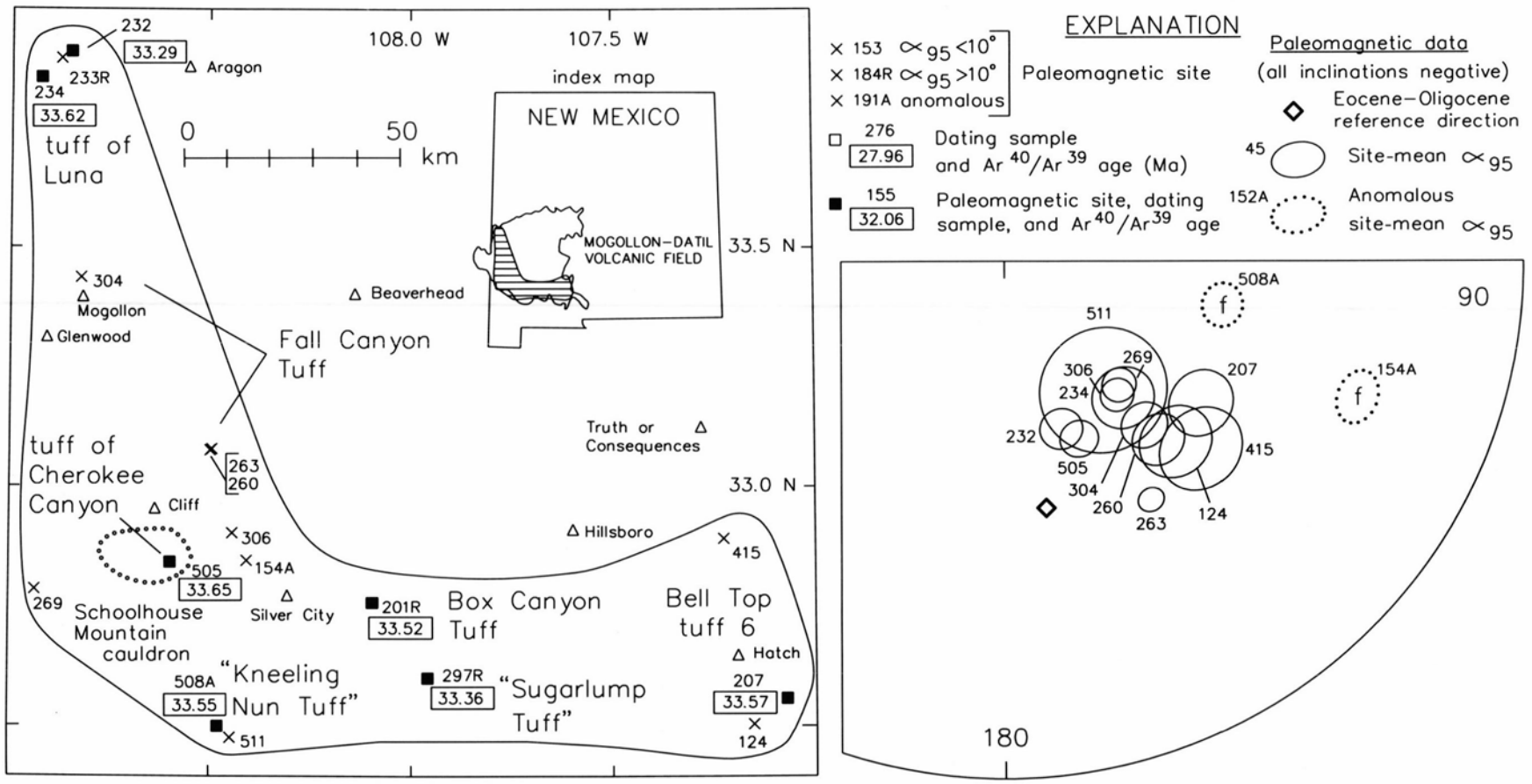

Box Canyon Tuff 33.5 Ma

FIGURE 16—Box Canyon Tuff. Site locations, areal extent, $^{40}Ar/^{39}Ar$ plateau ages, and site-mean paleomagnetic data. These data suggest a much larger large areal extent for this unit than was previously known (e.g. Elston, 1957). The probable source cauldron for this unit is the Schoolhouse Mountain cauldron (Wahl, 1980). Anomalous site-mean directions (dotted ellipses lettered f) probably reflect incorrectly determined paleohorizontal in areas of local structural complexity.

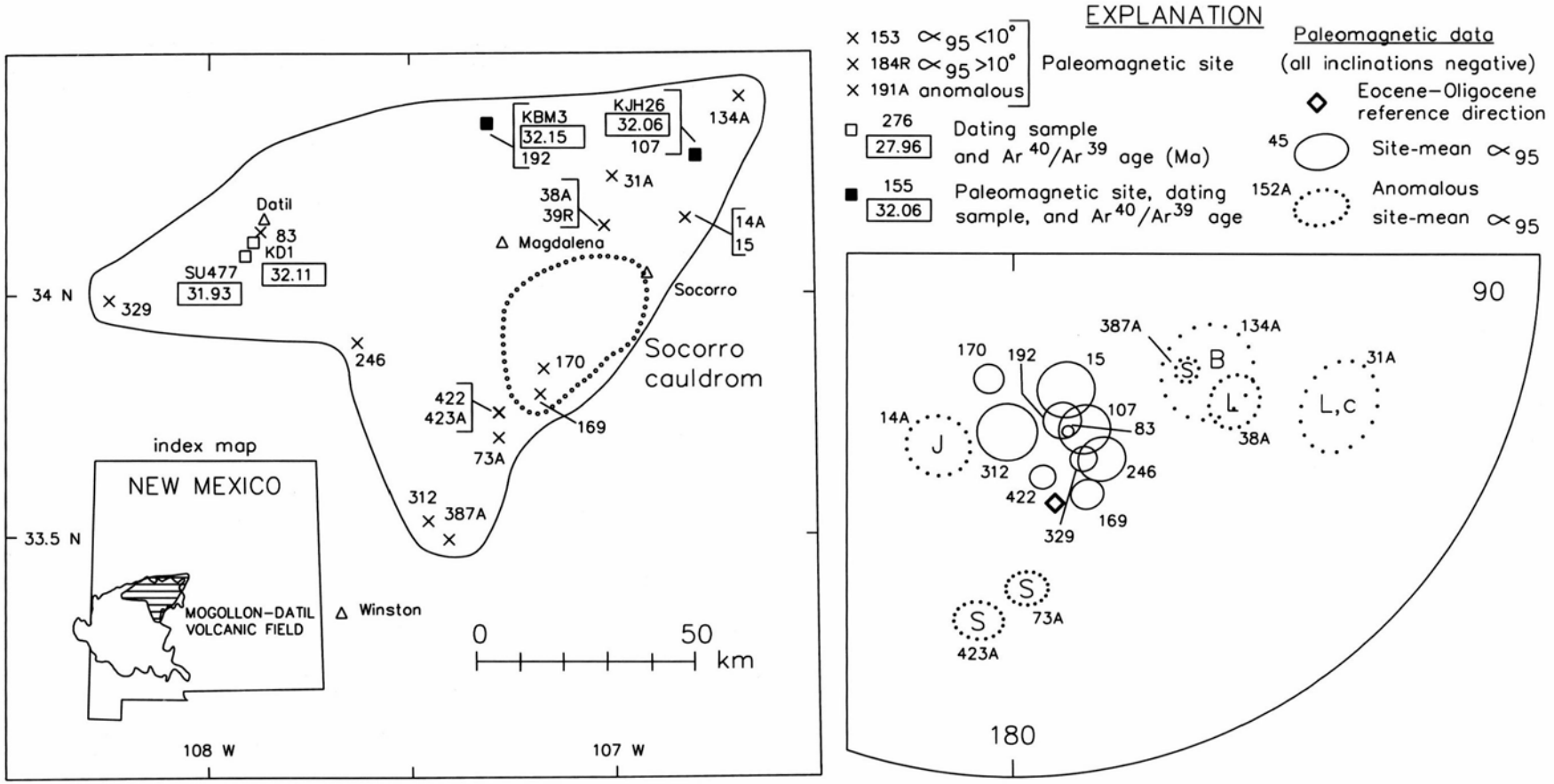

Hells Mesa Tuff 32.1 Ma

FIGURE 17—Hells Mesa Tuff. Site locations, areal extent, $^{40}Ar/^{39}Ar$ plateau ages, and site-mean paleomagnetic data. The Socorro cauldron is well-established as the source of Hells Mesa Tuff (Osburn and Chapin, 1983b). The large fraction of anomalous sites reflects tectonic rotations in highly extended areas (B=Black Butte, J=Joyita Hills, L=Lemitar Mountains, S=San Mateo Mountains). The anomalous direction of site 31 (dotted ellipse labelled c) may also reflect unremoved components of chemical remanence.

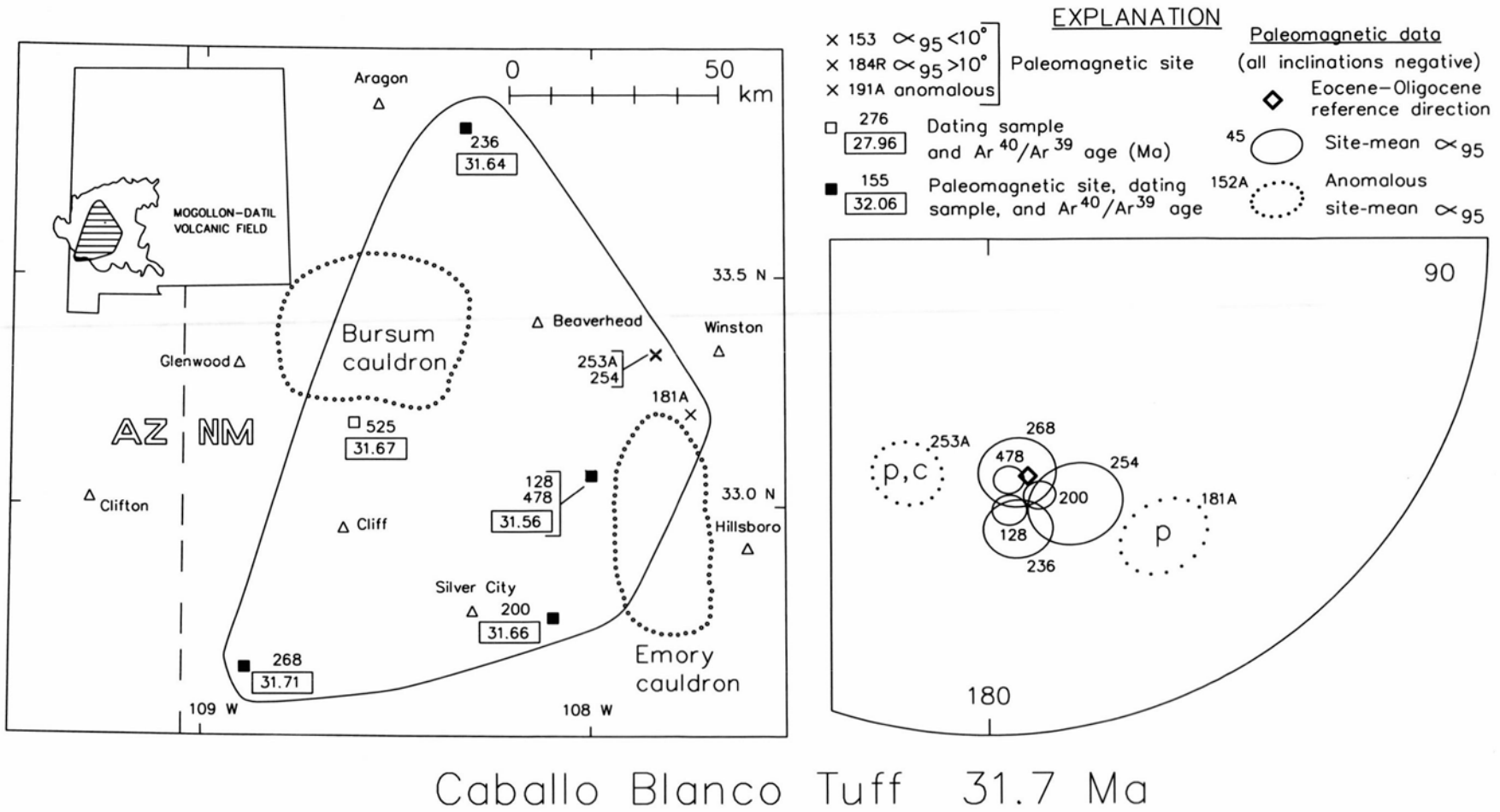

Caballo Blanco Tuff 31.7 Ma

FIGURE 18—Caballo Blanco Tuff. Site locations, areal extent, $^{40}Ar/^{39}Ar$ plateau ages, and site-mean paleomagnetic data. Possible sources for this unit include Bursum cauldron (Ratté et al., 1986) and Emory cauldron (Abbitz, 1989). Letters suggest reasons for anomalous site-mean directions (dotted ellipses, differing by more than 15° from the unit-mean direction): c=unremoved components of chemical remanence, p=incorrectly determined paleohorizontal at basal site in area of pre-eruptive topographic relief.

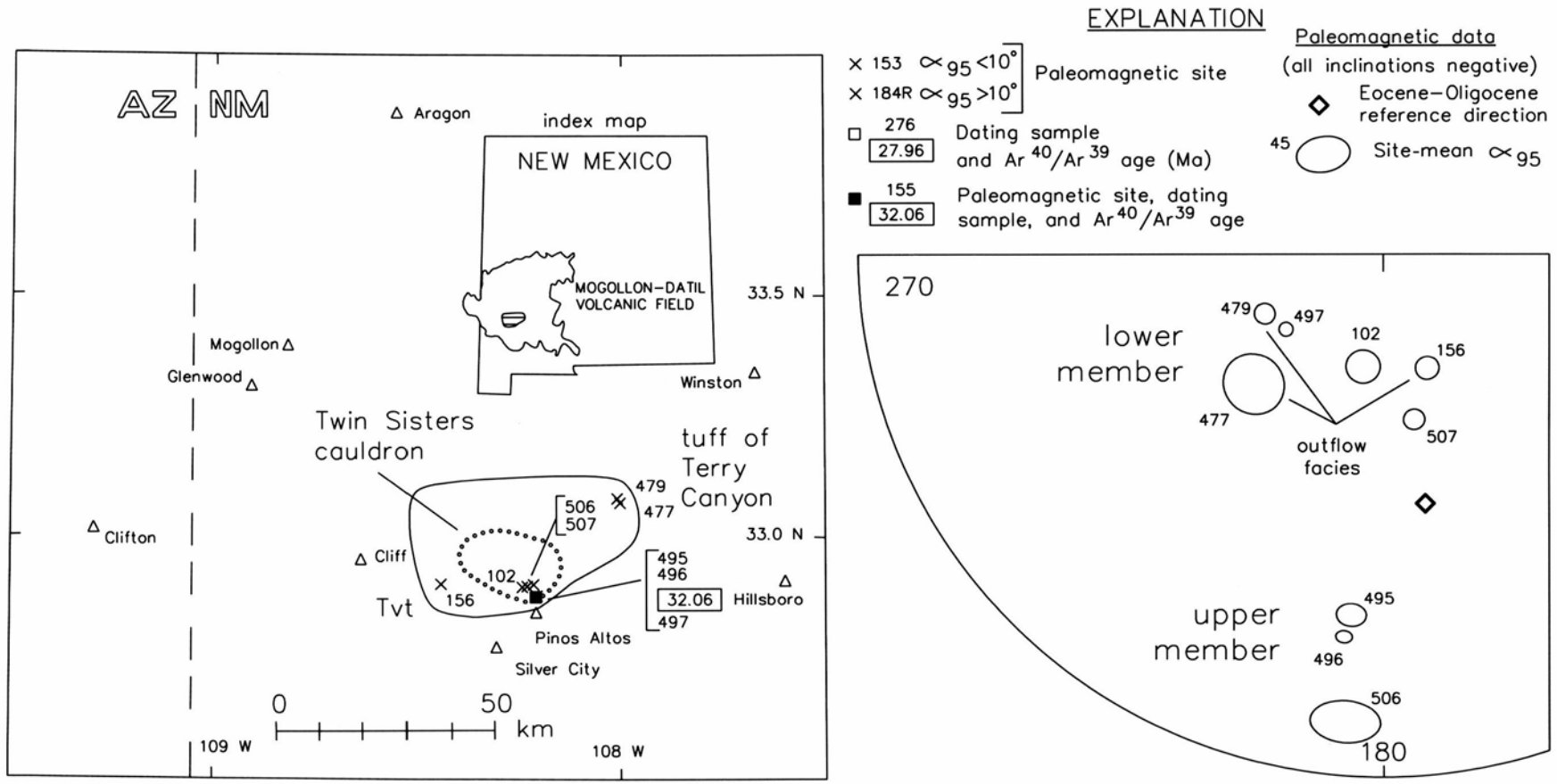

Tadpole Ridge Tuff 31.4 Ma

FIGURE 19—Upper and lower members of Tadpole Ridge Tuff. Site locations, areal extent, $^{40}Ar/^{39}Ar$ plateau ages, and site-mean paleomagnetic data. Both units were probably erupted from the Twin Sisters cauldron. The wide difference between the remanence directions of the upper an lower members indicates a time gap between their eruptions. Steep site-mean remanence directions in the outflow facies support correlation with the lower intracauldron member.

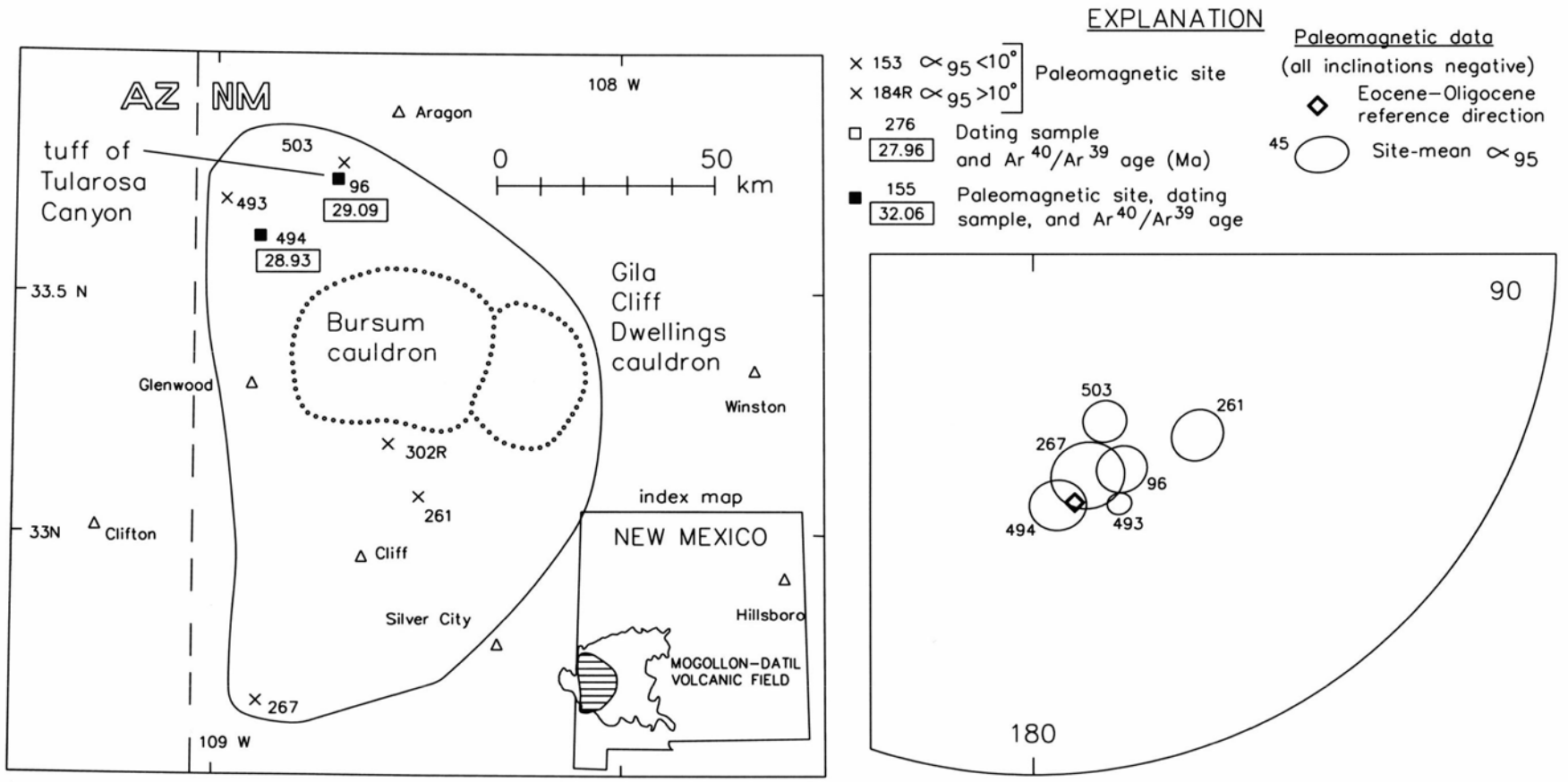

Davis Canyon Tuff 29.0 Ma

FIGURE 20—Davis Canyon Tuff. Site locations, areal extent, $^{40}Ar/^{39}Ar$ plateau ages, and site-mean paleomagnetic data. This unit may have been erupted from the Gila Cliff Dwellings cauldron (Ratté et al., 1984).

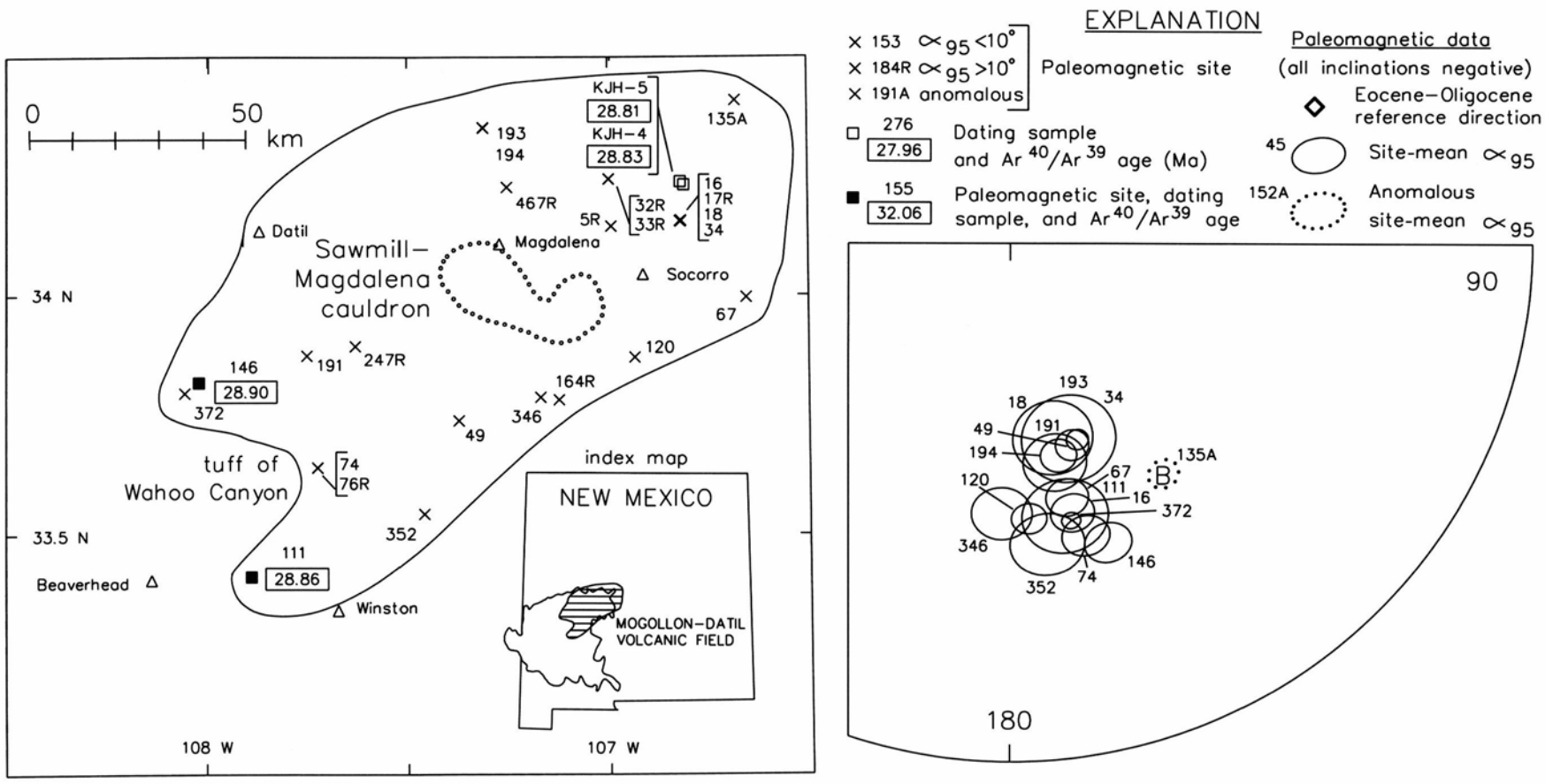

La Jencia Tuff 28.9 Ma

FIGURE 21—La Jencia Tuff. Site locations, areal extent, $^{40}Ar/^{39}Ar$ plateau ages, and site-mean paleomagnetic data. Sawmill–Magdalena cauldron is the well-established source of this unit. The anomalous direction of site 135 (dotted ellipse labelled B) reflects tectonic rotation at Black Butte.

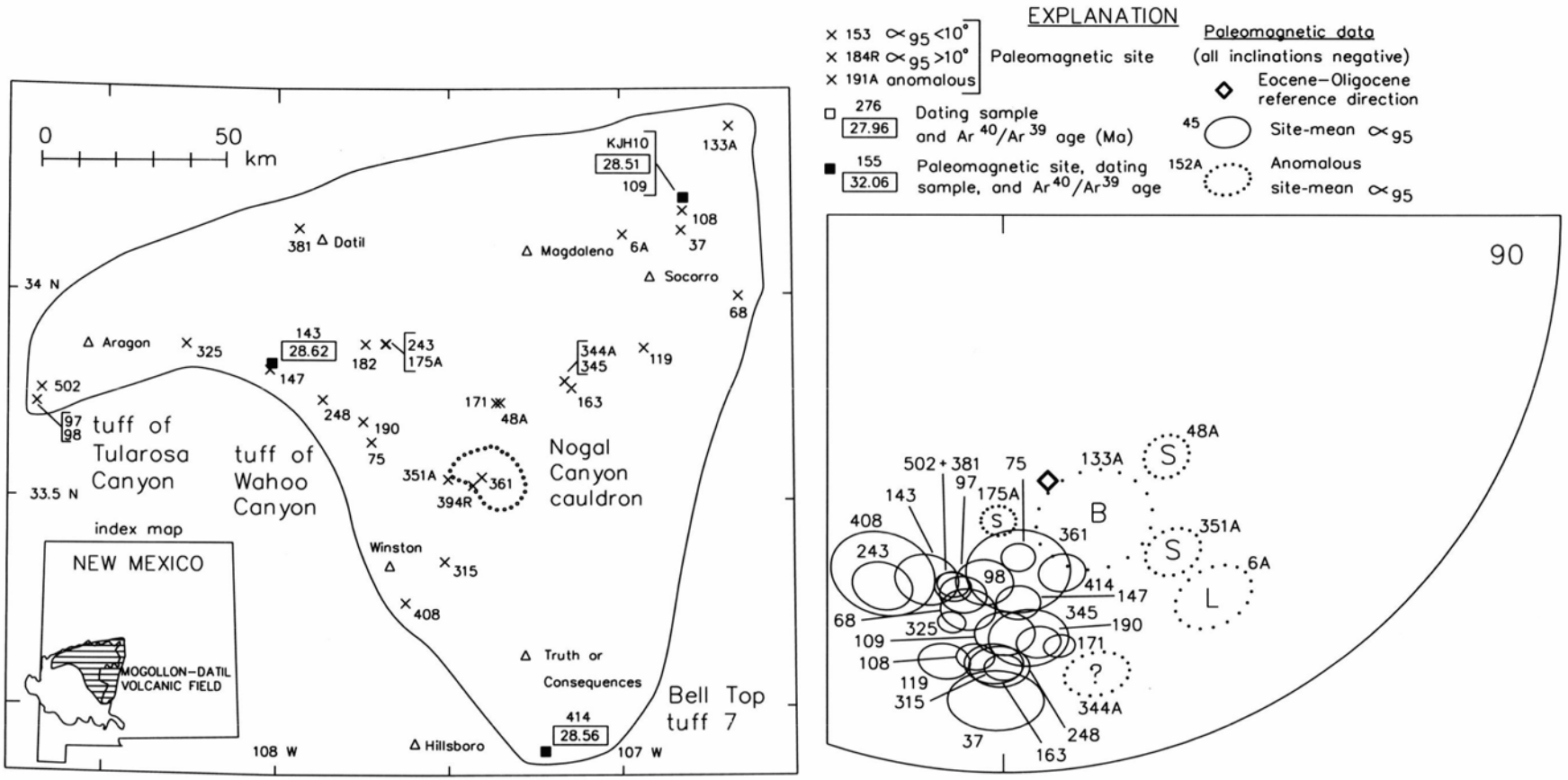

Vicks Peak Tuff 28.6 Ma

FIGURE 22—Vicks Peak Tuff. Site locations, areal extent, $^{40}Ar/^{39}Ar$ plateau ages, and site-mean paleomagnetic data. Vicks Peak Tuff is one of the most extensive ignimbrites in the field and includes Bell Top tuff 7 of Clemons (1976) and tuff of Tularosa Canyon of Rhodes and Smith (1976). Nogal Canyon cauldron is the source of the Vicks Peak Tuff. Letters suggest reasons for anomalous site-mean directions (dotted ellipses, differing by more than 15° from the unit-mean direction): ?=possible incorrect unit identification, B, L, and S=tectonic rotations in areas of high extension, respectively, Black Butte, Lemitar Mountains, and San Mateo Mountains. Paleomagnetic directions from sites 182 and 389 are excluded from stereographic projection because $\alpha_{95} > 8.5°$.

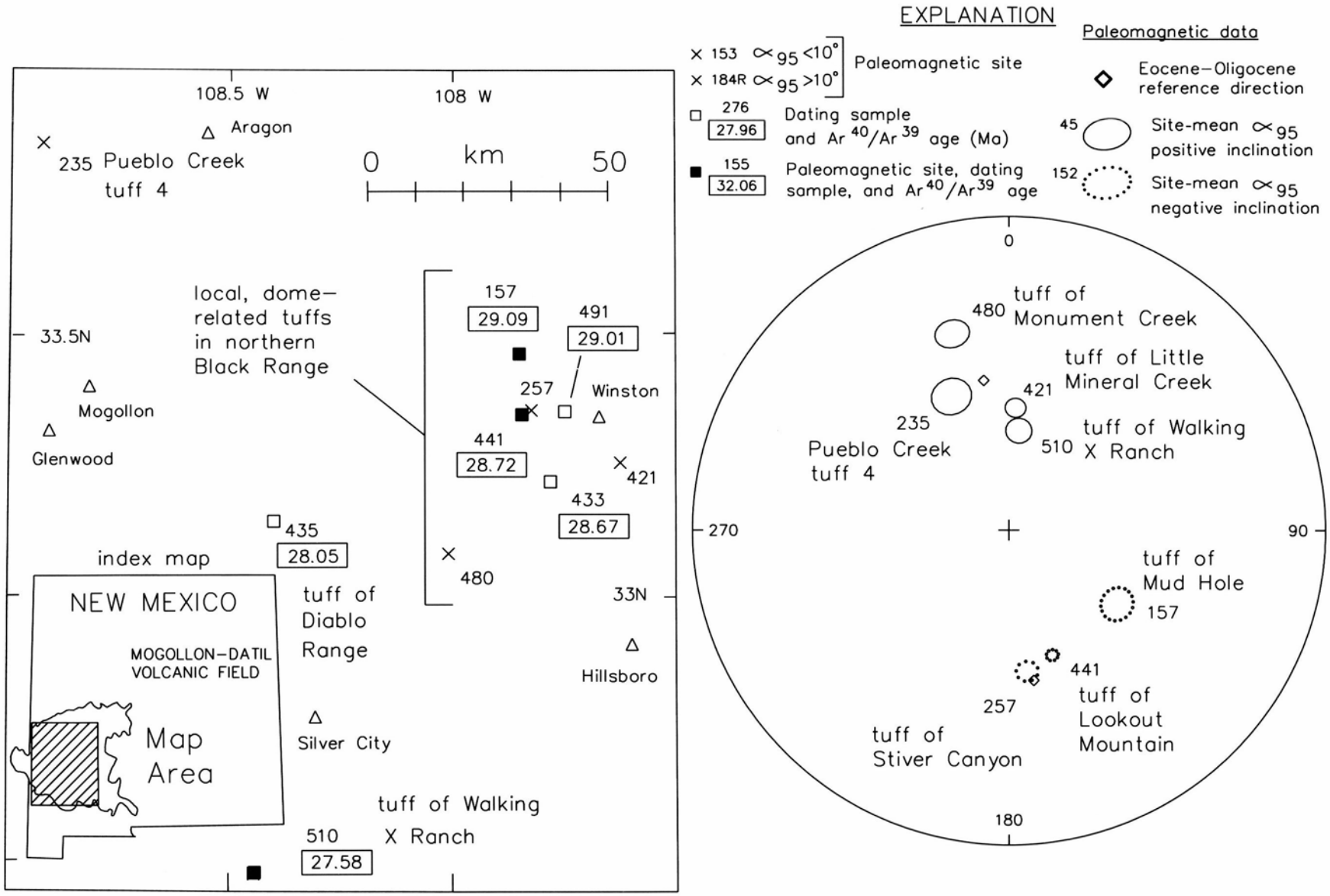

Local and poorly studied Episode 3 tuffs

FIGURE 23—Locally distributed 30 to 26 Ma ignimbrites in the western Mogollon–Datil volcanic field. Site locations, $^{40}Ar/^{39}Ar$ plateau ages, and site-mean paleomagnetic data. The tuff of Walking X Canyon may represent the distal fringe of a larger ignimbrite erupted from a source cauldron to the south. The other units, including tuff of Diablo Range, Pueblo Creek tuff 4, and local tuffs near Winston, were probably erupted during emplacement of rhyolitic domes.

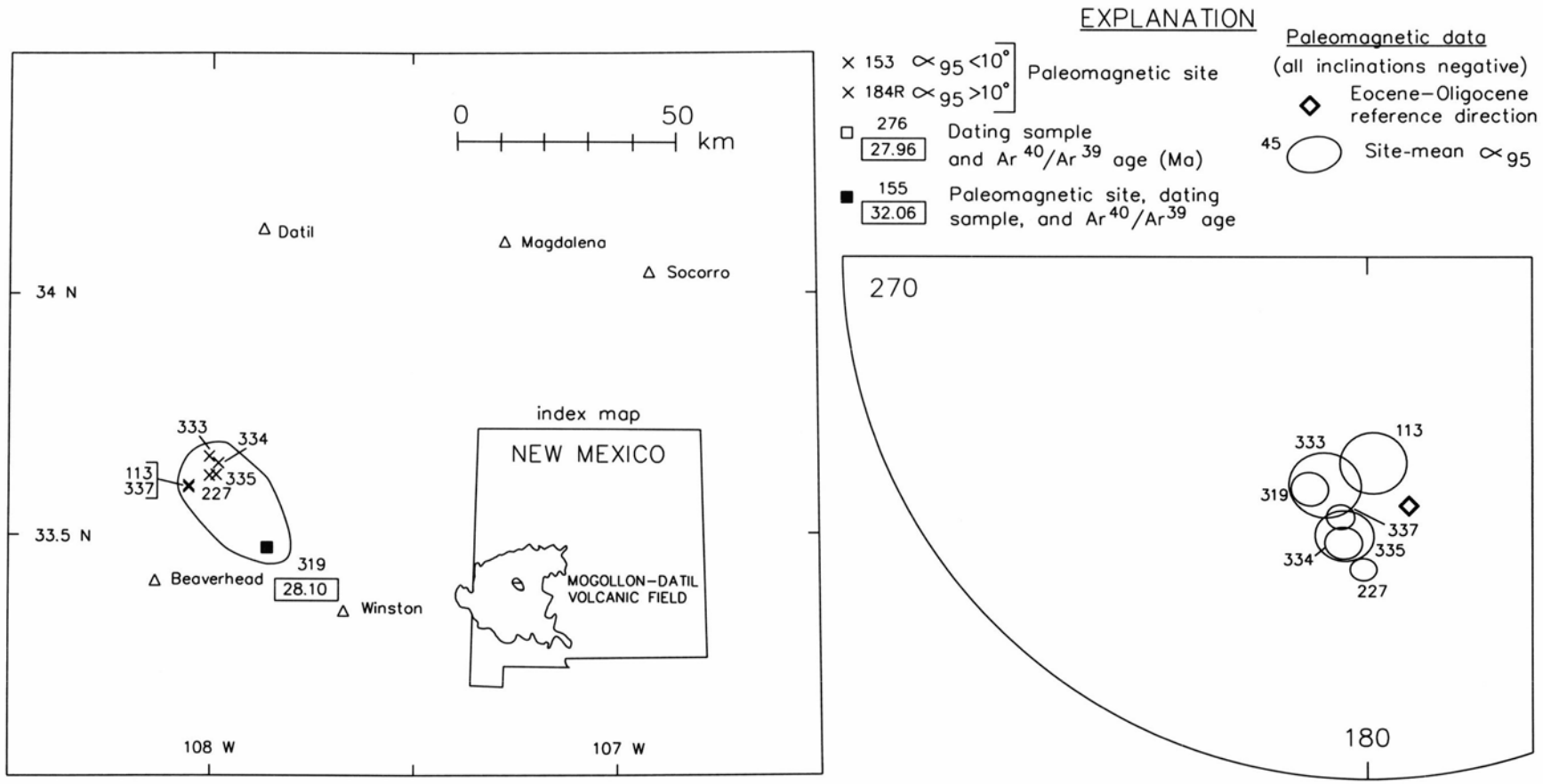

tuff of Garcia Camp 28.1 Ma

FIGURE 24—Tuff of Garcia Camp. Site locations, areal extent, $^{40}Ar/^{39}Ar$ plateau ages, and site-mean paleomagnetic data. This multi-cooling-unit tuff is part of a pyroclastic apron surrounding Indian Peak rhyolitic domes (Duffield et al., 1987).

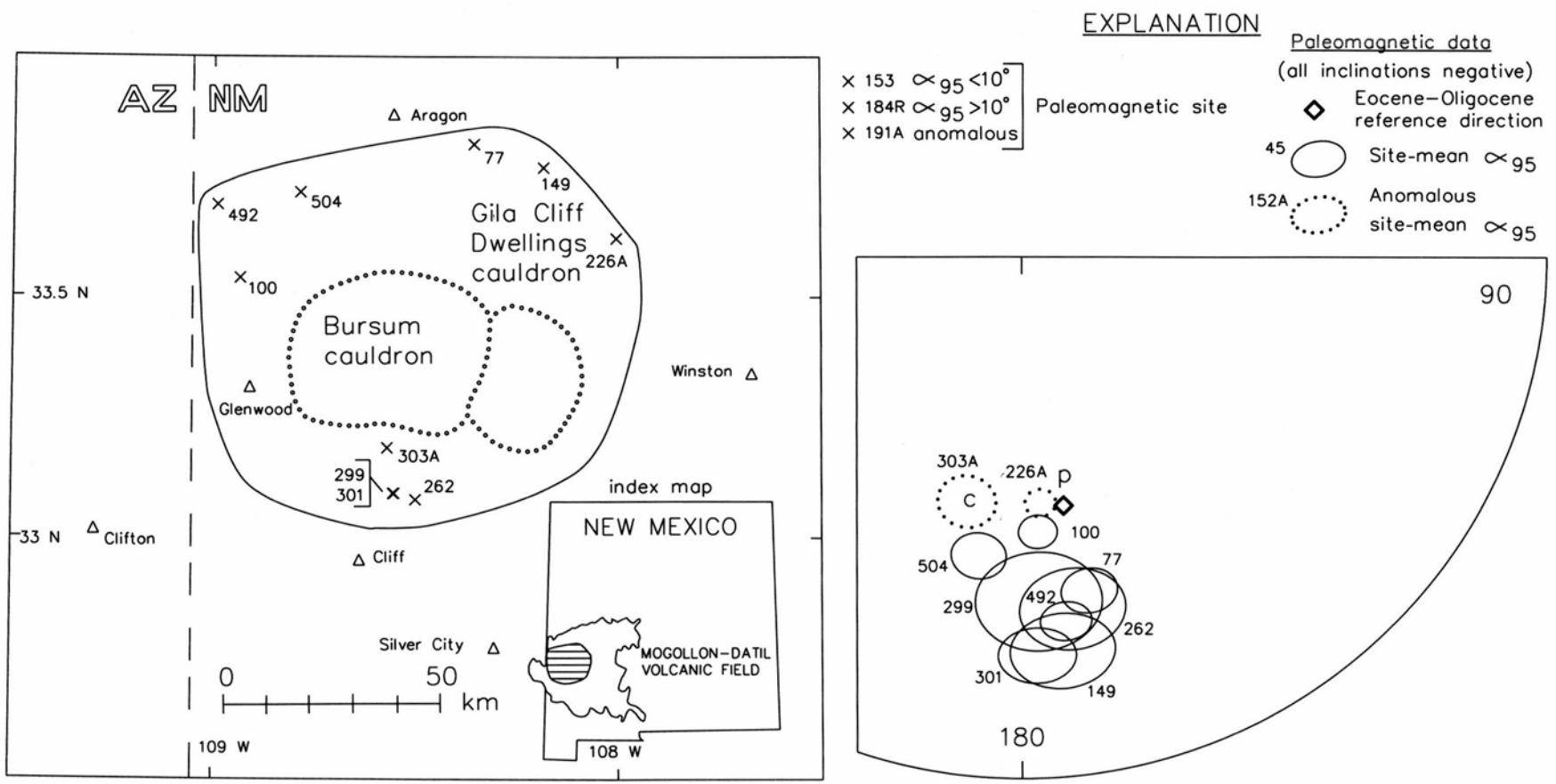

Shelley Peak Tuff 28.1 Ma

FIGURE 25—Shelly Peak Tuff. Site locations, areal extent, $^{40}Ar/^{39}Ar$ plateau ages, and site-mean paleomagnetic data. This unit may have been erupted from either the Gila Cliff Dwellings cauldron (Ratté et al., 1984) or the Bursum cauldron. Letters suggest reasons for anomalous site-mean directions (dotted ellipses, differing by more than 15° from the unit-mean direction): p=incorrectly determined paleohorizontal at basal site in area of pre-eruptive topographic relief, c=unremoved components of chemical remanence.

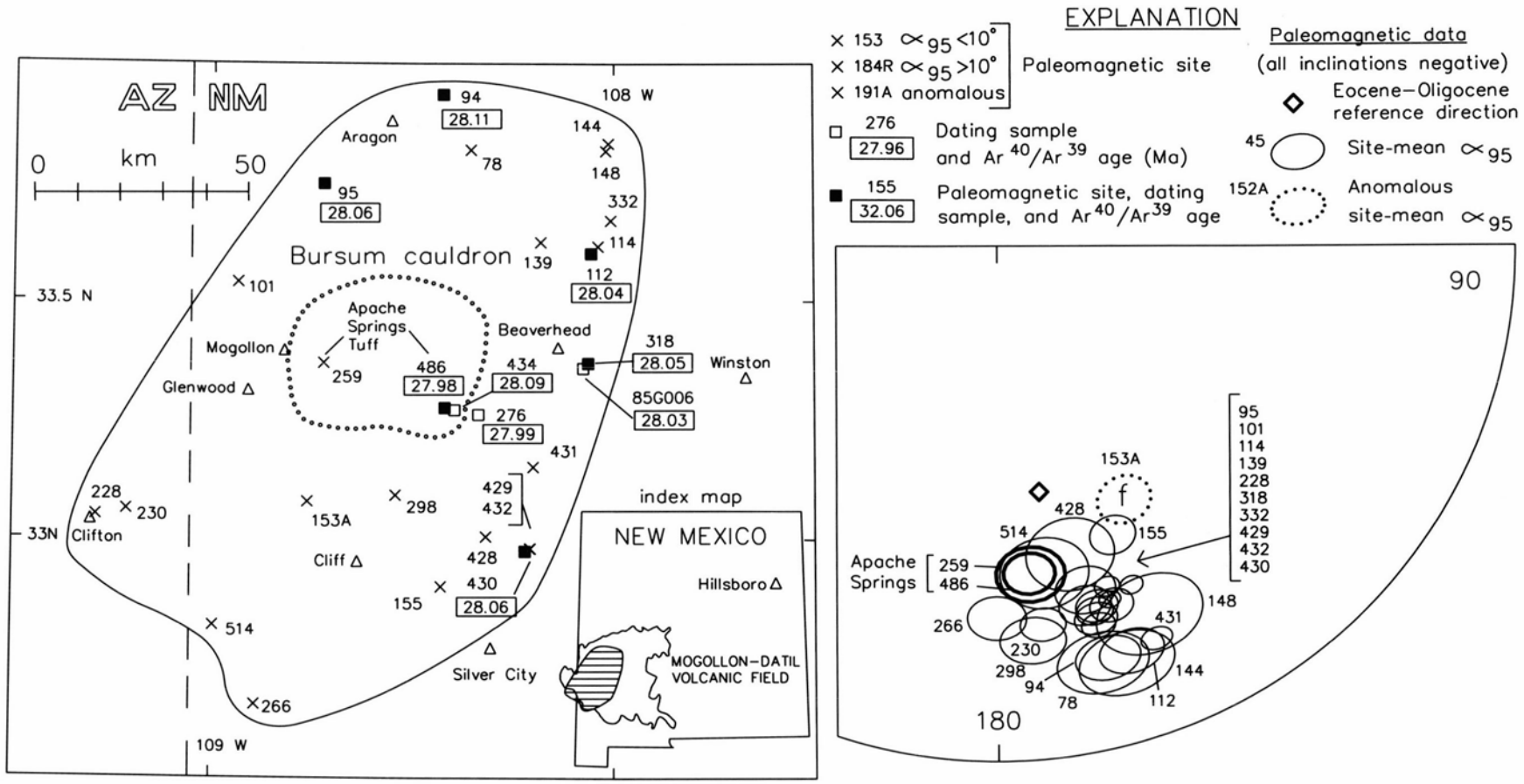

Bloodgood Canyon Tuff 28.1 Ma

FIGURE 26—Bloodgood Canyon Tuff and Apache Springs Tuff. Site locations, areal extent, $^{40}Ar/^{39}Ar$ plateau ages, and site-mean paleomagnetic data. These units represent outflow and intracaldera facies ignimbrites, respectively, erupted from the Bursum cauldron (Ratté et al., 1984). Paleomagnetic and $^{40}Ar/^{39}Ar$ data support the interpretation of the Bloodgood Canyon Tuff as the most widespread ignimbrite in the Mogollon–Datil volcanic field (Ratté et al., 1984). The anomalous direction of site 153 (dotted ellipse lettered f) probably reflects incorrectly determined paleohorizontal in an area of local structural complexity.

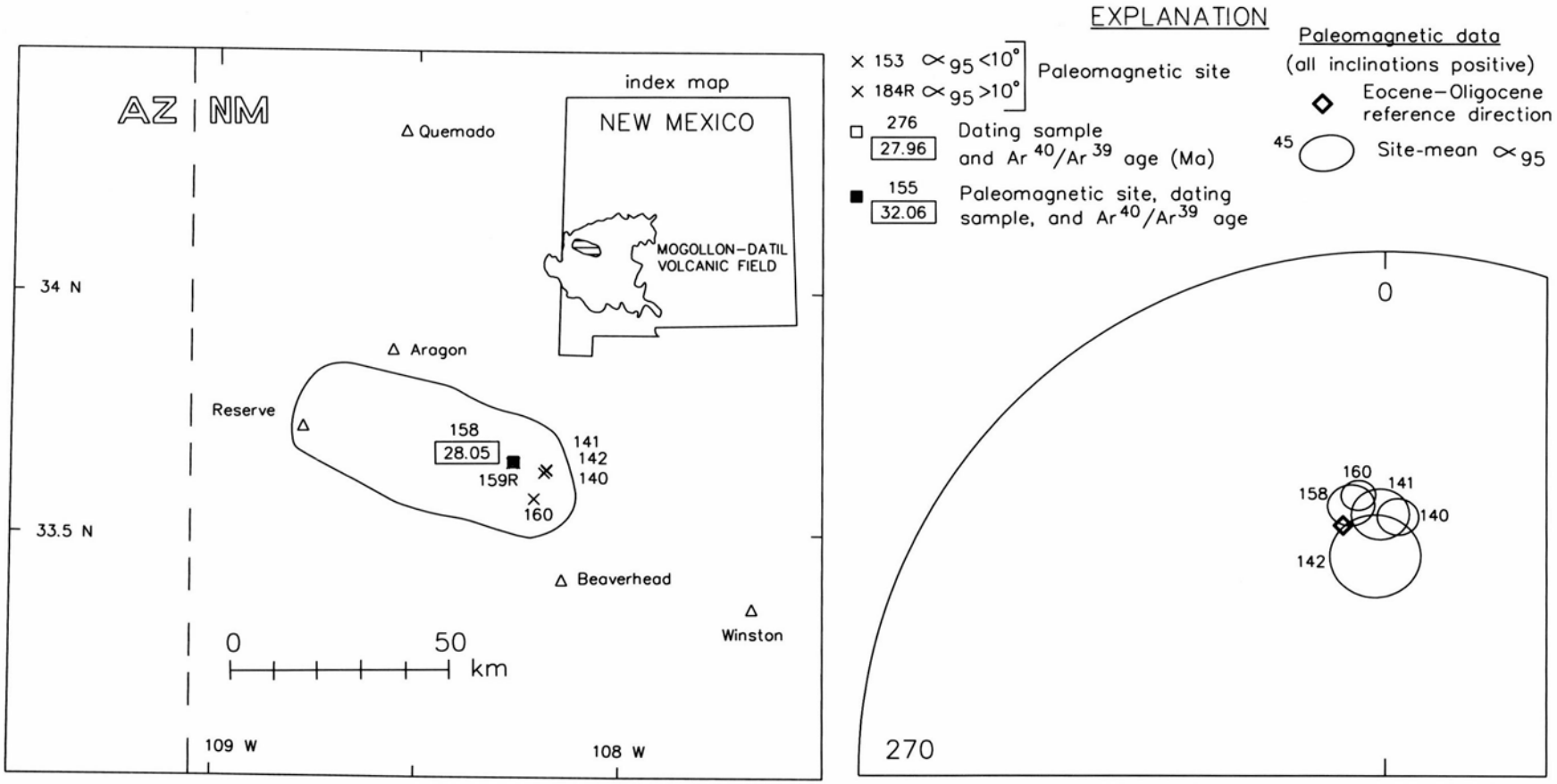

tuff of Triangle C Ranch 28.1 Ma

FIGURE 27—Tuff of Triangle C Ranch. Site locations, areal extent, $^{40}Ar/^{39}Ar$ plateau ages, and site-mean paleomagnetic data. This unit may have been erupted from the Bursum cauldron shortly after eruption of Bloodgood Canyon tuff.

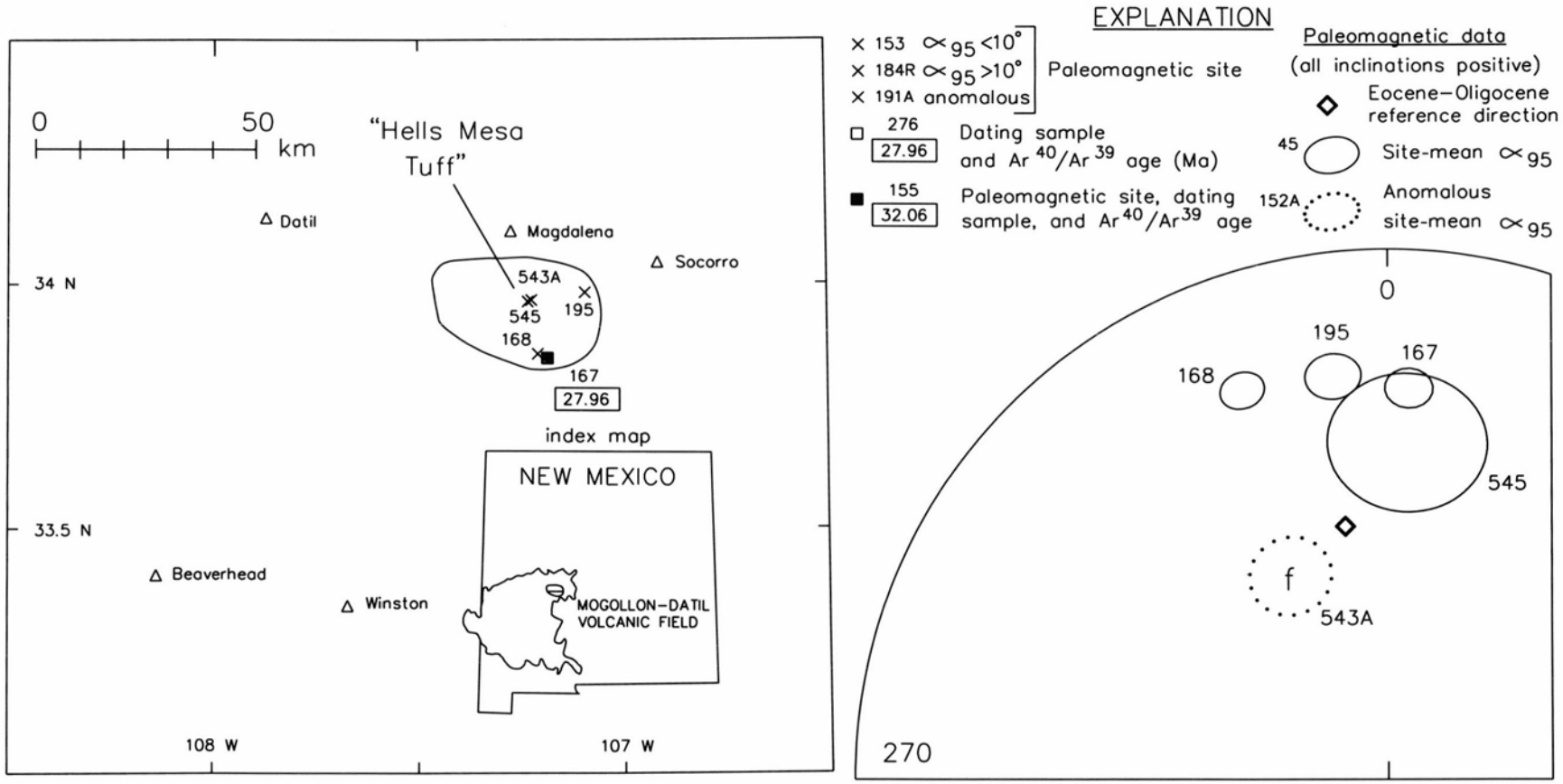

tuff of Caronita Canyon 28.0 Ma

FIGURE 28—Tuff of Caronita Canyon. Site locations, areal extent, $^{40}Ar/^{39}Ar$ plateau ages, and site-mean paleomagnetic data. This unit may represent a cogenetic precursor of the Lemitar Tuff. The anomalous direction of site 543 (dotted ellipse lettered f) probably reflects incorrectly determined paleohorizontal in an area of local structural complexity.

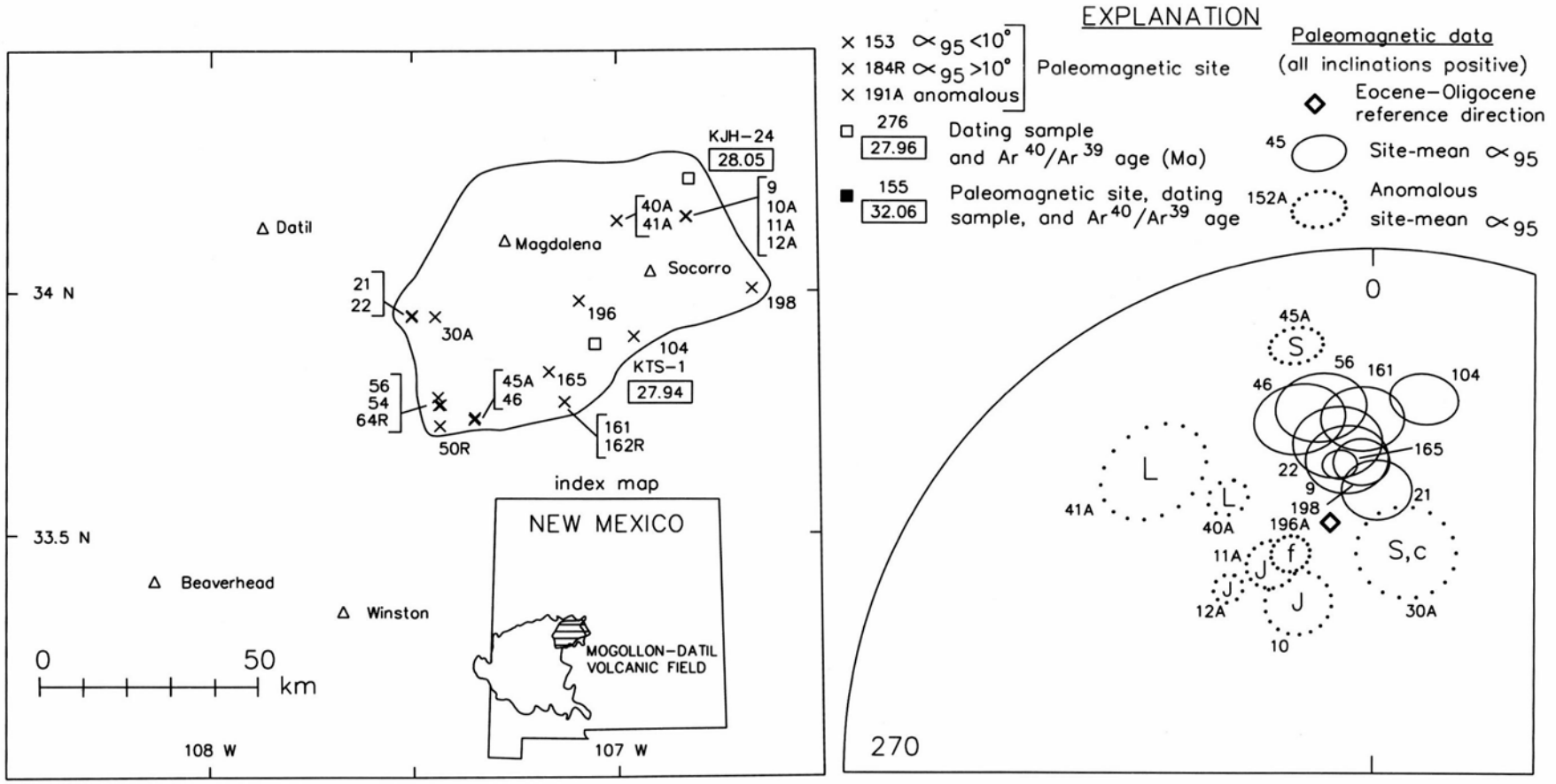

Lemitar Tuff 28.0 Ma

FIGURE 29—Lemitar Tuff. Site locations, areal extent, $^{40}Ar/^{39}Ar$ plateau ages, and site-mean paleomagnetic data. The source cauldron for this unit probably lies in the western Magdalena Mountains, although its margins have not yet been delineated. Letters suggest reasons for anomalous site-mean directions (dotted ellipses, differing by more than 15° from the unit-mean direction): c=unremoved components of chemical remanence, f=local structural complexity causing incorrect determination of paleohorizontal, J, L, and S=tectonic rotations in areas of high extension, respectively, Joyita Hills, Lemitar Mountains, and San Mateo Mountains. Paleomagnetic direction from site 54 is excluded from stereographic projection because $\alpha_{95} > 8.5°$.

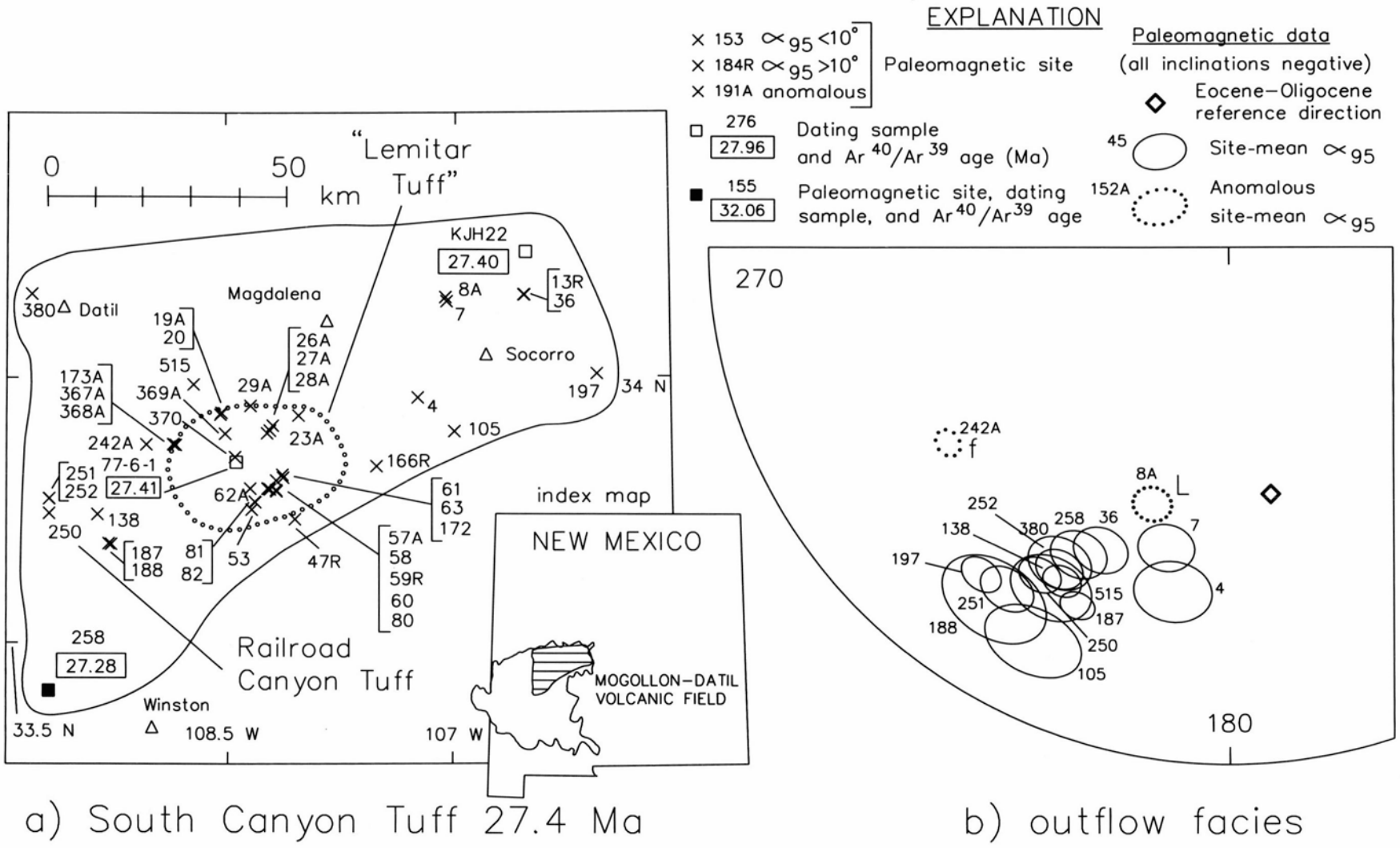

a) South Canyon Tuff 27.4 Ma

b) outflow facies

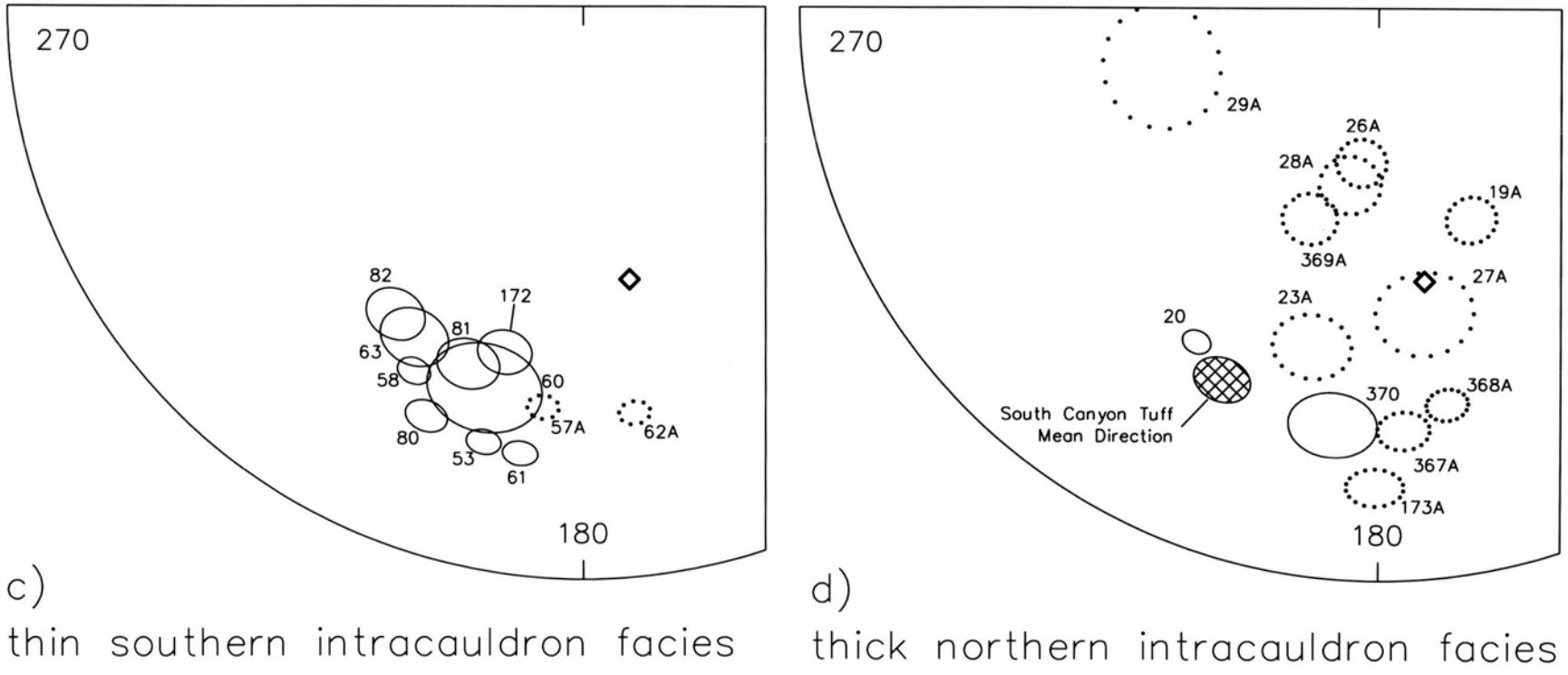

FIGURE 30—South Canyon Tuff. Site locations, areal extent, $^{40}Ar/^{39}Ar$ plateau ages, and site-mean paleomagnetic data. This unit was erupted from the Mt. Withington cauldron (a) (Ferguson, 1986). Site-mean remanence directions in the outflow (b) and shallow intracauldron facies (c) are well-grouped. Sites in thicker (>500 m) intracauldron facies (d) show scattered site-mean directions probably reflecting secular variation during protracted cooling. Letters suggest reasons for anomalous site-mean directions of outflow sites 8 and 242 (dotted ellipses, differing by more than 15° from the unit-mean direction): f=incorrectly determined paleohorizontal in an area of local structural complexity, L=tectonic rotation in the highly extended Lemitar Mountains area.

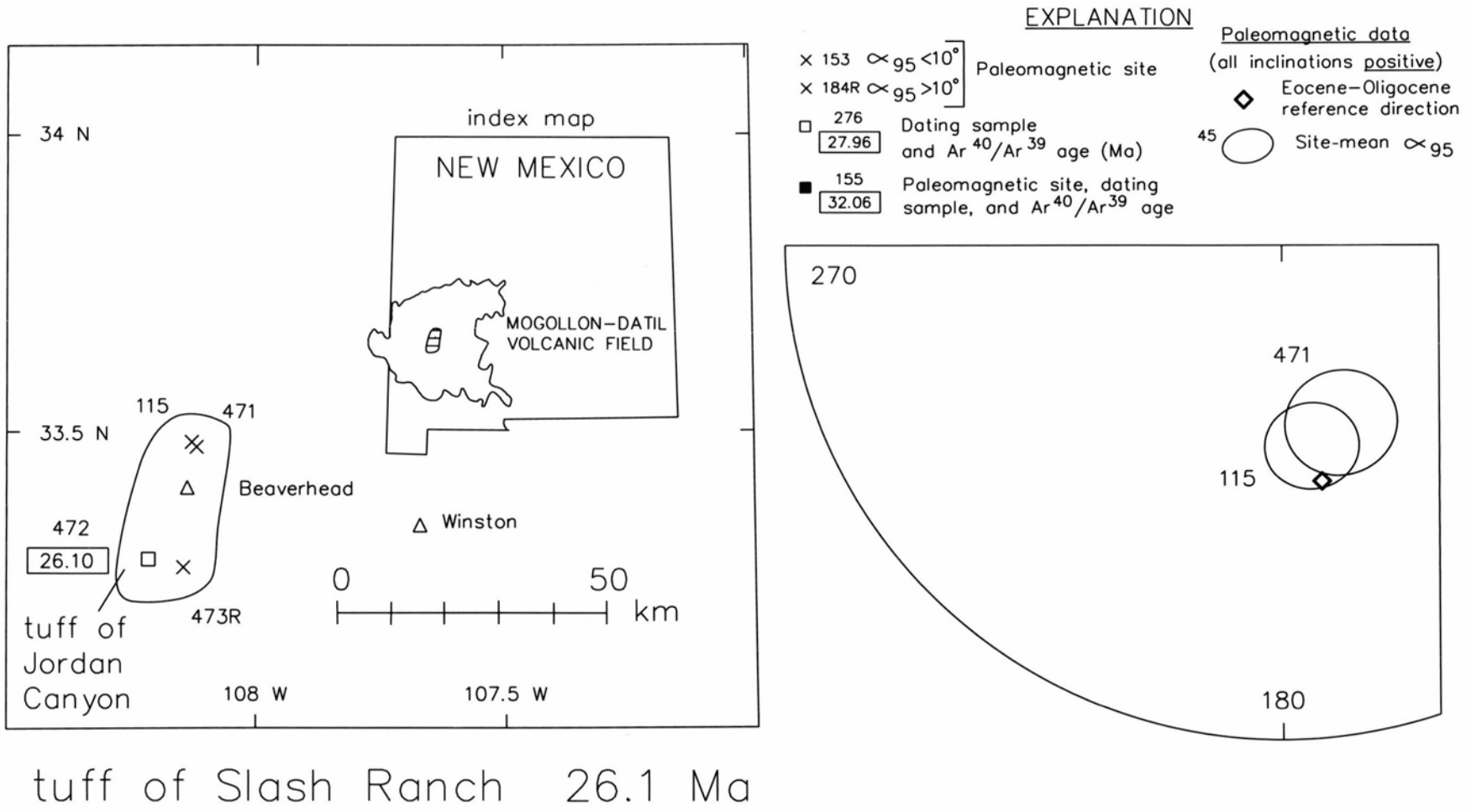

FIGURE 31—Tuff of Slash Ranch. Site locations, areal extent, $^{40}Ar/^{39}Ar$ plateau age, and site-mean paleomagnetic data. This relatively local, multi-flow unit is probably related to rhyolitic dome emplacement. Sites from this unit show unusual southerly, steeply downward paleomagnetic directions which may reflect emplacement during a geomagnetic field excursion.

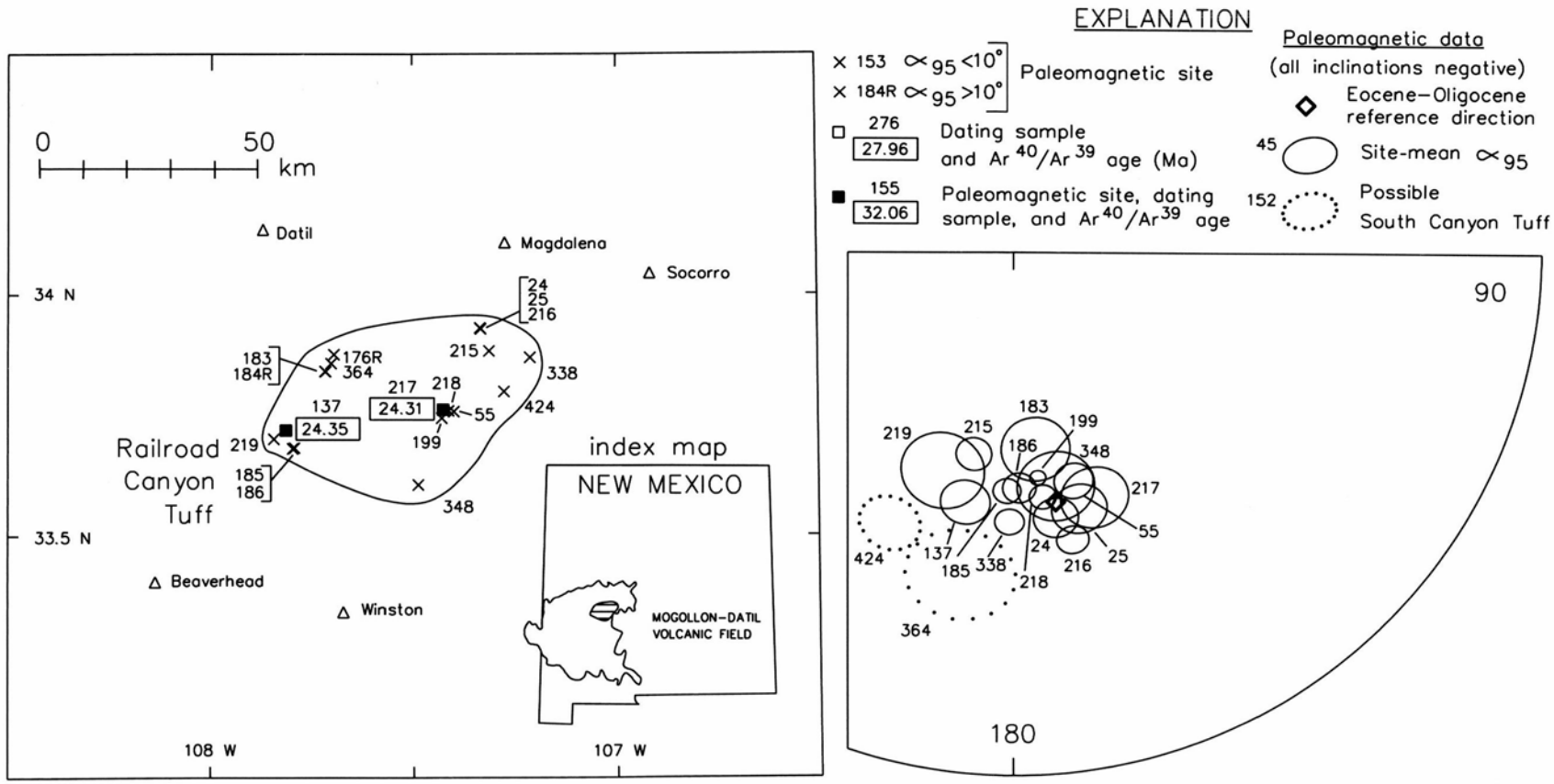

tuff of Turkey Springs 24.3 Ma

FIGURE 32—Tuff of Turkey Springs. Site locations, areal extent, $^{40}Ar/^{39}Ar$ plateau ages, and site-mean paleomagnetic data. The anomalous directions of outflow sites 364 and 424 (dotted) suggest the ignimbrite at these sites may be actually South Canyon Tuff rather than tuff of Turkey Springs.

APPENDIX 1—$^{40}Ar/^{39}Ar$ data from Mogollon–Datil ignimbrites. Units are listed in order of increasing age.

Explanation: Each data set is preceded by sample number, unit name, sample weight (grams), irradiation batch number, irradiation parameter (J), measured discrimination of atmospheric argon, and detector type (Faraday cup vs. electron multiplier). Columns in data sets give temperature of incremental heating steps, ratios of Ar isotopes (^{40}Ar=initial and radiogenic, ^{39}Ar=potassium-derived, ^{37}Ar=Calcium-derived, ^{36}Ar=initial), % of total ^{39}Ar in heating step, radiogenic yield of ^{40}Ar, moles of potassium-derived ^{39}Ar, K/Ca ratio calculated from $^{37}Ar/^{39}Ar$ ratio, age, and 1σ error. Lines following each data step show total gas K/Ca, total gas age, plateau temperature range, percent ^{39}Ar on the plateau, plateau age, and its error (method of Fleck et al., 1977).

	temp	$^{40}Ar/^{39}Ar$	$^{37}Ar/^{39}Ar$	$^{36}Ar/^{39}Ar$	$\%^{39}Ar$	%rad	moles ^{39}Ar	K/Ca	age(Ma)	1σ error
nm137	850	2.831	1.628e-02	6.861e-04	5.1	92.8	1.1e-12	31.9	23.54 ±	1.02
Turkey Springs	1125	2.752	1.560e-02	1.236e-04	26.6	98.7	6.0e-12	33.3	24.31 ±	0.10
wt = 0.1971	1250	2.780	1.542e-02	2.061e-04	45.1	97.8	1.0e-11	33.7	24.35 ±	0.07
RD56	1400	2.802	1.494e-02	2.374e-04	21.5	97.5	4.8e-12	34.8	24.45 ±	0.18
J = 0.004995	1550	2.927	1.521e-02	5.416e-04	1.6	94.5	3.7e-13	34.2	24.76 ±	1.21
disc = 296.5	total gas							33.8	24.33	
faraday	plateau	850- 1050			100.0				24.35 ±	0.09
nm217	850	2.924	1.823e-02	6.276e-04	4.2	93.7	9.5e-13	28.5	24.56 ±	0.83
Turkey Springs	1125	2.734	1.635e-02	1.176e-04	22.6	98.7	5.1e-12	31.8	24.22 ±	0.16
wt = 0.1983	1210	2.745	1.597e-02	1.394e-04	22.9	98.5	5.1e-12	32.6	24.26 ±	0.10
RD56	1375	2.756	1.566e-02	1.357e-04	47.5	98.5	1.1e-11	33.2	24.36 ±	0.09
J = 0.005007	1550	2.820	1.494e-02	2.776e-05	2.7	99.7	5.9e-13	34.8	25.29 ±	1.14
disc = 296.5	total gas							32.6	24.34	
faraday	plateau	850- 1550			100.0				24.31 ±	0.09
nm472	750	6.911	6.905e-02	1.012e-02	3.8	56.7	7.9e-13	7.5	35.18 ±	0.97
Jordan Canyon	1100	2.937	1.464e-02	1.440e-04	38.8	98.6	8.0e-12	35.5	26.04 ±	0.15
wt = 0.2036	1225	2.957	1.178e-02	1.488e-04	30.6	98.5	6.3e-12	44.1	26.20 ±	0.19
RD56	1350	2.986	1.097e-02	1.272e-04	25.6	98.7	5.3e-12	47.4	26.53 ±	0.17
J = 0.005023	1550	3.340	1.887e-02	6.584e-04	1.2	94.2	2.5e-13	27.6	28.27 ±	2.15
disc = 296.5	total gas							40.0	26.59	
faraday	plateau	1100- 1225			69.0				26.10 ±	0.12
kjh22	650	4.226	2.061e-02	6.537e-03	4.2	54.2	9.6e-13	25.2	28.35 ±	0.09
South Canyon	950	2.849	1.775e-02	2.078e-03	8.1	78.3	1.9e-12	29.3	27.62 ±	0.07
wt = 0.1405	1150	2.346	1.841e-02	4.421e-04	29.4	94.2	6.7e-12	28.2	27.37 ±	0.07
RD22	1250	2.361	1.381e-02	4.892e-04	26.7	93.7	6.1e-12	37.7	27.39 ±	0.07
J = 0.006917	1350	2.411	1.547e-02	6.401e-04	17.9	92.0	4.1e-12	33.6	27.45 ±	0.07
disc = 296.5	1450	2.667	1.735e-02	1.274e-03	10.6	85.7	2.4e-12	30.0	28.29 ±	0.07
faraday	1550	3.314	1.409e-02	3.551e-03	3.1	68.2	7.0e-13	36.9	27.98 ±	0.09
	total gas							31.6	27.57	
	plateau	1150- 1350			74.0				27.40 ±	0.07
78-6-1	900	3.662	2.762e-02	1.025e-03	28.2	91.6	1.4e-13	18.8	27.40 ±	0.08
South Canyon	1050	3.496	2.755e-02	4.488e-04	29.2	96.1	1.4e-13	18.9	27.43 ±	0.07
wt = 0.1584	1125	3.579	2.718e-02	7.304e-04	20.2	93.9	1.0e-13	19.1	27.43 ±	0.07
RD32	1200	3.868	2.704e-02	1.736e-03	11.1	86.6	5.5e-14	19.2	27.37 ±	0.07
J = 0.004562	1275	4.274	2.644e-02	3.006e-03	5.5	79.1	2.7e-14	19.7	27.61 ±	0.08
disc = 296.5	1400	4.820	2.698e-02	4.832e-03	4.0	70.3	2.0e-14	19.3	27.67 ±	0.08
faraday	1500	8.107	2.707e-02	1.597e-02	1.7	41.8	8.4e-15	19.2	27.64 ±	0.08
	total gas							19.0	27.44 ±	
	plateau	900- 1200							27.41 ±	0.07

APPENDIX 1, continued.

	temp	$^{40}Ar/^{39}Ar$	$^{37}Ar/^{39}Ar$	$^{36}Ar/^{39}Ar$	$\%^{39}Ar$	%rad	moles ^{39}Ar	K/Ca	age(Ma)	1σ error
nm258	700	5.774	2.456e-02	5.898e-03	2.5	69.7	4.9e-13	21.2	27.23 ±	0.12
South Canyon	1025	4.132	1.375e-02	3.247e-04	32.1	97.6	6.3e-12	37.8	27.26 ±	0.08
wt = 0.1972	1150	4.115	1.297e-02	2.558e-04	33.6	98.0	6.6e-12	40.1	27.29 ±	0.08
RD54	1300	4.175	1.269e-02	3.366e-04	29.1	97.5	5.7e-12	41.0	27.52 ±	0.08
J = 0.003777	1550	5.374	1.277e-02	4.189e-03	2.7	76.9	5.3e-13	40.7	27.93 ±	0.11
disc = 299.3	total gas							38.7	27.36	
faraday	plateau	1025- 1150			65.7				27.28 ±	0.10
nm510	1025	3.316	1.680e-02	8.543e-04	12.2	92.4	2.5e-12	31.0	27.57 ±	0.11
Walking X Canyon	1150	3.110	1.629e-02	1.890e-04	16.4	98.2	3.4e-12	31.9	27.49 ±	0.22
wt = 0.1994	1300	3.119	1.637e-02	2.017e-04	51.3	98.1	1.1e-11	31.8	27.54 ±	0.11
RD56	1400	3.109	1.596e-02	1.139e-04	17.5	98.9	3.6e-12	32.6	27.70 ±	0.15
J = 0.005028	1550	3.177	1.494e-02	6.223e-04	2.6	94.2	5.3e-13	34.8	28.42 ±	1.48
disc = 296.5	total gas							31.4	27.82	
faraday	plateau	1025- 1550			100.0				27.58 ±	0.10
kts1	900	3.896	2.283e-02	3.582e-03	11.40	72.7	1.6e-13	22.8	27.89 ±	0.08
Lemitar	1000	3.178	2.168e-02	1.133e-03	17.20	89.3	2.4e-13	24.0	27.94 ±	0.09
wt = 0.1016	1050	3.190	2.125e-02	1.137e-03	14.20	89.3	2.0e-13	24.5	28.04 ±	0.07
RD20	1100	3.138	2.100e-02	1.025e-03	13.70	90.2	1.9e-13	24.8	27.86 ±	0.06
J = 0.005499	1150	3.190	2.068e-02	1.111e-03	13.10	89.6	1.8e-13	25.1	28.12 ±	0.08
disc = 296.5	1200	3.295	2.079e-02	1.473e-03	11.00	86.7	1.5e-13	25.0	28.10 ±	0.10
faraday	1300	3.519	2.055e-02	2.296e-03	8.70	80.6	1.2e-13	25.3	27.91 ±	0.06
	1450	3.688	2.088e-02	2.830e-03	10.70	77.2	1.5e-13	24.9	28.02 ±	0.06
	total gas							24.5	27.98	
	plateau	900- 1100			56.5				27.94 ±	0.10
kjh24	650	3.719	1.876e-02	4.847e-03	6.9	61.4	2.7e-12	27.7	28.26 ±	0.07
Lemitar	900	2.463	2.021e-02	6.822e-04	12.4	91.6	4.8e-12	25.7	27.95 ±	0.07
wt = 0.2128	1000	2.338	1.670e-02	2.442e-04	22.2	96.7	8.5e-12	31.1	28.00 ±	0.07
RD22	1050	2.381	1.745e-02	3.760e-04	9.5	95.1	3.7e-12	29.8	28.05 ±	0.07
J = 0.006917	1125	2.350	1.535e-02	2.897e-04	11.8	96.2	4.6e-12	33.9	27.97 ±	0.07
disc = 296.5	1200	2.343	1.590e-02	2.188e-04	13.4	97.0	5.2e-12	32.7	28.15 ±	0.07
faraday	1300	2.365	1.581e-02	3.105e-04	11.4	95.9	4.4e-12	32.9	28.08 ±	0.07
	1550	2.394	1.588e-02	3.681e-04	12.4	95.3	4.8e-12	32.7	28.23 ±	0.07
	total gas							30.8	28.07	
	plateau	950- 1350			68.0				28.05 ±	0.07
nm167	650	4.610	2.035e-02	4.308e-03	7.9	72.3	3.9e-14	25.6	27.26 ±	0.08
Caronita Canyon	950	3.784	2.160e-02	1.281e-03	18.9	89.9	9.2e-14	24.1	27.81 ±	0.09
wt = 0.1282	1050	3.766	2.162e-02	1.159e-03	14.0	90.8	6.8e-14	24.1	27.96 ±	0.07
RD32	1125	3.706	2.161e-02	1.002e-03	16.8	91.9	8.2e-14	24.1	27.85 ±	0.08
J = 0.004569	1200	3.747	2.150e-02	1.067e-03	14.5	91.5	7.1e-14	24.2	28.03 ±	0.08
disc = 296.5	1275	3.854	2.137e-02	1.475e-03	10.9	88.6	5.3e-14	24.3	27.92 ±	0.09
faraday	1400	3.898	2.141e-02	1.580e-03	11.7	87.9	5.7e-14	24.3	28.02 ±	0.08
	1550	4.601	2.107e-02	3.715e-03	5.3	76.0	2.6e-14	24.7	28.60 ±	0.08
	total gas							24.3	27.91	
	plateau	1050- 1400			67.9				27.96 ±	0.07

APPENDIX 1, continued.

	temp	$^{40}Ar/^{39}Ar$	$^{37}Ar/^{39}Ar$	$^{36}Ar/^{39}Ar$	$\%^{39}Ar$	%rad	moles ^{39}Ar	K/Ca	age(Ma)	1σ error
nm158a	650	5.268	1.868e-02	6.085e-03	3.8	65.8	2.4e-14	27.8	28.47	± 0.08
Triangle C Ranch	950	3.639	1.503e-02	7.455e-04	11.2	93.8	7.0e-14	34.6	28.05	± 0.07
wt = 0.1518	1050	3.632	1.158e-02	7.923e-04	10.3	93.4	6.4e-14	44.9	27.88	± 0.07
RD32	1125	3.661	1.072e-02	8.718e-04	14.6	92.8	9.1e-14	48.5	27.92	± 0.08
J = 0.004591	1200	3.621	1.032e-02	7.543e-04	16.3	93.7	1.0e-13	50.4	27.88	± 0.08
disc = 296.5	1275	3.641	1.018e-02	7.687e-04	18.1	93.6	1.1e-13	51.1	28.00	± 0.08
faraday	1400	3.707	1.017e-02	9.615e-04	19.2	92.2	1.2e-13	51.1	28.08	± 0.09
	1550	4.285	9.963e-03	2.848e-03	6.5	80.2	4.0e-14	52.2	28.25	± 0.08
	total gas							46.2	28.01	
	plateau	950- 1275			70.5				27.95	± 0.08
nm158b	1000	4.197	1.520e-02	2.656e-03	19.7	81.2	7.6e-14	34.2	27.99	± 0.08
Triangle C Ranch	1150	3.720	1.070e-02	1.012e-03	21.4	91.8	8.3e-14	48.6	28.06	± 0.07
wt = 0.1518	1250	3.697	1.027e-02	8.976e-04	31.6	92.7	1.2e-13	50.6	28.15	± 0.07
RD32	1400	3.800	9.983e-03	1.243e-03	21.7	90.2	8.4e-14	52.1	28.16	± 0.08
J = 0.004591	1550	5.139	9.947e-03	5.755e-03	5.5	66.8	2.1e-14	52.3	28.21	± 0.08
disc = 296.5	total gas							46.2	28.11	
faraday	plateau	1150- 1550			80.2				28.15	± 0.07
nm487	700	5.581	2.491e-02	4.848e-03	4.3	74.3	7.2e-13	20.9	28.18	± 0.13
Apache Springs	1075	4.247	1.832e-02	4.555e-04	26.4	96.7	4.4e-12	28.4	27.93	± 0.08
wt = 0.2053	1250	4.209	1.647e-02	3.162e-04	37.5	97.7	6.2e-12	31.6	27.95	± 0.10
RD54	1450	4.299	1.581e-02	5.707e-04	26.9	96.0	4.5e-12	32.9	28.05	± 0.09
J = 0.003799	1550	4.857	1.559e-02	2.444e-03	5.0	85.0	8.2e-13	33.4	28.08	± 0.11
disc = 299.2	total gas							30.4	27.99	
faraday	plateau	1075- 1450			90.7				27.98	± 0.09
nm94	850	4.736	1.292e-02	5.172e-03	4.4	67.7	9.4e-13	40.3	28.66	± 0.78
Bloodgood Canyon	1140	3.308	1.201e-02	5.649e-03	24.1	49.5	5.2e-12	43.3	28.05	± 0.15
wt = 0.1999	1250	3.221	1.203e-02	2.602e-04	34.0	97.6	7.3e-12	43.2	28.08	± 0.09
RD56	1350	3.195	1.148e-02	1.526e-04	33.6	98.6	7.2e-12	45.3	28.13	± 0.09
J = 0.004990	1550	3.249	1.240e-02	2.101e-04	4.0	98.1	8.6e-13	41.9	28.45	± 0.51
disc = 296.5	total gas							43.8	28.13	
faraday	plateau	850- 1550			100.0				28.11	± 0.10
nm95	750	6.366	2.073e-02	1.007e-02	2.1	53.2	4.3e-13	25.1	30.27	± 0.94
Bloodgood Canyon	1100	3.373	1.305e-02	8.212e-04	19.2	92.8	3.9e-12	39.8	27.95	± 0.25
wt = 0.2018	1225	3.189	1.267e-02	1.941e-04	25.6	98.2	5.3e-12	41.1	27.98	± 0.15
RD56	1350	3.195	1.236e-02	1.693e-04	50.6	98.4	1.0e-11	42.1	28.08	± 0.09
J = 0.004990	1550	3.283	1.287e-02	5.674e-03	2.4	48.9	4.9e-13	40.4	27.79	± 0.84
disc = 296.5	total gas							40.9	28.22	
faraday	plateau	1100- 1550			97.7				28.06	± 0.10

APPENDIX 1, continued.

	temp	$^{40}Ar/^{39}Ar$	$^{37}Ar/^{39}Ar$	$^{36}Ar/^{39}Ar$	$\%^{39}Ar$	%rad	moles ^{39}Ar	K/Ca	age(Ma)	1σ error
nm112	800	3.987	1.951e-02	3.059e-03	3.4	77.3	7.0e-13	26.7	28.62 ±	0.57
Bloodgood Canyon	1050	3.259	1.448e-02	4.712e-04	14.3	95.7	2.9e-12	35.9	27.87 ±	0.14
wt = 0.1997	1175	3.166	1.412e-02	1.323e-04	17.3	98.8	3.5e-12	36.8	27.94 ±	0.23
RD56	1350	3.204	1.400e-02	2.161e-04	61.0	98.0	1.2e-11	37.2	28.06 ±	0.08
J = 0.004992	1550	3.259	1.324e-02	2.677e-04	4.0	97.6	8.0e-13	39.3	28.43 ±	1.12
disc = 296.5	total gas							36.0	28.25	
faraday	plateau	800- 1550			100.0				29.04 ±	0.10
nm276	700	3.002	2.107e-02	1.214e-02	1.6	55.1	2.4e-13	24.7	30.05 ±	0.28
Bloodgood Canyon	900	4.354	1.029e-02	8.640e-04	12.9	94.0	2.0e-12	50.5	27.90 ±	0.09
wt = 0.2123	1000	4.234	1.030e-02	4.606e-04	14.7	96.7	2.3e-12	50.5	27.90 ±	0.09
RD54	1100	4.539	1.067e-02	1.412e-03	20.3	90.7	3.2e-12	48.8	28.06 ±	0.09
J = 0.003808	1200	4.350	1.030e-02	7.672e-04	36.5	94.7	5.7e-12	50.5	28.07 ±	0.08
disc = 299.2	1300	4.630	1.065e-02	1.549e-03	12.1	90.0	1.9e-12	48.8	28.40 ±	0.09
faraday	1400	6.254	1.631e-02	6.847e-03	1.2	67.6	1.9e-13	31.9	28.81 ±	0.37
	1550	9.827	1.106e-02	1.911e-02	0.8	42.5	1.2e-13	47.0	28.45 ±	0.55
	total gas							48.8	28.10	
	plateau	900- 1200			84.4				27.99 ±	0.12
nm318	750	5.862	1.536e-02	5.571e-03	3.3	71.8	5.6e-13	33.8	28.67 ±	0.17
Bloodgood Canyon	1025	4.264	1.284e-02	5.610e-04	25.5	96.0	4.3e-12	40.5	27.86 ±	0.08
wt = 0.1977	1150	4.239	1.264e-02	4.177e-04	34.1	97.0	5.8e-12	41.1	27.98 ±	0.07
RD54	1300	4.251	1.232e-02	3.933e-04	33.3	97.1	5.6e-12	42.2	28.11 ±	0.07
J = 0.003803	1550	5.384	1.458e-02	3.980e-03	3.8	78.1	6.4e-13	35.7	28.61 ±	0.10
disc = 299.2	total gas							40.8	28.04	
faraday	plateau	1150- 1300			67.4				28.05 ±	0.07
nm430	750	4.418	1.300e-02	1.005e-03	25.3	93.2	4.5e-12	40.0	27.98 ±	0.08
Bloodgood Canyon	1050	4.233	1.254e-02	3.584e-04	45.9	97.4	8.2e-12	41.5	28.01 ±	0.07
wt = 0.1990	1150	4.265	1.214e-02	4.205e-04	25.5	97.0	4.5e-12	42.8	28.11 ±	0.08
RD54	1300	4.842	1.290e-02	2.367e-03	1.9	85.5	3.4e-13	40.3	28.12 ±	0.25
J = 0.003797	1550	7.192	1.297e-02	1.014e-02	1.4	58.3	2.5e-13	40.1	28.47 ±	0.20
disc = 299.2	total gas							41.4	28.04	
faraday	plateau	1050- 1150			71.4				28.06 ±	0.08
nm434	700	5.175	1.106e-02	3.410e-03	5.5	80.4	9.1e-13	47.0	28.39 ±	0.12
Bloodgood Canyon	1075	4.310	1.045e-02	6.685e-04	28.2	95.3	4.6e-12	49.8	28.02 ±	0.08
wt = 0.2044	1250	4.231	1.043e-02	3.890e-04	33.7	97.2	5.5e-12	49.9	28.04 ±	0.09
RD54	1450	4.318	1.050e-02	6.413e-04	28.7	95.5	4.7e-12	49.5	28.13 ±	0.08
J = 0.003811	1550	5.465	1.123e-02	4.399e-03	3.9	76.1	6.3e-13	46.3	28.37 ±	0.16
disc = 299.2	total gas							49.4	28.09	
faraday	plateau	1075- 1450			90.6				28.07 ±	0.09

APPENDIX 1, continued.

	temp	$^{40}Ar/^{39}Ar$	$^{37}Ar/^{39}Ar$	$^{36}Ar/^{39}Ar$	$\%^{39}Ar$	%rad	moles ^{39}Ar	K/Ca	age(Ma)	1σ error
nm434hfb	750	7.224	3.633e-02	1.111e-02	1.2	54.5	2.4e-13	14.3	34.90	± 1.95
Bloodgood Canyon	1025	3.215	1.096e-02	1.251e-04	19.2	98.9	3.8e-12	47.4	28.19	± 0.15
wt = 0.1995	1150	3.175	1.032e-02	3.885e-05	25.6	99.6	5.1e-12	50.4	28.07	± 0.17
RD56	1300	3.185	1.050e-02	5.877e-05	43.7	99.5	8.7e-12	49.5	28.10	± 0.12
J = 0.004966	1550	3.272	1.048e-02	3.387e-04	8.8	96.9	1.8e-12	49.6	28.14	± 0.40
disc = 296.5	1750	3.386	1.094e-02	1.100e-03	1.4	90.4	2.8e-13	47.5	27.18	± 2.57
faraday	total gas							48.9	28.18	
	plateau	1025-1750			98.8				28.12	± 0.10
85G006	750	5.691	3.035e-02	5.057e-03	4.3	73.7	6.3e-13	17.1	28.52	± 0.13
Bloodgood Canyon	1050	4.258	2.526e-02	5.000e-04	24.5	96.4	3.6e-12	20.6	27.94	± 0.08
wt = 0.2030	1150	4.195	2.348e-02	2.001e-04	39.4	98.5	5.8e-12	22.1	28.11	± 0.08
RD54	1550	4.679	2.017e-02	1.744e-03	31.8	88.9	4.6e-12	25.8	28.29	± 0.07
J = 0.003801	total gas							22.4	28.14	
disc = 299.2	plateau	1050- 1150			63.9				28.03	± 0.08
faraday										
nm435	700	6.623	1.553e-02	8.243e-03	3.1	63.2	5.3e-13	33.5	28.50	± 0.15
Diablo Range	1075	4.345	1.546e-02	7.756e-04	19.8	94.6	3.4e-12	33.6	28.02	± 0.08
wt = 0.2057	1250	4.210	1.521e-02	3.133e-04	28.2	97.7	4.8e-12	34.2	28.03	± 0.08
RD54	1450	4.215	1.521e-02	3.056e-04	42.6	97.7	7.3e-12	34.2	28.08	± 0.07
J = 0.003808	1550	4.606	1.541e-02	1.543e-02	6.3	90.0	1.1e-12	33.7	28.25	± 0.09
disc = 299.2	total gas							34.0	28.08	
faraday	plateau	1075- 1450			90.6				28.05	± 0.08
nm149a	650	7.386	2.219e-02	1.469e-02	2.7	41.2	1.5e-14	23.4	25.04	± 0.09
Shelley Peak	950	4.521	2.193e-02	3.568e-03	8.7	76.6	4.9e-14	23.7	28.47	± 0.08
wt = 0.1419	1050	4.147	2.076e-02	2.286e-03	9.8	83.6	5.5e-14	25.0	28.51	± 0.08
RD32	1125	4.074	2.087e-02	2.097e-03	12.8	84.7	7.1e-14	24.9	28.37	± 0.09
J = 0.004595	1200	4.042	2.018e-02	1.876e-03	15.8	86.2	8.8e-14	25.8	28.64	± 0.09
disc = 296.5	1275	4.026	1.969e-02	1.805e-03	17.4	86.6	9.7e-14	26.4	28.68	± 0.10
faraday	1400	3.853	1.973e-02	1.222e-03	27.0	90.5	1.5e-13	26.4	28.67	± 0.09
	1550	5.794	1.910e-02	7.489e-03	5.8	61.7	3.2e-14	27.2	29.40	± 0.09
	total gas							25.7	28.54	
	plateau	1200- 1400			60.2				28.67	± 0.08
nm149b	1125	4.227	2.101e-02	2.521e-03	40.2	82.3	7.9e-14	24.8	28.60	± 0.09
Shelley Peak	1400	3.927	1.975e-02	1.581e-03	50.8	88.0	1.0e-13	26.3	28.42	± 0.08
wt = 0.1419	1550	7.017	2.069e-02	1.198e-02	9.0	49.5	1.8e-14	25.1	28.55	± 0.08
RD32	total gas							25.6	28.50	
J = 0.004595	plateau	1125- 1550			100.0				28.52	± 0.09
disc = 296.5										
faraday										

APPENDIX 1, continued.

	temp	$^{40}Ar/^{39}Ar$	$^{37}Ar/^{39}Ar$	$^{36}Ar/^{39}Ar$	$\%^{39}Ar$	%rad	moles ^{39}Ar	K/Ca	age(Ma)	1σ error
nm319	750	6.319	2.248e-02	6.888e-03	3.2	67.7	6.1e-13	23.1	28.89	± 0.20
Garcia Camp	1025	4.343	2.088e-02	5.928e-04	20.5	95.9	3.9e-12	24.9	28.10	± 0.07
wt = 0.2126	1150	4.235	2.060e-02	2.647e-04	30.9	98.1	5.9e-12	25.2	28.03	± 0.08
RD54	1300	4.245	2.027e-02	2.354e-04	40.6	98.3	7.8e-12	25.7	28.15	± 0.07
J = 0.003771	1550	4.767	1.881e-02	2.010e-03	4.7	87.4	9.1e-13	27.7	28.13	± 0.11
disc = 299.2	total gas							25.4	28.13	
faraday	plateau	1025- 1300			92.1				28.10	± 0.09
nm116	900	7.032	1.632e-02	8.727e-03	4.3	63.3	2.7e-14	31.9	29.21	± 0.16
Taylor Creek Rhy.	1100	4.640	1.806e-02	1.317e-03	10.9	91.5	6.9e-14	28.8	27.88	± 0.08
wt = 0.1139	1200	4.570	1.789e-02	9.577e-04	14.6	93.7	9.2e-14	29.1	28.11	± 0.07
RD42	1300	4.600	1.785e-02	9.774e-04	18.8	93.6	1.2e-13	29.1	28.27	± 0.08
J = 0.003668	1450	4.680	1.794e-02	1.250e-03	35.5	92.0	2.2e-13	29.0	28.26	± 0.08
disc = 297.5	1550	5.475	1.784e-02	3.962e-03	15.8	78.5	1.0e-13	29.1	28.23	± 0.10
faraday	total gas							29.1	28.24	
	plateau	1220- 1550			84.7				28.23	± 0.10
85G003	700	5.611	2.752e-02	4.882e-03	2.7	74.2	4.6e-13	18.9	28.38	± 0.10
Taylor Creek Rhy.	1075	4.210	2.386e-02	3.773e-04	23.7	97.3	4.0e-12	21.8	27.90	± 0.09
wt = 0.2109	1250	4.182	2.232e-02	2.527e-04	43.5	98.1	7.3e-12	23.3	27.96	± 0.08
RD54	1450	4.260	2.157e-02	4.705e-04	24.5	96.6	4.1e-12	24.1	28.05	± 0.08
J = 0.003807	1550	4.819	2.074e-02	2.130e-03	5.6	86.8	9.4e-13	25.1	28.51	± 0.11
disc = 299.2	total gas							23.1	28.01	
faraday	plateau	1075- 1450			91.7				27.97	± 0.10
kjh10	650	6.015	4.845e-02	1.253e-02	3.5	38.4	3.8e-13	10.7	28.58	± 0.10
Vicks Peak	900	3.088	7.601e-03	2.597e-03	6.9	75.0	7.6e-13	68.4	28.66	± 0.09
wt = 0.0925	1000	2.788	1.511e-02	1.387e-03	6.0	85.1	6.7e-13	34.4	29.37	± 0.08
RD22	1100	2.617	9.280e-03	1.090e-03	10.2	87.5	1.1e-12	56.0	28.35	± 0.08
J = 0.006917	1200	2.504	5.580e-03	6.524e-04	14.7	92.1	1.6e-12	93.2	28.55	± 0.07
disc = 296.5	1300	2.555	1.250e-02	8.523e-04	15.2	89.9	1.7e-12	41.6	28.45	± 0.07
faraday	1550	2.425	1.211e-02	3.883e-04	43.5	95.1	4.8e-12	42.9	28.54	± 0.08
	total gas							43.2	28.57	
	plateau	950- 1350			73.4				28.51	± 0.08
nm143	650	5.771	1.295e-02	7.582e-03	5.6	61.1	2.3e-14	40.2	28.99	± 0.08
Vicks Peak	950	4.450	1.104e-02	3.348e-03	15.4	77.7	6.3e-14	47.1	28.42	± 0.08
wt = 0.1395	1050	4.279	1.031e-02	2.665e-03	10.8	81.5	4.4e-14	50.5	28.67	± 0.09
RD32	1125	3.979	1.212e-02	1.713e-03	19.5	87.2	7.9e-14	42.9	28.52	± 0.07
J = 0.004595	1200	4.032	1.135e-02	1.848e-03	18.5	86.3	7.5e-14	45.8	28.62	± 0.08
disc = 296.5	1275	4.288	1.085e-02	2.685e-03	14.3	81.4	5.8e-14	47.9	28.69	± 0.08
faraday	1400	4.138	1.093e-02	2.147e-03	10.2	84.5	4.2e-14	47.6	28.76	± 0.07
	1550	4.792	1.080e-02	4.336e-03	5.7	73.2	2.3e-14	48.1	28.82	± 0.07
	total gas							46.1	28.63	
	plateau	1050- 1275			63.1				28.62	± 0.08

APPENDIX 1, continued.

	temp	$^{40}Ar/^{39}Ar$	$^{37}Ar/^{39}Ar$	$^{36}Ar/^{39}Ar$	$\%^{39}Ar$	%rad	moles ^{39}Ar	K/Ca	age(Ma)	1σ error
nm414	750	7.845	9.396e-03	1.183e-02	3.2	55.4	4.6e-13	55.3	29.33	± 0.24
Vicks Peak	1025	4.545	5.884e-03	1.065e-03	18.9	98.0	2.7e-12	88.4	28.51	± 0.08
wt = 0.1947	1150	4.432	6.504e-03	6.336e-04	41.9	95.7	6.1e-12	79.9	28.61	± 0.08
RD54	1300	4.651	6.298e-03	7.584e-04	30.1	95.1	4.4e-12	82.6	29.84	± 0.10
J = 0.003771	1550	5.782	7.564e-03	4.693e-03	5.9	75.9	8.6e-13	68.7	29.62	± 0.12
disc = 299.2	total gas							80.3	29.05	
faraday	plateau	1025- 1150			60.8				28.56	± 0.08
nm502	850	4.397	1.125e-02	4.014e-03	5.5	73.0	1.0e-12	46.2	28.89	± 0.57
Vicks Peak	1075	3.480	8.976e-03	8.789e-04	13.8	92.5	2.6e-12	57.9	28.99	± 0.37
wt = 0.1982	1200	3.539	9.379e-03	4.300e-04	24.7	96.4	4.6e-12	55.4	30.68	± 0.14
RD56	1350	3.522	1.046e-02	3.776e-04	51.4	96.8	9.6e-12	49.7	30.69	± 0.09
J = 0.005030	1550	3.615	1.074e-02	5.258e-04	4.5	95.7	8.5e-13	48.4	31.12	± 0.90
disc = 296.5	total gas							52.8	30.37	
faraday	plateau	1200- 1550			81.0				30.69	± 0.11
nm433	700	9.423	2.333e-02	1.755e-02	1.3	44.9	2.1e-13	22.3	28.89	± 0.52
Lookout Mountain	1050	4.438	1.579e-02	7.695e-04	46.4	94.8	7.4e-12	32.9	28.70	± 0.10
wt = 0.2064	1150	4.267	1.638e-02	2.566e-04	25.3	98.1	4.1e-12	31.7	28.56	± 0.08
RD54	1300	4.496	1.617e-02	9.460e-04	26.0	93.7	4.2e-12	32.2	28.74	± 0.09
J = 0.003812	1550	8.111	1.842e-02	1.273e-02	0.9	53.5	1.4e-13	28.2	29.63	± 0.56
disc = 299.2	total gas							32.2	28.69	
faraday	plateau	1050- 1300			97.8				28.67	± 0.12
nm441	750	6.940	1.378e-02	8.647e-03	4.4	63.1	7.5e-13	37.7	29.86	± 0.18
Lookout Mountain	1050	4.394	1.374e-02	6.225e-04	36.5	95.7	6.2e-12	37.8	28.67	± 0.09
wt = 0.2121	1150	4.299	1.449e-02	2.907e-04	31.0	97.9	5.3e-12	35.9	28.69	± 0.08
RD54	1300	4.396	1.455e-02	5.549e-04	24.1	96.2	4.1e-12	35.7	28.82	± 0.08
J = 0.003809	1550	5.743	1.443e-02	4.862e-03	4.0	74.9	6.8e-13	36.0	29.33	± 0.16
disc = 299.2	total gas							36.6	28.79	
faraday	plateau	1050- 1300			91.6				28.72	± 0.11
kjh4	900	3.601	1.862e-02	2.160e-03	16.7	82.2	1.9e-13	27.9	29.11	± 0.08
La Jencia	1000	3.078	1.830e-02	4.860e-04	19.2	95.2	2.2e-13	28.4	28.84	± 0.06
wt = 0.1001	1050	3.073	1.810e-02	4.706e-04	16.1	95.3	1.9e-13	28.7	28.83	± 0.07
RD20	1100	3.143	1.791e-02	7.003e-04	14.1	93.3	1.6e-13	29.0	28.86	± 0.07
J = 0.005499	1150	3.240	1.766e-02	1.052e-03	12.1	90.3	1.4e-13	29.4	28.79	± 0.09
disc = 296.5	1200	3.323	1.767e-02	1.320e-03	9.5	88.1	1.1e-13	29.4	28.82	± 0.07
faraday	1300	3.524	1.743e-02	1.823e-03	7.1	84.6	8.2e-14	29.8	29.33	± 0.09
	1450	4.104	1.788e-02	3.995e-03	5.3	71.1	6.1e-14	29.1	28.73	± 0.08
	total gas							28.8	28.91	
	plateau	1000- 1200			71.0				28.82	± 0.07

APPENDIX 1, continued.

	temp	$^{40}Ar/^{39}Ar$	$^{37}Ar/^{39}Ar$	$^{36}Ar/^{39}Ar$	$\%^{39}Ar$	%rad	moles ^{39}Ar	K/Ca	age(Ma)	1σ error
kjh5	900	3.769	1.956e-02	2.693e-03	11.20	78.8	1.2e-13	26.6	29.22	± 0.07
La Jencia	1000	3.150	1.917e-02	8.814e-04	12.80	91.6	1.3e-13	27.1	28.39	± 0.06
wt = 0.0931	1050	3.088	1.894e-02	5.431e-04	19.00	94.7	2.0e-13	27.5	28.77	± 0.08
RD20	1100	3.119	1.859e-02	6.262e-04	15.80	93.9	1.7e-13	28.0	28.84	± 0.07
J = 0.005499	1150	3.374	1.823e-02	1.516e-03	13.40	86.6	1.4e-13	28.5	28.75	± 0.07
disc = 296.5	1200	3.244	1.837e-02	1.022e-03	11.60	90.6	1.2e-13	28.3	28.91	± 0.08
faraday	1300	3.391	1.826e-02	1.649e-03	9.10	85.5	9.6e-14	28.5	28.53	± 0.06
	1450	4.034	1.864e-02	3.709e-03	6.90	72.7	7.3e-14	27.9	28.87	± 0.09
	total gas							27.8	28.78	
	plateau	1050- 1200			59.8				28.81	± 0.09
nm146a	650	10.927	1.841e-02	2.635e-02	1.7	28.7	8.0e-15	28.2	25.77	± 0.10
La Jencia	950	5.183	2.184e-02	5.870e-03	7.0	66.5	3.2e-14	23.8	28.29	± 0.07
wt = 0.1513	1050	4.580	2.196e-02	3.488e-03	9.1	77.4	4.2e-14	23.7	29.11	± 0.07
RD32	1125	4.225	2.162e-02	2.346e-03	14.9	83.5	6.9e-14	24.1	28.97	± 0.07
J = 0.004590	1200	4.155	2.156e-02	2.137e-03	14.4	84.7	6.7e-14	24.1	28.90	± 0.08
disc = 296.5	1275	4.140	2.142e-02	2.026e-03	15.5	85.4	7.2e-14	24.3	29.05	± 0.09
faraday	1400	4.003	2.150e-02	1.576e-03	23.2	88.3	1.1e-13	24.2	29.01	± 0.08
	1550	4.398	2.116e-02	2.925e-03	14.3	80.2	6.6e-14	0.0	28.98	± 0.08
	total gas							24.2	29.11	
	plateau	1125- 1550			82.3				28.98	± 0.08
nm146b	1000	5.604	2.196e-02	1.046e-02	15.1	53.1	2.2e-14	23.7	28.82	
La Jencia	1400	4.110	2.133e-02	1.989e-03	70.2	85.6	1.0e-13	24.4	28.89	± 0.07
wt = 0.1513	1550	5.742	2.164e-02	1.096e-02	14.7	51.9	2.1e-14	24.0	28.74	± 0.07
RD32	total gas							24.2	28.86	
J = 0.004590	plateau	1000- 1550			100.0				28.82	± 0.08
disc = 296.5										
faraday										
nm111	900	5.465	2.564e-02	3.722e-03	9.3	79.8	7.3e-14	20.3	28.82	± 0.09
La Jencia	1100	4.554	2.474e-02	6.571e-04	21.2	95.6	1.7e-13	21.0	28.78	± 0.07
wt = 0.1130	1200	4.496	2.319e-02	4.095e-04	20.2	97.2	1.6e-13	22.4	28.89	± 0.08
RD42	1300	4.484	2.293e-02	3.579e-04	24.2	97.5	1.9e-13	22.7	28.90	± 0.08
J = 0.003692	1450	4.542	2.221e-02	6.642e-04	19.0	95.6	1.5e-13	23.4	28.69	± 0.08
disc = 297.5	1550	4.929	2.106e-02	1.807e-03	6.0	89.1	4.7e-14	24.7	29.01	± 0.09
faraday	total gas							22.2	28.83	
	plateau	900- 1300			74.9				28.86	± 0.09
nm157	750	7.750	2.529e-02	1.155e-02	3.5	55.9	5.6e-13	20.6	29.56	± 0.17
Mud Hole	1025	4.606	2.110e-02	1.307e-03	27.0	91.5	4.3e-12	24.6	28.77	± 0.09
wt = 0.1895	1150	4.435	2.039e-02	5.751e-04	36.4	96.1	5.8e-12	25.5	29.07	± 0.13
RD54	1300	4.470	1.868e-02	5.965e-04	29.0	96.0	4.6e-12	27.8	29.26	± 0.08
J = 0.038124	1550	5.588	1.995e-02	4.081e-03	4.0	78.3	6.3e-13	26.1	29.86	± 0.09
disc = 299.2	total gas							25.7	29.09	
faraday	plateau	1150- 1300			65.4				29.16	± 0.11

APPENDIX 1, continued.

	temp	$^{40}Ar/^{39}Ar$	$^{37}Ar/^{39}Ar$	$^{36}Ar/^{39}Ar$	$\%^{39}Ar$	%rad	moles ^{39}Ar	K/Ca	age(Ma)	1σ error
nm96	1000	4.054	1.771e-02	1.680e-03	24.9	87.6	7.8e-14	29.4	29.04	± 0.08
Davis Canyon	1400	3.730	1.717e-02	5.628e-04	67.0	95.4	2.1e-13	30.3	29.10	± 0.08
wt = 0.0963	1550	4.537	1.708e-02	3.277e-03	8.1	78.6	2.6e-14	30.5	29.14	± 0.08
RD32	total gas							30.1	29.09	
J = 0.004569	plateau	1000- 1550			100.0				29.09	± 0.08
disc = 296.5										
faraday										
nm494	1150	3.350	1.209e-02	4.748e-04	40.2	95.8	4.2e-13	43.0	28.70	± 0.08
Davis Canyon	1250	3.344	1.221e-02	3.505e-04	27.6	96.9	2.9e-13	42.6	28.97	± 0.08
wt = 0.0535	1350	3.313	1.171e-02	2.867e-04	32.1	97.4	3.4e-13	44.4	28.86	± 0.08
RD56	total gas							43.3	28.83	
J = 0.004995	plateau	1250- 1350			60.0				28.93	± 0.10
disc = 296.5										
multiplier										
nm491	850	3.385	4.191e-02	6.216e-04	6.2	94.6	1.2e-12	12.4	28.83	± 0.49
L. Mineral Creek	1125	3.266	3.311e-02	1.862e-04	20.5	98.3	3.9e-12	15.7	28.90	± 0.19
wt = 0.1677	1225	3.305	2.702e-02	2.988e-04	25.9	97.3	5.0e-12	19.2	28.96	± 0.15
RD56	1350	3.316	2.324e-02	3.137e-04	33.5	97.2	6.4e-12	22.4	29.02	± 0.10
J = 0.005030	1550	3.335	2.417e-02	2.992e-04	13.9	97.3	2.7e-12	21.5	29.22	± 0.18
disc = 296.5	total gas							19.5	28.99	
faraday	plateau	850- 1550			100.0				29.01	± 0.10
nm496	1135	3.646	6.316e-02	5.450e-04	29.8	95.6	2.7e-13	8.2	31.34	± 0.09
Tadpole Ridge	1210	3.649	5.221e-02	5.047e-04	29.6	95.9	2.7e-13	10.0	31.48	± 0.11
wt = 0.0491	1250	3.726	4.634e-02	8.102e-04	20.6	93.6	1.9e-13	11.2	31.36	± 0.12
RD56	1270	3.763	4.606e-02	8.936e-04	14.8	93.0	1.4e-13	11.3	31.48	± 0.15
J = 0.005031	1325	3.816	4.179e-02	1.330e-03	5.2	89.7	4.8e-14	12.4	30.79	± 0.16
disc = 296.5	total gas							10.0	31.38	
multiplier	plateau	1135- 1270			95.0				31.39	± 0.11
nm200	900	5.475	9.299e-03	2.198e-03	8.6	88.0	1.2e-13	55.9	31.75	± 0.08
Caballo Blanco	1100	4.974	8.338e-03	5.825e-04	19.5	96.4	2.7e-13	62.4	31.60	± 0.08
wt = 0.1196	1200	4.959	8.415e-03	5.383e-04	20.7	96.7	2.9e-13	61.8	31.59	± 0.08
RD42	1300	4.973	8.127e-03	5.367e-04	24.3	96.7	3.4e-13	64.0	31.68	± 0.11
J = 0.003684	1450	5.059	8.320e-03	8.134e-04	22.1	95.1	3.1e-13	62.5	31.71	± 0.09
disc = 297.5	1550	6.661	8.670e-03	6.044e-03	4.7	73.1	6.5e-14	60.0	32.08	± 0.09
faraday	total gas							61.9	31.68	
	plateau	900- 1450			95.3				31.66	± 0.11

APPENDIX 1, continued.

	temp	$^{40}Ar/^{39}Ar$	$^{37}Ar/^{39}Ar$	$^{36}Ar/^{39}Ar$	$\%^{39}Ar$	%rad	moles ^{39}Ar	K/Ca	age(Ma)	1σ error
nm236	850	5.011	1.148e-02	5.048e-03	2.6	70.2	5.6e-13	45.3	31.52	± 0.65
Caballo Blanco	1150	3.671	8.485e-03	4.630e-04	27.9	96.3	6.1e-12	61.3	31.66	± 0.13
wt = 0.1541	1250	3.640	8.316e-03	3.862e-04	38.5	96.9	8.4e-12	62.5	31.58	± 0.09
RD56	1350	3.600	8.015e-03	1.902e-04	30.5	98.4	6.6e-12	64.9	31.75	± 0.11
J = 0.005010	1550	4.000	8.601e-03	8.447e-04	0.5	93.8	1.2e-13	60.5	33.60	± 3.61
disc = 296.5	total gas							62.4	31.66	
faraday	plateau	850- 1550			100.0				31.64	± 0.11
nm268	700	6.197	1.168e-02	5.087e-03	3.1	75.7	6.3e-13	44.5	31.93	± 0.11
Caballo Blanco	1075	4.784	8.288e-03	4.529e-04	23.4	97.1	4.8e-12	62.7	31.64	± 0.10
wt = 0.1954	1250	4.767	7.922e-03	3.688e-04	42.6	97.6	8.7e-12	65.6	31.69	± 0.08
RD54	1450	4.816	8.012e-03	4.757e-04	26.7	97.7	5.5e-12	64.9	31.81	± 0.08
J = 0.003809	1550	5.715	9.046e-03	3.411e-03	4.2	82.3	8.6e-13	57.5	32.03	± 0.13
disc = 299.2	total gas							63.4	31.73	
faraday	plateau	1075- 1450			92.7				31.71	± 0.12
nm478	700	5.972	1.122e-02	4.185e-03	3.0	79.2	6.3e-13	46.4	32.23	± 0.12
Caballo Blanco	1075	4.834	9.249e-03	7.121e-04	13.6	95.5	2.9e-12	56.2	31.47	± 0.09
wt = 0.2063	1250	4.736	8.670e-03	3.476e-04	25.9	97.7	5.5e-12	60.0	31.54	± 0.09
RD54	1450	4.754	8.530e-03	3.462e-04	48.8	97.7	1.0e-11	61.0	31.66	± 0.09
J = 0.003810	1550	4.911	8.718e-03	8.033e-04	8.8	95.1	1.9e-12	59.6	31.81	± 0.10
disc = 299.2	total gas							59.4	31.63	
faraday	plateau	1075- 1450			88.2				31.56	± 0.12
nm525	850	3.740	9.891e-03	8.697e-04	3.4	93.1	9.4e-13	52.6	31.32	± 0.79
Caballo Blanco	1140	3.557	8.230e-03	1.655e-04	14.7	98.6	4.1e-12	63.2	31.54	± 0.17
wt = 0.2005	1240	3.601	7.735e-03	3.089e-04	28.2	97.5	7.8e-12	67.2	31.56	± 0.10
RD56	1375	3.578	7.569e-03	1.665e-04	50.7	98.6	1.4e-11	68.7	31.73	± 0.09
J = 0.005028	1550	3.669	7.458e-03	2.414e-04	3.0	98.1	8.2e-13	69.7	32.36	± 1.19
disc = 296.5	total gas							66.9	31.66	
faraday	plateau	850- 1550			100.0				31.67	± 0.11
khj26	900	3.720	9.052e-03	1.474e-03	13.2	86.1	2.2e-13	57.4	32.23	± 0.10
Hells Mesa	1000	3.384	8.629e-03	3.432e-04	13.0	96.8	2.2e-13	60.3	32.22	± 0.09
wt = 0.0967	1050	3.418	8.274e-03	4.310e-04	15.3	96.1	2.6e-13	62.8	32.30	± 0.07
RD20	1100	3.389	8.099e-03	3.722e-04	12.6	96.6	2.1e-13	64.2	32.19	± 0.08
J = 0.005499	1150	3.429	8.136e-03	5.044e-04	11.6	95.5	2.0e-13	63.9	32.19	± 0.08
disc = 296.5	1200	3.469	8.029e-03	5.861e-04	11.8	94.9	2.0e-13	64.8	32.34	± 0.07
faraday	1250	3.577	8.117e-03	9.865e-04	8.7	91.7	1.5e-13	64.1	32.25	± 0.08
	1450	3.725	8.066e-03	1.492e-03	13.8	88.0	2.3e-13	64.5	32.23	± 0.10
	total gas							62.5	32.24	
	plateau	900- 1450			100.0				32.25	± 0.08

APPENDIX 1, continued.

	temp	$^{40}Ar/^{39}Ar$	$^{37}Ar/^{39}Ar$	$^{36}Ar/^{39}Ar$	$\%^{39}Ar$	%rad	moles ^{39}Ar	K/Ca	age(Ma)	1σ error
kjh26	650	4.234	3.491e-03	5.468e-03	3.6	61.7	1.0e-12	149.0	32.32	± 0.09
Hells Mesa	950	2.767	7.239e-03	5.851e-04	12.8	93.6	3.7e-12	71.8	32.02	± 0.08
wt = 0.1373	1050	2.699	5.805e-03	3.420e-04	18.4	96.1	5.4e-12	89.6	32.06	± 0.08
RD22	1150	2.656	5.001e-03	1.896e-04	21.7	97.7	6.3e-12	104.0	32.08	± 0.09
J = 0.006917	1250	2.687	5.089e-03	2.840e-04	19.6	96.7	5.7e-12	102.2	32.13	± 0.08
disc = 296.5	1350	2.728	7.616e-03	4.083e-04	15.1	95.4	4.4e-12	68.3	32.18	± 0.11
faraday	1450	3.014	3.442e-03	1.345e-03	8.0	86.6	2.3e-12	151.1	32.29	± 0.09
	1650	7.312	3.382e-02	1.568e-02	0.7	36.6	2.0e-13	15.4	33.09	± 0.22
	total gas							88.6	32.13	
	plateau	950- 1350			87.6				32.10	± 0.11
kjh26	700	6.080	1.393e-02	4.495e-03	3.0	78.1	6.7e-13	37.3	32.32	± 0.12
Hells Mesa	1075	4.798	9.163e-03	3.594e-04	23.0	97.7	5.1e-12	56.7	31.91	± 0.08
wt = 0.2023	1250	4.816	8.395e-03	3.856e-04	47.0	97.5	1.1e-11	61.9	31.98	± 0.08
RD54	1450	4.881	8.388e-03	5.590e-04	22.1	96.5	4.9e-12	62.0	32.08	± 0.08
J = 0.003808	1550	6.063	1.053e-02	4.613e-03	4.9	77.4	1.1e-12	49.4	31.97	± 0.11
disc = 299.2	total gas							55.4	32.00	
faraday	plateau	1075- 1450			92.1				31.99	± 0
kjh26	850	3.707	1.158e-02	5.064e-04	3.6	96.0	9.8e-13	44.9	31.82	± 0.24
Hells Mesa	1150	3.615	8.764e-03	1.388e-04	32.2	98.9	8.8e-12	59.3	31.93	± 0.11
wt = 0.2013	1250	3.682	8.344e-03	3.367e-04	38.0	97.3	1.0e-11	62.3	32.01	± 0.09
RD56	1325	3.679	8.248e-03	2.651e-04	24.9	97.9	6.8e-12	63.0	32.17	± 0.10
J = 0.004998	1550	3.830	7.714e-03	1.420e-03	1.3	89.0	3.5e-13	67.4	32.59	± 2.05
disc = 296.5	total gas							61.0	32.03	
faraday	plateau	850- 1250			73.8				31.99	± 0.11
kjh26-hfa	850	3.730	1.095e-02	4.258e-04	3.7	96.6	1.1e-12	47.5	32.22	± 0.55
Hells Mesa	1140	3.590	8.834e-03	8.092e-05	38.6	99.3	1.1e-11	58.9	31.88	± 0.10
wt = 0.2010	1240	3.596	8.151e-03	7.205e-05	30.5	99.4	8.9e-12	63.8	31.97	± 0.10
RD56	1375	3.622	8.140e-03	9.348e-05	26.9	99.2	7.9e-12	63.9	32.14	± 0.12
J = 0.005002	1550	4.401	9.800e-03	3.120e-03	0.3	79.1	7.9e-14	53.1	31.27	± 7.25
disc = 296.5	total gas							61.3	31.99	
faraday	plateau	850- 1240			72.8				32.03	± 0.11
kjh26-hfb	850	3.731	1.068e-02	4.518e-04	3.1	96.4	8.8e-13	48.7	32.18	± 0.45
Hells Mesa	1150	3.585	8.687e-03	4.626e-05	38.3	99.6	1.1e-11	59.9	31.94	± 0.10
wt = 0.2018	1250	3.596	8.070e-03	6.717e-05	31.7	99.4	8.8e-12	64.4	32.00	± 0.09
RD56	1325	3.614	7.841e-03	6.550e-05	26.2	99.5	7.3e-12	66.3	32.16	± 0.12
J = 0.005004	1550	3.724	9.112e-03	7.967e-04	0.7	93.7	2.1e-13	57.1	31.19	± 2.08
disc = 296.5	total gas							62.6	32.02	
faraday	plateau	850- 1550			100.0				32.01	± 0.11

APPENDIX 1, continued.

	temp	$^{40}Ar/^{39}Ar$	$^{37}Ar/^{39}Ar$	$^{36}Ar/^{39}Ar$	$\%^{39}Ar$	%rad	moles ^{39}Ar	K/Ca	age(Ma)	1σ error
kd1	900	3.843	9.032e-03	1.853e-03	14.9	85.6	1.5e-13	57.6	32.34	± 0.08
Hells Mesa	1050	3.372	8.441e-03	3.608e-04	27.1	96.7	2.8e-13	61.6	32.05	± 0.06
wt = 0.0576	1150	3.347	8.022e-03	2.324e-04	27.1	97.8	2.8e-13	64.8	32.17	± 0.08
RD20	1250	3.460	7.943e-03	5.724e-04	19.6	95.0	2.0e-13	65.5	32.30	± 0.09
J = 0.005499	1350	3.810	8.183e-03	1.837e-03	8.5	85.6	8.7e-14	63.5	32.07	± 0.08
disc = 296.5	1450	5.516	1.114e-02	7.469e-03	2.7	59.9	2.8e-14	46.7	32.48	± 0.09
faraday	total gas							62.1	32.19	
	plateau	1050- 1150			54.2				32.11	± 0.10
kbm3	650	5.454	2.159e-02	9.135e-03	3.5	50.4	1.1e-12	24.1	34.00	± 0.14
Hells Mesa	950	2.795	3.299e-02	5.391e-04	14.0	94.2	4.3e-12	15.8	32.55	± 0.06
wt = 0.1986	1050	2.658	7.585e-03	1.925e-04	23.1	97.7	7.0e-12	68.6	32.10	± 0.06
RD22	1150	2.714	8.116e-03	3.839e-04	26.4	95.6	8.0e-12	64.1	32.10	± 0.06
J = 0.006917	1250	2.691	5.228e-03	2.680e-04	28.3	96.9	8.6e-12	99.5	32.24	± 0.06
disc = 296.5	1450	3.242	7.616e-03	2.078e-03	3.9	80.9	1.2e-12	68.3	32.43	± 0.09
faraday	1550	6.039	4.000e-02	1.151e-02	0.9	43.6	2.7e-13	13.0	32.58	± 0.13
	total gas							45.7	32.28	
	plateau	1050- 1250			77.8				32.15	± 0.11
SU-4-77	750	7.228	4.985e-02	1.030e-02	1.1	57.8	2.1e-14	10.4	33.44	± 0.20
Hells Mesa	900	4.449	2.285e-02	1.341e-03	5.3	91.0	9.6e-14	22.8	32.40	± 0.09
wt = 0.1329	1000	4.329	1.490e-02	1.116e-03	18.1	92.3	3.3e-13	34.9	31.97	± 0.10
RD16	1050	4.512	1.112e-02	1.726e-03	19.2	88.6	3.5e-13	46.8	31.98	± 0.09
J = 0.004476	1100	4.897	1.025e-02	3.065e-03	14.0	81.4	2.5e-13	50.7	31.89	± 0.09
disc = 296.5	1150	4.987	9.851e-03	3.345e-03	27.2	80.1	4.9e-13	52.8	31.96	± 0.09
faraday	1200	8.495	1.024e-02	1.528e-02	15.0	46.8	2.7e-13	50.8	31.81	± 0.11
	total gas							53.8	31.97	
	plateau	1000- 1200			93.5				31.92	± 0.11
nm201	900	5.499	1.095e-02	1.572e-03	8.6	91.5	1.1e-13	47.5	33.14	± 0.09
Box Canyon	1100	5.269	1.008e-02	6.530e-04	17.2	96.2	2.2e-13	51.6	33.40	± 0.09
wt = 0.1126	1200	5.306	9.839e-03	7.149e-04	16.3	95.9	2.1e-13	52.9	33.52	± 0.09
RD42	1300	5.340	9.606e-03	8.420e-04	16.2	95.2	2.0e-13	54.1	33.50	± 0.10
J = 0.003686	1450	5.313	9.722e-03	6.949e-04	26.7	96.0	3.4e-13	53.5	33.61	± 0.09
disc = 297.5	1550	5.678	9.570e-03	1.877e-03	14.9	90.1	1.9e-13	54.3	33.71	± 0.09
faraday	total gas							52.7	33.52	
	plateau	1100- 1450			76.4				33.52	± 0.12
nm207	700	7.193	1.687e-02	7.487e-03	4.0	69.2	4.5e-13	30.8	33.87	± 0.15
Box Canyon	1075	5.275	1.096e-02	1.152e-03	20.6	93.4	2.3e-12	47.4	33.55	± 0.10
wt = 0.1005	1250	5.503	1.038e-02	1.923e-03	34.4	89.6	3.9e-12	50.1	33.55	± 0.09
RD54	1450	5.408	9.844e-03	1.576e-03	32.0	91.3	3.6e-12	52.8	33.60	± 0.11
J = 0.003808	1550	6.404	9.725e-03	4.765e-03	8.9	77.9	9.9e-13	53.5	33.97	± 0.14
disc = 299.2	total gas							49.4	33.61	
faraday	plateau	1075- 1450			87.1				33.57	± 0.09

APPENDIX 1, continued.

	temp	$^{40}Ar/^{39}Ar$	$^{37}Ar/^{39}Ar$	$^{36}Ar/^{39}Ar$	$\%^{39}Ar$	%rad	moles ^{39}Ar	K/Ca	age(Ma)	1σ error
nm232	700	6.109	1.498e-02	4.153e-03	2.0	79.8	4.7e-13	34.7	33.23	± 0.12
Box Canyon?	1075	5.015	1.030e-02	4.895e-04	20.4	97.0	4.7e-12	50.5	33.15	± 0.10
wt = 0.2080	1250	5.063	9.621e-03	5.506e-04	23.2	96.7	5.4e-12	54.1	33.35	± 0.09
RD54	1450	5.043	9.272e-03	4.829e-04	35.0	97.1	8.1e-12	56.1	33.35	± 0.09
J = 0.003812	1550	5.259	9.306e-03	1.095e-03	19.4	93.7	4.5e-12	55.9	33.59	± 0.10
disc = 299.2	total gas							53.7	33.36	
faraday	plateau	1075- 1450			78.6				33.29	± 0.14
nm234	700	6.158	1.327e-02	4.156e-03	1.9	80.0	4.5e-13	39.2	33.55	± 0.17
Box Canyon?	1075	4.991	9.788e-03	3.544e-04	19.1	97.8	4.4e-12	53.1	33.26	± 0.09
wt = 0.1996	1250	5.016	9.365e-03	2.679e-04	29.6	98.3	6.9e-12	55.5	33.60	± 0.10
RD54	1450	5.054	9.235e-03	3.733e-04	43.5	97.7	1.0e-11	56.3	33.64	± 0.10
J = 0.003812	1550	5.488	9.604e-03	1.864e-03	5.9	89.9	1.4e-12	54.1	33.60	± 0.10
disc = 299.2	total gas							54.9	33.55	
faraday	plateau	1250- 1450			73.0				33.62	± 0.10
nm297	700	6.945	1.126e-02	6.748e-03	6.9	71.2	1.1e-12	46.2	33.66	± 0.11
Box Canyon	1075	5.103	9.559e-03	7.050e-04	30.7	95.8	4.9e-12	54.4	33.28	± 0.09
wt = 0.1842	1250	5.039	9.540e-03	4.095e-04	50.8	97.5	8.1e-12	54.5	33.44	± 0.10
RD54	1450	6.214	1.084e-02	4.179e-03	7.6	80.0	1.2e-12	48.0	33.86	± 0.13
J = 0.003808	1550	6.197	1.168e-02	5.087e-03	4.0	75.7	6.3e-13	44.5	31.92	± 0.11
disc = 299.2	total gas							52.8	33.38	
faraday	plateau	1075- 1250			81.5				33.36	± 0.10
nm505	850	3.840	2.477e-02	3.798e-04	5.7	97.1	1.1e-12	21.0	33.51	± 0.43
Box Canyon	1150	3.765	2.434e-02	9.714e-05	31.3	99.2	5.9e-12	21.4	33.59	± 0.10
wt = 0.1981	1250	3.821	2.265e-02	2.521e-04	34.1	98.1	6.5e-12	23.0	33.65	± 0.10
RD56	1310	3.861	2.171e-02	3.593e-04	25.5	97.3	4.8e-12	24.0	33.74	± 0.11
J = 0.005028	1550	3.972	2.176e-02	5.539e-04	3.4	95.9	6.6e-13	23.9	34.24	± 0.38
disc = 296.5	total gas							22.6	33.67	
faraday	plateau	1150-1310			91.0				33.65	± 0.12
nm508	850	4.424	1.078e-02	2.262e-03	3.6	84.9	1.0e-12	48.2	33.77	± 0.54
Box Canyon	1150	3.829	9.783e-03	3.552e-04	21.5	97.3	6.0e-12	53.2	33.49	± 0.12
wt = 0.2017	1240	3.768	9.816e-03	2.795e-04	9.7	97.8	2.7e-12	53.0	33.14	± 0.18
RD56	1325	3.771	9.449e-03	1.295e-04	63.0	99.0	1.8e-11	55.0	33.55	± 0.10
J = 0.005031	1550	3.852	9.326e-03	4.671e-04	2.1	96.4	6.0e-13	55.8	33.43	± 0.54
disc = 296.5	total gas							54.2	33.50	
faraday	plateau	1325-1550			65.1				33.55	± 0.12
nm240	900	5.654	1.883e-02	1.656e-03	10.1	91.3	1.4e-13	27.6	33.72	± 0.09
Blue Canyon	1100	5.259	1.765e-02	3.888e-04	21.1	97.7	2.8e-13	29.5	33.58	± 0.09
wt = 0.1300	1200	5.264	1.753e-02	4.009e-04	20.4	97.7	2.7e-13	29.7	33.59	± 0.09
RD42	1300	5.287	1.744e-02	4.144e-04	28.2	97.6	3.8e-13	29.8	33.71	± 0.10
J = 0.003656	1450	5.402	1.736e-02	6.808e-04	17.4	96.2	2.3e-13	30.0	33.95	± 0.09
disc = 297.5	1550	6.270	2.056e-02	3.333e-03	2.8	84.2	3.8e-14	25.3	34.50	± 0.13
faraday	total gas							29.3	33.72	
	plateau	900- 1300			79.8				33.64	± 0.11

APPENDIX 1, continued.

	temp	$^{40}Ar/^{39}Ar$	$^{37}Ar/^{39}Ar$	$^{36}Ar/^{39}Ar$	$\%^{39}Ar$	%rad	moles ^{39}Ar	K/Ca	age(Ma)	1σ error
nm328	1125	3.847	1.777e-02	2.878e-04	23.1	97.8	2.2e-13	29.3	33.74	0.10
Blue Canyon	1180	3.785	1.762e-02	1.501e-04	23.5	98.8	2.2e-13	29.5	33.56	0.09
wt = 0.1001	1205	3.810	1.728e-02	2.315e-04	18.9	98.2	1.8e-13	30.1	33.57	0.10
RD56	1235	3.832	1.754e-02	2.689e-04	10.1	97.9	9.5e-14	29.7	33.67	0.09
J = 0.005020	1260	3.829	1.723e-02	2.138e-04	11.7	98.3	1.1e-13	30.2	33.76	0.09
disc = 296.5	1290	3.838	1.729e-02	2.452e-04	10.5	98.1	9.9e-14	30.1	33.78	0.09
multiplier	1325	3.880	1.856e-02	4.416e-04	2.3	96.6	2.2e-14	28.0	33.63	0.11
	total gas							29.7	33.66	
	plateau	1125-1325			100.0				33.68	0.12
80-12-6a	650	5.747	1.917e-02	5.327e-03	3.3	72.5	2.2e-14	27.1	34.22	0.09
Blue Canyon	950	4.447	1.920e-02	1.034e-03	10.1	93.0	6.6e-14	27.1	33.97	0.09
wt = 0.1568	1050	4.372	1.891e-02	7.735e-04	9.7	94.7	6.4e-14	27.5	33.98	0.10
RD32	1125	4.316	1.898e-02	6.181e-04	15.0	95.7	9.8e-14	27.4	33.90	0.09
J = 0.004595	1200	4.319	1.882e-02	6.056e-04	14.7	95.8	9.7e-14	27.6	33.95	0.09
disc = 296.5	1275	4.314	1.883e-02	5.354e-04	12.3	96.2	8.0e-14	27.6	34.08	0.09
faraday	1400	4.297	1.868e-02	4.589e-04	22.4	96.7	1.5e-13	27.8	34.13	0.12
	1550	4.464	1.865e-02	9.779e-04	12.6	93.4	8.3e-14	27.9	34.24	0.09
	total gas							27.6	34.05	
	plateau	950- 1400			84.2				34.00	0.09
80-12-6b	1000	4.615	1.926e-02	1.585e-03	15.5	89.8	5.9e-14	27.0	34.01	0.09
Blue Canyon	1150	4.306	1.920e-02	5.888e-04	24.5	95.9	9.4e-14	27.4	33.89	0.09
wt = 0.1568	1275	4.257	1.875e-02	3.799e-04	38.0	97.3	1.5e-13	27.7	33.99	0.10
RD32	1400	4.410	1.871e-02	8.270e-04	18.0	94.4	6.9e-14	27.8	34.16	0.09
J = 0.004595	1550	5.819	1.855e-02	5.527e-03	4.0	71.9	1.5e-14	28.0	34.33	0.09
disc = 296.5	total gas							27.6	34.01	
faraday	plateau	1000- 1275			78.0				33.96	0.08
nm468	850	4.232	2.045e-02	1.371e-03	4.8	90.4	8.2e-13	25.4	34.34	0.34
Rockhouse Canyon	1150	3.898	1.763e-02	2.356e-04	34.0	98.2	5.8e-12	29.5	34.34	0.13
wt = 0.1491	1250	3.949	1.646e-02	3.938e-04	36.0	97.1	6.2e-12	31.6	34.38	0.11
RD56	1325	3.961	1.614e-02	3.668e-04	23.8	97.3	4.1e-12	32.2	34.56	0.12
J = 0.005020	1550	4.102	1.621e-02	1.463e-03	1.4	89.5	2.5e-13	32.1	32.94	1.71
disc = 296.5	total gas							30.7	34.39	
faraday	plateau	1150-1325			93.8				34.42	0.12
nm239	900	6.395	1.813e-02	3.744e-03	10.0	82.6	9.5e-14	28.7	35.04	0.09
Rockhouse Canyon	1100	5.536	1.586e-02	9.111e-04	19.2	95.1	1.8e-13	32.8	34.89	0.10
wt = 0.1034	1200	5.473	1.564e-02	7.481e-04	21.7	95.9	2.0e-13	33.3	34.79	0.09
RD42	1300	5.532	1.564e-02	8.642e-04	17.0	95.3	1.6e-13	33.2	34.96	0.09
J = 0.003711	1450	5.672	1.521e-02	1.377e-03	22.5	92.7	2.1e-13	34.2	34.88	0.10
disc = 297.5	1550	5.846	1.518e-02	1.832e-03	9.6	90.7	9.1e-14	34.3	35.14	0.09
faraday	total gas							32.9	34.92	
	plateau	1100- 1450			80.3				34.88	0.11

APPENDIX 1, continued.

	temp	$^{40}Ar/^{39}Ar$	$^{37}Ar/^{39}Ar$	$^{36}Ar/^{39}Ar$	$\%^{39}Ar$	%rad	moles ^{39}Ar	K/Ca	age(Ma)	1σ error
nm296	850	4.292	1.823e-02	1.916e-03	4.1	86.8	7.4e-13	28.5	32.74 ±	0.56
Table Mountain	1160	3.978	1.656e-02	3.996e-04	30.2	97.0	5.5e-12	31.4	33.92 ±	0.12
wt = 0.1498	1250	3.835	1.479e-02	6.872e-04	40.5	94.7	7.4e-12	35.2	34.06 ±	0.15
RD56	1350	4.036	1.516e-02	4.542e-04	24.6	96.7	4.5e-12	34.3	34.27 ±	0.12
J = 0.004917	1550	4.422	1.822e-02	9.421e-04	0.7	93.7	1.2e-13	28.5	36.30 ±	2.93
disc = 296.5	total gas							32.6	34.03	
faraday	plateau	1160-1250			70.7				33.96 ±	0.12
nm454	850	4.753	2.832e-02	2.951e-03	4.3	81.7	5.7e-13	18.4	34.62 ±	1.07
Mimbres Peak	1125	3.997	2.259e-02	4.689e-04	20.6	96.5	2.7e-12	23.0	34.40 ±	0.45
wt = 0.1338	1225	3.940	1.973e-02	2.921e-04	25.6	97.8	3.4e-12	26.4	34.39 ±	0.29
RD56	1350	3.963	1.856e-02	2.910e-04	42.4	97.8	5.7e-12	28.0	34.59 ±	0.12
J = 0.004992	1550	4.137	2.072e-02	8.109e-04	7.1	94.2	9.5e-13	25.1	34.76 ±	0.45
disc = 296.5	total gas							25.9	34.51	
faraday	plateau	850-1550			100.0				34.57 ±	0.12
nm231	700	6.641	5.182e-02	5.101e-03	10.0	77.3	1.2e-12	10.0	34.95 ±	0.12
Bishop Peak	1075	5.459	4.996e-02	1.241e-03	33.3	93.2	3.9e-12	10.4	34.67 ±	0.10
wt = 0.1539	1250	5.467	4.633e-02	1.237e-03	30.7	93.3	3.6e-12	11.2	34.74 ±	0.10
RD54	1450	5.576	4.508e-02	1.503e-03	20.1	92.0	2.3e-12	11.5	34.94 ±	0.09
J = 0.003812	1550	6.688	4.597e-02	5.244e-03	5.8	76.8	6.8e-13	11.3	34.98 ±	0.18
disc = 299.2	total gas							10.9	34.79	
faraday	plateau	1075- 1250			64.0				34.70 ±	0.10
nm92	850	4.533	8.582e-03	1.937e-03	3.4	87.4	9.5e-13	60.6	35.37 ±	0.72
Kneeling Nun	1160	4.031	8.426e-03	4.384e-04	26.3	96.8	7.4e-12	61.7	34.84 ±	0.11
wt = 0.2028	1260	4.055	8.244e-03	4.841e-04	43.4	96.5	1.2e-11	63.1	34.94 ±	0.10
RD56	1350	3.959	8.122e-03	2.192e-04	26.5	98.4	7.4e-12	64.0	35.14 ±	0.11
J = 0.004999	1550	4.564	5.665e-03	2.585e-03	0.5	83.3	1.4e-13	91.8	34.00 ±	6.30
disc = 296.5	total gas							63.0	34.97	
faraday	plateau	850-1260			73.0				34.90 ±	0.12
nm202	850	4.068	1.347e-02	2.968e-04	3.0	97.8	8.3e-13	38.6	35.64 ±	0.94
Kneeling Nun	1150	3.921	1.059e-02	1.188e-04	26.0	99.1	7.1e-12	49.1	34.80 ±	0.13
wt = 0.2000	1250	3.933	1.043e-02	1.441e-04	26.7	98.9	7.3e-12	49.8	34.84 ±	0.11
RD56	1350	3.934	1.015e-02	1.069e-04	43.3	99.2	1.2e-11	51.2	34.95 ±	0.10
J = 0.005013	1550	4.040	1.153e-02	1.044e-03	1.0	92.4	2.7e-13	45.1	33.52 ±	2.57
disc = 296.5	total gas							49.9	34.89	
faraday	plateau	850-1550			100.0				34.89 ±	0.12
nm208	750	6.062	1.120e-02	3.025e-03	6.2	85.2	1.3e-12	46.4	35.00 ±	0.11
Kneeling Nun	1050	5.249	8.672e-03	4.148e-04	20.9	97.6	1.4e-12	60.0	34.72 ±	0.09
wt = 0.1984	1250	5.271	8.224e-03	4.450e-04	32.9	97.4	7.0e-12	63.2	34.81 ±	0.11
RD54	1450	5.298	7.694e-03	4.624e-04	33.0	97.3	7.0e-12	67.6	34.96 ±	0.10
J = 0.003794	1550	5.712	9.070e-03	1.825e-03	7.0	90.5	1.5e-12	57.3	35.03 ±	0.12
disc = 299.2	total gas							62.0	34.87	
faraday	plateau	1050- 1450			86.8				34.83 ±	0.15

APPENDIX 1, continued.

	temp	$^{40}Ar/^{39}Ar$	$^{37}Ar/^{39}Ar$	$^{36}Ar/^{39}Ar$	$\%^{39}Ar$	%rad	moles ^{39}Ar	K/Ca	age(Ma)	1σ error
nm294	850	4.089	7.594e-03	7.651e-04	3.8	94.5	6.3e-13	68.5	34.70	± 0.69
Kneeling Nun	1150	3.909	7.907e-03	7.825e-05	26.9	99.4	4.4e-12	65.8	34.89	± 0.22
wt = 0.1144	1250	3.931	8.822e-03	2.399e-05	29.3	99.8	4.8e-12	58.9	35.08	± 0.26
RD56	1350	3.931	8.372e-03	1.228e-04	38.5	99.1	6.3e-12	62.1	34.96	± 0.15
J = 0.005025	1550	4.096	1.298e-02	8.952e-04	1.5	93.5	2.4e-13	40.1	34.43	± 1.86
disc = 296.5	total gas							62.1	34.96	
faraday	plateau	850-1550			100.0				34.96	± 0.13
nm498	850	3.985	9.114e-03	2.569e-04	6.3	98.1	1.7e-12	57.1	35.13	± 0.30
Kneeling Nun	1160	3.931	8.375e-03	7.686e-05	32.6	99.4	8.7e-12	62.1	35.11	± 0.10
wt = 0.2001	1240	3.973	8.475e-03	1.925e-04	30.9	98.6	8.2e-12	61.4	35.18	± 0.16
RD56	1340	3.967	8.184e-03	1.433e-04	28.6	98.9	7.6e-12	63.5	35.25	± 0.10
J = 0.005029	1550	4.049	8.520e-03	2.441e-04	1.5	98.2	4.1e-13	61.0	35.73	± 1.47
disc = 296.5	total gas							61.9	35.18	
faraday	plateau	850-1550			100.0				35.17	± 0.12
nm110	650	8.066	9.238e-03	1.231e-02	4.0	54.8	1.9e-14	56.3	36.29	± 0.10
Kneeling Nun	950	5.124	8.870e-03	2.780e-03	8.6	83.9	4.2e-14	58.6	35.27	± 0.09
wt = 0.1137	1050	4.885	8.549e-03	1.991e-03	8.1	87.8	4.0e-14	60.8	35.22	± 0.09
RD32	1125	4.655	8.544e-03	1.231e-03	12.3	92.1	6.0e-14	60.9	35.18	± 0.09
J = 0.004595	1200	4.679	8.578e-03	1.267e-03	16.3	91.9	8.0e-14	60.6	35.29	± 0.09
disc = 296.5	1275	4.628	8.515e-03	1.021e-03	14.1	93.4	6.9e-14	61.1	35.46	± 0.09
faraday	1400	4.591	8.483e-03	9.387e-04	18.2	93.8	8.9e-14	61.3	35.36	± 0.09
	1550	4.727	8.411e-03	1.426e-03	18.5	91.0	9.1e-14	61.8	35.30	± 0.09
	total gas							60.7	35.34	
	plateau	1200- 1550			67.1				35.35	± 0.12
nm465	850	3.927	9.790e-03	4.354e-04	3.1	96.7	6.8e-13	53.1	34.11	± 0.74
Kneeling Nun	1160	4.426	8.033e-03	7.687e-05	27.2	99.5	6.0e-12	64.7	39.45	± 0.12
wt = 0.1988	1240	4.892	7.499e-03	8.280e-05	33.3	99.5	7.4e-12	69.3	43.56	± 0.20
RD56	1550	5.980	7.239e-03	9.871e-05	33.9	99.5	7.5e-12	71.8	53.11	± 0.17
J = 0.005021	1550	6.699	7.578e-03	2.947e-05	2.5	99.9	5.6e-13	68.6	59.63	± 1.44
disc = 296.5	total gas							68.4	45.81	
faraday	no plateau									
nm206	850	6.277	5.011e-02	3.652e-03	12.0	82.8	1.6e-12	10.4	35.29	± 0.10
Bell Top tuff 4	1000	5.557	4.939e-02	1.381e-03	15.6	92.6	2.1e-12	10.5	34.96	± 0.11
wt = 0.2105	1250	5.340	4.735e-02	6.457e-04	39.8	96.4	5.4e-12	11.0	34.96	± 0.10
RD54	1450	5.420	4.646e-02	8.295e-04	27.4	95.4	3.7e-12	11.2	35.13	± 0.10
J = 0.003801	1550	6.487	4.708e-02	4.383e-03	5.3	80.0	7.2e-13	11.0	35.24	± 0.20
disc = 299.2	total gas							10.9	35.06	
faraday	plateau	1000- 1450			82.7				35.01	± 0.13

APPENDIX 1, continued.

	temp	$^{40}Ar/^{39}Ar$	$^{37}Ar/^{39}Ar$	$^{36}Ar/^{39}Ar$	$\%^{39}Ar$	%rad	moles ^{39}Ar	K/Ca	age(Ma)	1σ error
nm209	850	4.604	5.390e-02	2.533e-03	6.0	83.7	9.9e-13	9.6	34.50	± 0.90
Bell Top tuff 4	1150	4.059	5.026e-02	5.604e-04	26.4	95.9	4.4e-12	10.3	34.83	± 0.21
wt = 0.1977	1250	4.204	4.681e-02	1.012e-03	39.3	92.9	6.5e-12	11.1	34.93	± 0.13
RD56	1350	4.057	4.360e-02	4.887e-04	20.4	96.4	3.4e-12	11.9	35.00	± 0.16
J = 0.005007	1550	4.183	4.357e-02	8.313e-04	7.9	94.1	1.3e-12	11.9	35.22	± 0.40
disc = 296.5	total gas							11.1	34.91	
faraday	plateau	850-1550			100.0				34.94	± 0.12
nm501	850	4.900	4.617e-02	3.457e-03	5.9	79.2	1.2e-12	11.3	34.86	± 0.35
Bell Top tuff 4	1150	4.108	4.623e-02	7.497e-04	24.6	94.6	5.0e-12	11.2	34.94	± 0.13
wt = 0.2006	1250	4.244	4.141e-02	1.217e-03	39.1	91.5	8.0e-12	12.6	34.92	± 0.14
RD56	1300	4.258	4.082e-02	1.081e-03	27.2	92.5	5.5e-12	12.7	35.39	± 0.11
J = 0.005031	1550	4.516	4.289e-02	1.811e-03	3.2	88.1	6.4e-13	12.1	35.77	± 0.63
disc = 296.5	total gas							12.2	35.08	
faraday	plateau	1150-1250			63.8				34.93	± 0.12
nm460	850	4.376	3.155e-02	1.590e-03	3.9	89.3	7.8e-13	16.5	35.05	± 0.37
upper Sugarlump	1150	4.001	2.227e-02	3.389e-04	24.4	97.5	4.9e-12	23.4	35.00	± 0.13
wt = 0.2003	1250	4.109	2.176e-02	6.184e-04	34.5	95.6	6.9e-12	23.9	35.23	± 0.10
RD56	1550	4.052	2.122e-02	3.730e-04	34.8	97.3	7.0e-12	24.5	35.36	± 0.10
J = 0.005022	1550	4.195	2.234e-02	6.149e-04	2.4	95.7	4.8e-13	23.3	36.01	± 0.49
disc = 296.5	total gas							23.7	35.23	
faraday	plateau	1150-1250			58.9				35.17	± 0.12
nm238	900	6.150	4.185e-02	2.257e-03	10.7	89.1	9.7e-14	12.4	35.79	± 0.09
Farr Ranch	1100	5.588	4.236e-02	4.885e-04	20.2	97.4	1.8e-13	12.3	35.54	± 0.09
wt = 0.1129	1200	5.588	4.145e-02	5.632e-04	14.4	97.0	1.3e-13	12.5	35.39	± 0.09
RD42	1300	5.620	4.005e-02	5.693e-04	15.7	97.0	1.4e-13	13.0	35.58	± 0.10
J = 0.003656	1450	5.680	3.974e-02	7.463e-02	23.3	96.1	2.1e-13	13.1	35.64	± 0.10
disc = 297.5	1550	5.870	3.901e-03	1.388e-03	15.7	93.0	1.4e-13	13.3	35.64	± 0.09
faraday	total gas							12.8	35.59	
	plateau	1100- 1550			89.3				35.57	± 0.13
nm85a	900	5.184	4.222e-02	2.898e-03	20.2	83.4	9.1e-14	12.3	35.45	± 0.11
Datil Well	1050	4.767	4.192e-02	1.440e-03	25.9	91.0	1.2e-13	12.4	35.57	± 0.10
wt = 0.1440	1125	4.780	4.155e-02	1.511e-03	23.1	90.6	1.0e-13	12.5	35.50	± 0.09
RD32	1200	5.212	4.161e-02	2.902e-03	12.3	83.5	5.6e-14	12.5	35.68	± 0.09
J = 0.004590	1275	5.650	4.105e-02	4.337e-03	6.5	77.3	3.0e-14	12.7	35.79	± 0.10
disc = 296.5	1400	5.490	4.151e-02	3.815e-03	8.1	79.4	3.7e-14	12.5	35.74	± 0.10
faraday	1550	6.768	4.194e-02	8.105e-03	3.9	64.6	1.8e-14	12.4	35.82	± 0.10
	total gas							12.4	35.58	
	plateau	900- 1200			81.5				35.55	± 0.10

APPENDIX 1, continued.

	temp	$^{40}Ar/^{39}Ar$	$^{37}Ar/^{39}Ar$	$^{36}Ar/^{39}Ar$	$\%^{39}Ar$	%rad	moles ^{39}Ar	K/Ca	age(Ma)	1σ error
nm85b	900	6.249	4.182e-02	6.450e-03	12.8	69.5	3.8e-14	12.4	35.58 ±	0.12
Datil Well	1050	4.910	4.249e-02	1.983e-03	17.3	88.0	5.2e-14	12.2	35.42 ±	0.10
wt = 0.0983	1125	4.867	4.173e-02	1.841e-03	19.0	88.8	5.7e-14	12.5	35.42 ±	0.09
RD32	1400	4.812	4.137e-02	1.574e-03	42.3	90.3	1.3e-13	12.6	35.61 ±	0.13
J = 0.004590	1550	5.996	4.092e-02	5.472e-03	8.6	73.0	2.6e-14	12.7	35.87 ±	0.10
disc = 296.5	total gas							12.4	35.56	
faraday	plateau	900- 1400			91.4				35.51 ±	0.10
nm529	850	4.201	2.974e-02	7.790e-04	5.9	94.5	9.5e-13	17.5	35.55 ±	0.45
Squaw Mountain	1150	4.041	2.933e-02	1.997e-04	34.0	98.5	5.5e-12	17.7	35.66 ±	0.12
wt = 0.1984	1225	4.226	2.799e-02	7.445e-04	32.4	94.8	5.2e-12	18.6	35.87 ±	0.13
RD56	1375	4.899	2.748e-02	2.837e-03	20.1	82.9	3.2e-12	18.9	36.36 ±	0.23
J = 0.005013	1550	5.481	2.799e-02	4.596e-03	7.6	75.2	1.2e-12	18.6	36.91 ±	0.48
disc = 296.5	total gas							18.7	35.96	
faraday	plateau	850-1225			72.3				30.69 ±	0.11
nm483	850	4.667	3.552e-03	2.245e-03	8.1	85.8	1.5e-12	146.4	35.97 ±	0.51
Cueva	1150	4.278	3.128e-03	8.778e-04	46.9	93.9	8.9e-12	166.2	36.10 ±	0.11
wt = 0.2021	1225	4.278	3.277e-03	8.006e-04	28.6	94.5	5.5e-12	158.7	36.30 ±	0.11
RD56	1350	4.332	3.170e-03	1.098e-03	11.3	92.5	2.1e-12	164.0	35.99 ±	0.20
J = 0.005030	1550	4.687	3.695e-03	1.916e-03	5.1	87.9	9.7e-13	140.7	37.01 ±	0.23
disc = 296.5	total gas							160.9	36.18	
faraday	plateau	850-1350			95.0				36.20 ±	0.13
nm482	850	4.178	4.180e-03	5.429e-04	7.9	96.2	1.4e-12	124.4	36.01 ±	0.24
Cueva	1125	4.113	4.767e-03	3.455e-04	23.8	97.5	4.2e-12	109.1	35.94 ±	0.14
wt = 0.1985	1235	4.057	5.762e-03	5.099e-04	42.8	96.3	7.5e-12	90.3	35.01 ±	0.10
RD56	1375	4.197	4.714e-03	5.127e-04	23.6	96.4	4.1e-12	110.3	36.24 ±	0.15
J = 0.005017	1550	4.371	4.634e-03	1.686e-03	1.9	88.6	3.4e-13	112.2	34.68 ±	1.83
disc = 296.5	total gas							102.6	35.60	
faraday	no plateau									

APPENDIX 2—Site-mean paleomagnetic data from Mogollon–Datil ignimbrites. Units are listed in order of increasing age.

Explanation: demag is alternating field demagnetization level for site-mean data (PCA = directions determined by principal component analysis); n/nt denotes number of samples used in site mean/total or number of sites used in unit mean/total; inc, dec, and int are site-mean inclination, declination, and intensity; k is Fisher (1953) precision parameter; α_{95} is radius of cone of 95% confidence, type denotes demagnetization behavior: 1=TRM, 2=TRM+IRM, 3=TRM+CRM, 4=TRM+lithic-hosted components; letters following type number identify sites rejected from unit-mean calculations: R = α_{95}>10° and A = anomalous site-mean direction differing by >15° from unit-mean direction, following letter gives probable reason: Aa=possible miscorrelated unit, Ab=basal site in area of pre-eruptive topographic relief, Ac=local structural complexity and/or poor paleohorizontal indicators, Ad=tectonically extended area, Ae=unremoved CRM or IRM components, Af=secular variation recorded by thick intracaldera facies.

Unit name (age)	site	lat [°N]	long [°W]	dip	strike	demag [mT]	n/nt	inc	dec	intensity [A/m]	k	α_{95}	type	
* Turkey Springs	mean						15/19	-51.8	175.9		112	3.6		
(24.3 Ma)	024	33.931	107.334	22	332	30	7/8	-47.4	171.0	1.0e-01	345	3.3	1	
	025	33.930	107.333	22	332	40	6/8	-48.1	165.7	1.1e-01	275	4.1	1	
	055	33.761	107.425	32	120	30	8/8	-52.8	165.4	1.7e-01	369	2.9	2	
	137	33.719	107.812	0	0	30	5/8	-49.7	190.9	2.3e-01	449	3.6	2	
	183	33.840	107.715	6	200	40	7/8	-58.9	173.8	6.7e-02	139	5.1	2	
	185	33.681	107.795	4	180	30	8/8	-52.3	181.6	3.1e-01	747	2.0	1	
	186	33.682	107.791	4	180	30	8/8	-52.8	178.7	7.5e-02	521	2.4	1	
	199	33.744	107.429	10	330	30	8/8	-54.3	174.0	8.4e-02	2250	1.2	1	
	215	33.929	107.333	30	3	30	8/8	-57.7	191.1	2.3e-01	442	2.6	1	
	216	33.883	107.312	22	334	30	8/8	-43.3	168.4	1.9e-01	569	2.3	1	
	217	33.757	107.399	10	259	30	9/9	-49.2	161.8	1.1e-01	107	5.0	2	
	218	33.759	107.412	25	316	30	8/8	-51.1	173.3	9.5e-02	802	2.0	1	
	219	33.701	107.842	0	0	40	6/8	-53.8	197.9	1.0e-01	119	6.2	2	
	338	33.869	107.211	20	35	30	8/8	-47.2	180.9	4.6e-02	677	2.1	1	
	348	33.605	107.487	12	130	30	7/8	-52.5	169.8	1.7e-01	114	5.7	2	
	364	33.857	107.700	6	145	40	6/8	-37.4	189.3	7.5e-02	77	7.7	2	Aa
	424	33.799	107.275	8	0	40	6/8	-42.5	204.4	2.6e-01	231	4.4	2	Aa
	176	33.875	107.693	15	165	80	3/8	-41.1	171.7	3.0e-03	43	19.0	4	R
	184	33.840	107.713	6	200	40	8/8	-72.1	301.2	2.9e-01	1	180.0	4	R
* Slash Ranch	mean						2/3	57.6	166.9		371	13.0		
(26.1 Ma)	115	33.481	108.129	0	0	20	7/8	56.2	171.7	1.6e-02	68	7.4	1	
	471	33.472	108.119	0	0	20	8/8	58.9	161.8	8.7e-03	39	8.9	2	
	473	33.270	108.145	0	0	100	3/8	40.1	60.4	1.7e-03	9	43.6	4	R
South Canyon	mean outflow						15/20	-30.2	204.3		66	4.7		
outflow	mean outflow and thin intracaldera						24/33	-30.7	202.1		70	3.5		
facies	004	33.963	107.068	40	330	20	8/8	-32.9	189.3	5.9e-02	106	5.4	1	
(27.4 Ma)	007	34.144	107.002	35	150	20	7/8	-38.3	191.5	2.2e-02	195	4.3	2	
	036	34.156	106.828	43	185	30	7/8	-36.5	202.9	1.3e-01	237	3.9	1	
	105	33.898	106.986	30	302	20	8/8	-15.9	206.4	1.5e-01	76	6.4	1	
	138	33.743	107.793	0	0	30	6/8	-29.1	207.6	1.1e-01	471	3.1	1	
	187	33.687	107.768	4	180	40	6/8	-25.7	202.9	3.2e-02	782	2.4	1	
	188	33.686	107.763	4	180	30	8/8	-19.2	213.6	3.5e-02	59	7.3	1	
	197	34.006	106.664	42	180	30	8/8	-21.8	217.0	1.2e-01	379	2.9	1	
	250	33.745	107.903	0	0	30	8/8	-27.7	209.9	1.2e-01	343	3.0	2	
	251	33.772	107.903	0	0	40	8/8	-22.3	212.9	3.1e-02	218	3.8	2	
	252	33.773	107.902	0	0	30	8/8	-30.3	207.7	1.7e-01	274	3.4	1	
	258	33.410	107.904	8	180	30	9/9	-34.2	206.0	5.4e-02	162	4.1	1	
	380	34.158	107.942	0	0	40	8/8	-31.3	208.1	4.6e-02	152	4.5	2	
	515	33.987	107.574	0	0	30	6/9	-26.5	207.5	1.1e-02	141	5.7	2	
	008	34.152	107.004	35	150	20	7/8	-44.6	195.5	1.6e-01	298	3.5	2	A
	242	33.874	107.682	15	145	30	8/8	-9.0	236.7	1.5e-01	515	2.4	1	Ac
	013	34.156	106.826	33	195	30	8/8	-14.2	197.9	2.5e-01	18	13.5	2	R
	166	33.833	107.162	25	358	80	6/8	-38.0	202.3	2.4e-02	37	11.2	2	R

APPENDIX 2, continued.

Unit name (age)	site	lat [°N]	long [°W]	dip	strike	demag [mT]	n/nt	inc	dec	intensity [A/m]	k	α_{95}	type	
South Canyon	mean							-31.3	198.4		87	5.6		
southern	053	33.765	107.435	13	36	40	8/8	-23.0	192.8	3.2e-01	718	2.1	2	
intracaldera	058	33.791	107.406	22	5	40	8/8	-30.5	204.7	1.7e-01	706	2.1	1	
facies	060	33.789	107.388	9	355	30	8/8	-31.6	194.4	3.8e-01	61	7.1	2	
(27.4 Ma)	061	33.806	107.387	17	4	40	7/8	-22.2	188.0	5.9e-01	852	2.1	2	
	063	33.807	107.367	2	21	40	7/8	-37.2	211.1	3.0e-01	244	3.9	2	
	080	33.791	107.407	27	5	30	15/15	-27.6	199.7	2.1e-01	188	2.8	1	
	081	33.766	107.436	17	78	40	7/8	-34.6	197.1	2.5e-01	175	4.6	1	
	082	33.751	107.443	19	60	40	8/8	-35.4	206.8	1.0e-01	157	4.4	1	
	172	33.817	107.373	33	5	40	8/8	-38.0	192.7	1.7e-01	258	3.5	1	
	057	33.790	107.402	14	196	30	8/8	-28.1	182.6	1.7e-01	491	2.5	1	Af
	062	33.791	107.446	12	350	30	5/8	-29.2	172.9	1.1e-01	1612	1.9	2	Af
	047	33.733	107.346	9	329	30	8/8	-19.0	188.1	1.9e-02	5	29.2	4	R
	059	33.786	107.387	16	48	40	8/8	-42.8	174.0	7.6e-01	8	20.5	4	R
South Canyon	mean						12/12	-46.2	186.7		13	12.7		
northern	019	33.930	107.513	13	233	30	7/8	-56.9	156.5	7.9e-01	318	3.4	2	Af
intracaldera	020	33.934	107.511	11	260	30	8/8	-35.1	210.7	2.5e-01	378	2.9	1	Af
facies	023	33.929	107.337	22	345	40	6/8	-42.5	189.2	2.4e-01	156	5.4	1	
(27.4 Ma)	026	33.910	107.395	55	0	40	7/8	-67.8	186.2	8.1e-01	309	3.4	1	Af
	027	33.896	107.408	35	342	30	7/8	-45.0	171.5	2.3e-01	90	6.4	1	Af
	028	33.900	107.401	27	349	30	6/8	-64.4	189.0	3.2e-01	256	4.2	1	Af
	029	33.947	107.445	10	75	40	6/8	-58.0	254.6	5.5e-01	63	8.5	2	Af
	173	33.873	107.615	32	237	30	7/8	-17.3	180.4	8.0e-01	342	3.3	1	Af
	367	33.874	107.620	20	210	30	8/8	-26.9	176.6	2.0e+00	310	3.2	1	Af
	368	33.875	107.621	20	210	40	8/8	-30.4	170.2	1.9e-01	468	2.6	2	Af
	369	33.894	107.502	20	290	30	8/8	-58.2	197.9	8.5e-01	220	3.7	2	Af
	370	33.850	107.480	18	350	30	7/8	-27.5	186.2	4.4e-02	128	5.4	2	
* Walking X Canyon														
(27.6 Ma)	510	32.476	108.442	25	315	40	7/8	64.0	5.7	6.0e-02	334	3.3	1	
Lemitar	mean						10/21	36.6	356.9		128	4.3		
(28.0 Ma)	009	34.156	106.823	45	180	30	6/8	39.8	355.4	3.2e-02	136	5.8	1	
	021	33.950	107.502	22	85	30	6/8	45.1	0.9	3.7e-01	181	5.0	1	
	022	33.953	107.501	12	120	30	6/8	36.7	354.0	9.0e-02	120	6.2	2	
	046	33.737	107.349	16	336	40	8/8	31.7	348.4	9.3e-02	81	6.2	2	
	054	33.768	107.432	0	0	40	8/8	42.2	2.2	2.2e-01	33	9.7	3	
	056	33.784	107.438	17	349	PCA	8/8	30.3	352.0	9.0e-02	85	6.1	3	
	104	33.908	106.955	30	317	30	8/8	28.8	7.8	6.4e-01	149	4.6	2	
	161	33.774	107.127	5	333	40	8/8	32.9	358.4	7.8e-02	98	5.6	2	
	165	33.836	107.165	30	346	30	8/8	37.3	353.0	4.4e-01	164	4.3	1	
	198	34.007	106.663	42	180	30	8/8	40.4	358.0	6.3e-02	199	3.9	2	
	010	34.156	106.823	45	180	30	6/8	61.1	336.6	1.8e-01	180	5.0	1	A
	011	34.156	106.824	45	180	30	8/10	53.8	337.9	5.6e-01	88	6.0	1	A
	012	34.156	106.825	67	180	40	8/8	53.4	322.2	4.5e-01	639	2.2	1	A
	030	33.950	107.444	45	32	40	5/8	54.9	8.7	3.5e-01	109	7.4	2	A
	040	34.147	106.995	55	185	30	6/8	40.0	333.2	4.4e-02	412	3.3	1	A
	041	34.148	106.996	55	185	30	13/12	29.9	324.2	3.1e-01	31	7.6	3	A
	045	33.741	107.348	16	328	40	8/8	18.4	349.9	5.4e-01	269	3.4	1	A
	196	33.983	107.090	22	357	30	6/8	55.3	341.1	3.1e-02	347	3.6	1	Ac
	050	33.724	107.434	8	298	40	7/8	26.4	352.4	4.5e-01	32	10.9	3	R
	064	33.812	107.372	8	355	PCA	4/8	42.4	341.5	1.2e-01	67	11.3	3	R
	162	33.774	107.127	5	333	40	8/8	40.4	332.1	1.5e+00	4	34.3	2	R

APPENDIX 2, continued.

Unit name (age)	site	lat [°N]	long [°W]	dip	strike	demag [mT]	n/nt	inc	dec	intensity [A/m]	k	α_{95}	type	
* Caronita Canyon	mean						4/5	41.5	354.2		71	11.0		
(28.0 Ma)	167	33.847	107.184	24	2	30	8/8	40.6	3.1	1.4e-01	429	2.7	1	
	168	33.856	107.207	38	336	30	7/8	37.5	339.6	5.9e-01	609	2.5	1	
	195	33.982	107.091	22	357	30	6/8	38.6	352.3	5.6e-02	472	3.1	1	
	545	33.955	107.290	22	350	30	7/7	47.7	3.3	9.3e-02	45	9.1	2	
	543	33.960	107.250	28	5	30	6/6	62.2	334.5	2.0e-02	190	4.9	2	Ac
* Triangle C Ranch	mean						5/6	49.2	357.3		304	4.4		
(28.1 Ma)	140	33.625	108.181	0	0	40	8/8	49.1	2.9	2.0e-02	340	3.0	2	
	141	33.631	108.174	0	0	30	8/8	48.7	359.0	1.4e-02	175	4.2	1	
	142	33.629	108.174	0	0	80	6/8	55.5	357.5	2.9e-02	101	6.7	2	
	158	33.645	108.254	0	0	40	8/8	46.9	352.9	2.8e-02	268	3.4	2	
	160	33.571	108.205	0	0	35	8/8	45.4	354.6	1.8e-01	500	2.5	1	
	159	33.645	108.259	0	0	40	5/8	52.3	354.6	6.9e-03	42	11.9	2	R
Bloodgood Canyon	mean						22/23	-27.1	165.3		100	3.1		
(28.1 Ma)	078	33.818	108.355	5	130	40	8/8	-17.7	166.0	6.2e-02	90	5.9	1	
	094	33.935	108.425	0	0	40	7/8	-18.4	165.2	2.2e-01	208	4.2	1	
	095	33.747	108.722	16	220	40	8/8	-31.3	162.4	2.0e-01	999	1.8	1	
	101	33.540	108.935	13	190	40	7/8	-29.0	166.5	1.7e-01	288	3.6	1	
	112	33.601	108.056	5	170	30	7/8	-18.4	161.9	3.8e-02	208	4.2	2	
	114	33.616	108.039	2	112	30	7/8	-24.9	165.3	4.5e-02	711	2.3	2	
	139	33.625	108.181	0	0	40	8/14	-28.9	162.6	6.1e-01	1395	1.5	1	
	144	33.833	108.013	0	0	30	8/8	-16.4	163.0	4.2e-02	83	6.1	2	
	148	33.817	108.019	0	0	80	4/8	-23.7	157.8	6.1e-02	160	7.2	2	
	155	32.902	108.428	25	335	40	8/8	-39.5	158.5	8.0e-02	280	3.3	2	
	228	33.050	109.290	10	182	40	7/8	-27.6	165.3	1.8e-01	583	2.5	1	
	230	33.062	109.213	9	282	30	8/8	-26.9	173.3	2.5e-01	329	3.1	1	
	266	32.654	108.888	17	300	30	6/8	-28.5	180.2	1.2e-01	284	4.0	1	
	298	33.093	108.541	24	273	40	7/8	-24.1	175.0	3.2e-01	193	4.4	2	
	318	33.371	108.063	0	0	30	8/8	-30.1	158.7	2.2e-01	1206	1.6	1	
	332	33.670	108.007	0	0	40	8/8	-27.8	162.6	2.3e-01	343	3.0	2	
	428	33.006	108.316	0	0	30	7/8	-38.4	166.9	2.9e-01	93	6.3	1	
	429	32.985	108.202	0	0	40	7/8	-31.7	165.9	8.4e-02	209	4.2	2	
	430	32.976	108.219	0	0	40	8/8	-26.2	165.4	1.7e-01	365	2.9	1	
	431	33.153	108.199	8	270	10	9/9	-19.1	158.2	8.1e-02	611	2.1	1	
	432	32.982	108.207	8	270	30	8/8	-28.4	164.8	8.7e-02	369	2.9	2	
	514	32.820	108.993	16	22	30	5/11	-36.0	172.0	2.6e-01	152	6.2	2	
	153	33.080	108.760	30	135	40	8/8	-44.3	153.7	3.0e-01	196	4.0	1	Ac
Apache Springs	mean						2/2	-35.8	166.1		69	30.6		
(28.1 Ma)	259	33.371	108.721	25	160	30	8/8	-34.7	157.7	5.3e-01	100	5.6	1	
	486	33.272	108.410	0	0	30	6/8	-36.3	174.6	8.0e-02	344	3.6	2	
Shelley Peak	mean						8/10	-32.7	174.8		76	6.4		
(28.1 Ma)	077	33.818	108.355	5	130	30	8/8	-35.0	168.6	4.9e-01	201	3.9	2	
	100	33.539	108.934	14	140	30	8/8	-45.1	179.2	3.2e-01	204	3.9	1	
	149	33.770	108.183	0	0	100	3/8	-24.9	174.1	4.2e-01	318	6.9	2	
	262	33.079	108.498	14	295	40	8/8	-32.2	171.8	5.2e-01	60	7.2	2	
	299	33.092	108.551	24	273	30	5/8	-27.1	167.7	2.4e-01	65	9.6	1	
	301	33.092	108.553	24	273	30	6/8	-24.4	177.8	2.2e-01	167	5.1	1	
	492	33.692	108.990	10	200	30	8/8	-30.3	173.1	2.3e-01	254	3.5	1	
	504	33.718	108.783	15	307	30	8/8	-41.6	188.2	2.9e-01	201	3.9	1	
	149	33.770	108.183	0	0	100	3/8	-24.9	174.1	4.2e-01	318	6.9	2	
	303	33.187	108.568	8	310	40	7/8	-50.2	192.6	1.8e-01	200	4.3	2	Ae

APPENDIX 2, continued.

Unit name (age)	site	lat [°N]	long [°W]	dip	strike	demag [mT]	n/nt	inc	dec	intensity [A/m]	k	α_{95}	type	
* Garcia Camp	mean						7/7	-48.8	185.4		137	5.2		
(28.1 Ma)	113	33.601	108.055	5	170	20	8/8	-57.5	178.3	5.4e+01	125	5.0	1	
	227	33.622	108.003	5	95	40	8/8	-39.9	180.7	1.3e-01	873	1.9	1	
	319	33.473	107.860	0	0	30	8/8	-52.2	193.8	7.5e-02	409	2.7	1	
	333	33.661	108.003	0	0	30	7/8	-53.3	190.4	1.5e-01	130	5.3	2	
	334	33.648	107.980	0	0	30	9/8	-44.2	184.7	4.9e-02	371	2.7	1	
	335	33.623	107.986	0	0	80	7/8	-45.4	184.6	1.7e-02	206	4.2	2	
	337	33.597	108.055	0	0	30	8/8	-48.5	185.8	4.8e-01	745	2.0	1	
Vicks Peak	mean						24/32	-27.9	182.8		84	3.3		
(28.6 Ma)	037	34.156	106.822	35	180	30	6/8	-13.8	180.9	8.2e-02	149	5.5	2	
	068	33.996	106.656	60	160	40	7/8	-29.6	185.1	2.5e-01	307	3.5	2	
	075	33.641	107.725	12	120	40	8/8	-38.4	177.5	5.3e-02	621	2.2	2	
	097	33.739	108.700	20	212	30	8/8	-34.3	182.9	7.8e-02	225	3.7	1	
	098	33.739	108.700	20	212	40	8/8	-32.5	184.3	2.3e-02	208	3.9	1	
	108	34.203	106.817	30	182	40	7/8	-21.6	183.6	3.9e-02	691	2.3	2	
	109	34.235	106.815	41	187	30	8/8	-27.4	180.0	2.2e-01	191	4.0	1	
	119	33.870	106.933	33	2	40	6/8	-20.3	187.5	9.4e-02	459	3.1	1	
	143	33.833	108.014	0	0	40	8/8	-33.5	191.8	1.7e-01	183	4.1	2	
	147	33.817	108.020	0	0	40	8/8	-31.0	177.8	1.0e-01	390	2.8	2	
	163	33.773	107.144	14	22	40	8/8	-20.5	181.2	2.0e-02	247	3.5	2	
	171	33.738	107.352	16	336	40	8/8	-23.1	172.6	5.5e-01	823	1.9	1	
	182	33.879	107.742	5	0	100	5/8	-23.5	184.5	1.7e-2	61	9.8	2	
	190	33.691	107.749	8	160	40	8/8	-24.1	175.3	4.0e-02	419	2.7	1	
	243	33.880	107.683	15	145	40	8/8	-30.6	198.0	2.1e-01	204	3.9	1	
	248	33.744	107.866	2	192	40	8/8	-20.0	180.5	3.4e-02	235	3.6	2	
	315	33.351	107.512	30	335	40	8/8	-19.9	180.0	7.3e-02	595	2.3	1	
	325	33.880	108.265	0	0	30	8/8	-27.2	187.2	1.1e-01	1002	1.8	1	
	345	33.790	107.165	40	330	40	7/8	-24.9	176.6	3.5e-02	152	4.9	2	
	361	33.557	107.406	0	0	30	5/8	-36.1	177.6	2.0e-01	130	6.8	1	
	381	34.161	107.936	0	0	40	8/8	-33.1	187.7	9.6e-02	542	2.4	1	
	408	33.251	107.626	14	40	30	7/8	-32.5	198.5	2.8e-02	81	6.8	1	
	414	32.891	107.224	10	0	40	8/8	-35.2	170.7	5.2e-02	331	3.1	1	
	502	33.771	108.687	11	222	30	8/8	-33.5	187.7	2.9e-02	720	2.1	1	
	006	34.146	106.993	75	174	20	5/8	-24.6	150.5	1.2e-01	122	7.0	1	A
	048	33.737	107.364	9	329	30	8/8	-46.6	146.0	1.8e-02	300	3.2	2	A
	133	34.409	106.681	10	212	40	8/8	-42.3	163.4	1.1e-01	51	7.8	2	A
	175	33.880	107.685	24	135	40	8/8	-44.3	180.9	6.8e-02	559	2.4	1	A
	344	33.790	107.164	40	330	40	8/8	-17.1	168.5	1.3e-01	206	3.9	2	Aa
	351	33.552	107.503	20	132	30	8/8	-32.8	153.3	2.3e-01	227	3.7	1	A
	389	33.571	107.396	15	0	30	7/8	-46.3	173.7	4.5e-03	47	8.9	2	A
	394	33.536	107.431	15	0	80	4/8	-34.1	181.6	3.5e-03	54	12.6	2	R
* Lookout Mountain														
(28.7 Ma)	441	33.354	107.823	10	180	40	8/8	-55.4	160.8	8.6e-02	1383	1.5	1	
La Jencia	mean						15/24	-49.3	168.2		112	3.6		
(28.9 Ma)	016	34.157	106.818	28	180	40	7/8	-45.6	167.0	1.6e-02	358	3.2	2	
	018	34.155	106.819	28	180	100	6/8	-58.4	167.7	8.4e-02	122	6.0	2	
	034	34.156	106.821	35	180	30	7/8	-57.6	163.4	4.4e-01	74	7.1	1	
	049	33.738	107.372	7	353	30	8/8	-57.1	161.2	1.3e-01	1132	1.7	1	
	067	33.983	106.677	60	160	30	8/8	-48.3	167.4	7.8e-01	319	3.1	1	
	074	33.641	107.722	5	300	30	8/8	-41.3	165.5	1.1e-01	261	3.4	1	
	111	33.412	107.888	14	197	40	8/8	-45.3	168.6	5.9e-01	80	6.2	2	
	120	33.870	106.935	33	2	30	8/8	-45.7	176.0	3.1e-01	471	2.6	1	
	146	33.817	108.021	0	0	40	8/8	-39.1	161.9	1.8e+00	268	3.4	2	
	191	33.874	107.749	2	235	40	8/8	-54.4	168.5	7.4e-01	139	4.7	2	
	193	34.352	107.312	5	110	40	8/8	-55.8	167.2	1.5e-01	479	2.5	1	

APPENDIX 2, continued.

Unit name (age)	site	lat [°N]	long [°W]	dip	strike	demag [mT]	n/nt	inc	dec	intensity [A/m]	k	α_{95}	type
	194	34.351	107.311	5	110	30	7/8	-56.5	163.0	1.0e-01	500	2.7	1
	346	33.787	107.170	40	330	30	8/8	-46.6	181.7	1.1e-01	157	4.4	1
	352	33.543	107.459	36	325	30	6/8	-41.0	172.9	3.1e-02	160	5.3	2
	372	33.795	108.056	0	0	30	8/8	-44.4	167.6	1.2e+00	1647	1.4	1
	135	34.408	106.681	10	212	40	8/8	-45.7	146.5	7.5e-02	585	2.3	2 A
	005	34.145	106.992	99	158	40	2/8	-60.2	133.8	2.5e-02	460	11.7	1 R
	017	34.156	106.818	28	180	80	3/8	-40.4	155.6	3.0e-02	121	11.2	2 R
	032	34.244	106.998	40	172	50	3/10	-70.0	142.0	9.6e-03	144	10.3	1 R
	033	34.244	106.999	40	172	50	6/8	-51.3	122.6	4.1e-02	6	31.5	3 R
	076	33.640	107.722	5	270	40	5/8	-14.2	167.7	2.7e-03	5	36.9	4 R
	164	33.782	107.124	16	112	100	8/8	-68.2	195.0	1.7e-01	3	37.3	2 R
	247	33.893	107.628	16	70	40	8/8	-50.5	212.9	2.1e+00	5	26.2	2 R
	467	34.227	107.253	0	0	40	12/12	-40.9	161.4	3.0e-01	6	18.7	2 R
Davis Canyon	mean						6/7	53.9	159.6		81	7.5	
(29.0 Ma)	096	33.738	108.699	20	211	30	8/8	-53.2	157.7	2.7e-02	217	3.8	1
	261	33.079	108.498	5	310	40	8/8	-51.3	137.9	2.7e-01	192	4.0	2
	267	32.654	108.891	17	300	30	8/8	-56.0	169.0	6.1e-02	90	5.9	1
	493	33.696	108.976	10	200	50	8/8	-48.0	161.0	5.0e-01	964	1.8	1
	494	33.620	108.891	6	290	40	8/8	-49.9	174.4	2.4e-02	177	4.2	1
	503	33.772	108.686	11	222	10	8/8	-61.4	156.9	2.5e-02	289	3.3	2
	302	33.188	108.572	8	310	40	7/8	-18.3	184.8	3.4e-01	8	23.3	4 R
* Mudhole (29.1 Ma)	157	33.461	107.850	10	180	30	8/8	-55.9	124.5	2.8e-02	173	4.2	1
Stiver Canyon (approx. 29 Ma)	257	33.345	107.844	5	220	40	8/8	-52.7	172.6	4.1e-02	421	2.7	1
* Little Mineral Creek (29.0 Ma)	421	33.255	107.624	14	40	40	8/8	58.0	3.1	9.4e-02	459	2.6	1
* Monument Creek (approx. 29 Ma)	480	33.082	108.009	10	270	30	5/8	35.2	344.0	8.8e-02	363	4.0	1
* Pueblo Creek tuff 4 (approx. 30 Ma)	235	33.859	108.927	9	264	30	7/8	51.8	336.9	2.1e+00	148	5.0	2
Tadpole Ridge	mean						3/3	-23.3	185.2		58	16.3	
upper member	495	32.879	108.206	5	329	50	6/8	-31.3	185.1	2.0e-01	1087	2.0	1
(31.3 Ma)	496	32.879	108.206	5	329	50	8/8	-27.3	185.9	1.0e-01	2537	1.1	2
	506	32.902	108.214	0	0	30	8/8	-11.2	184.7	3.0e-01	172	4.2	1
Tadpole Ridge	mean						6/6	-71.1	203.8		38	11.0	
lower member	102	32.897	108.241	6	343	30	8/8	-72.2	190.2	1.3e+00	449	2.6	1
(approx. 31.3 Ma)	156	32.903	108.441	25	335	30	8/8	-71.0	159.1	4.6e-01	944	1.8	1
	477	33.071	108.002	9	260	30	8/8	-61.3	224.8	3.3e-01	141	4.7	1
	479	33.080	108.009	10	270	30	8/8	-69.4	243.3	1.9e+00	1233	1.6	2
	497	32.877	108.208	5	329	40	8/8	-70.9	232.3	5.3e-01	2635	1.1	1
	507	32.899	108.229	0	0	30	8/8	-63.7	169.5	3.8e-01	1190	1.6	1
Caballo Blanco	mean						6/8	-46.0	171.4		229	4.4	
(31.7 Ma)	128	33.067	107.999	3	197	30	9/9	-44.4	175.6	2.4e-01	378	2.7	1
	200	32.758	108.096	0	0	30	7/8	-46.3	168.7	7.0e-01	620	2.4	2
	236	33.827	108.327	2	190	30	6/8	-40.9	174.2	2.3e-01	167	5.2	2
	254	33.331	107.833	21	200	40	6/8	-43.1	161.9	1.3e-02	89	7.2	2
	268	32.649	108.888	10	310	30	6/8	-50.8	173.0	1.6e-01	126	6.0	2

APPENDIX 2, continued.

Unit name (age)	site	lat [°N]	long [°W]	dip	strike	demag [mT]	n/nt	inc	dec	intensity [A/m]	k	α_{95}	type	
Cooney	mean						3/3	-46.7	168.6		21	28.0		
(approx. 34 Ma)	079	33.384	108.816	13	115	40	8/8	-51.4	145.5	1.9e-01	160	4.4	2	
	229	33.058	109.229	8	317	40	8/8	-54.1	182.8	2.2e-01	190	4.0	1	
	305	33.376	108.834	0	0	30	8/8	-31.4	175.3	2.1e-02	750	2.0	1	
Rockhouse Canyon	mean						8/11	-55.6	144.8		105	5.4		
(approx. 34.4 Ma)	070	33.998	106.655	43	175	40	7/8	-55.6	162.9	5.6e-02	155	4.9	2	
	086	34.159	107.851	7	152	40	6/8	-50.1	144.2	4.5e-02	338	3.7	2	
	089	33.910	108.196	6	180	80	7/8	-54.5	141.8	2.4e-02	113	5.7	2	
	239	33.989	108.068	5	195	30	8/8	-56.8	145.7	2.5e-01	2067	1.2	1	
	371	33.796	108.056	0	0	40	7/8	-55.5	163.7	6.1e-02	491	2.7	1	
	403	33.463	107.812	13	140	40	8/8	-55.6	133.4	1.4e-01	823	1.9	1	
	439	33.905	108.197	3	120	30	8/8	-50.8	135.7	1.7e-01	279	3.3	2	
	468	34.306	107.633	15	135	30	8/8	-61.4	130.0	2.0e-01	201	3.9	1	
	517	33.938	107.617	21	202	30	6/8	-49.7	173.9	1.0e-01	606	2.7	2	Ac
	145	33.817	108.021	0	0	30	8/8	28.6	45.0	1.2e-02	2	69.1	3	R
	405	33.435	107.812	13	160	30	8/8	-35.4	151.8	1.1e-04	2	53.7	1	R
* Lebya Well	mean						4/4	-61.7	171.2		73	10.8		
(approx. 35 Ma)	088	33.911	108.194	6	145	40	8/8	-63.6	163.1	2.4e-01	234	3.6	2	
	231	33.973	108.981	4	274	40	8/8	-50.9	174.4	6.8e+00	397	2.8	1	
	438	33.905	108.195	3	120	30	8/8	-71.7	162.1	2.0e-01	101	5.6	2	
	436	33.957	108.219	0	0	40	5/8	-59.9	180.0	2.3e+00	79	8.7	2	
	404	33.434	107.812	13	160	40	7/8	-46.5	144.8	4.9e-02	102	6.0	1	Aa
Kneeling Nun	mean						21/28	-43.7	167.1		71	3.8		
(34.9 Ma)	092	33.916	108.198	3	122	40	8/8	-47.5	165.3	1.7e-01	96	5.7	2	
	103	32.850	107.888	40	152	30	8/8	-44.6	163.2	1.6e-01	113	5.2	1	
	110	33.466	107.807	12	180	20	6/8	-47.7	170.5	4.6e-02	299	3.9	1	
	118	33.331	107.746	0	0	20	8/8	-45.5	166.3	1.7e-01	259	3.5	1	
	123	32.487	107.133	5	250	30	8/8	-35.9	162.0	1.8e-01	168	4.3	1	
	126	32.835	107.595	13	322	30	8/8	-54.3	164.5	2.5e-01	47	8.2	2	
	179	33.386	107.719	0	0	30	8/8	-43.2	176.3	3.4e-02	889	1.9	1	
	202	32.761	108.094	0	0	30	8/8	-52.7	179.5	5.4e-01	171	4.2	1	
	208	32.556	107.077	7	225	40	8/8	-44.6	158.0	1.4e-01	42	8.7	3	
	210	33.293	107.630	18	25	PCA	8/8	-43.5	148.8	6.0e-01	88	5.9	3	
	256	33.344	107.821	8	195	30	8/8	-41.6	169.7	4.2e-01	488	2.5	1	
	294	32.588	107.920	0	0	10	8/8	-39.0	175.0	5.3e-01	515	2.4	1	
	295	32.597	107.966	0	0	40	8/8	-46.5	168.5	5.2e-01	850	1.9	1	
	314	33.355	107.516	24	0	PCA	7/8	-45.5	155.4	3.5e-01	78	6.9	3	
	324	33.921	108.205	9	110	40	7/8	-31.4	171.8	1.3e-01	43	9.3	2	
	374	33.901	108.202	2	300	30	8/8	-41.5	161.1	1.3e-01	401	2.8	2	
	383	33.985	108.160	0	0	30	4/8	-33.6	178.6	5.9e-02	290	5.4	2	
	416	32.892	107.227	10	0	40	8/8	-38.8	181.3	4.5e-01	515	2.4	1	
	420	33.274	107.604	11	111	PCA	5/8	-32.1	177.6	3.2e-01	550	3.3	3	
	456	32.680	107.841	8	42	30	8/8	-44.6	146.6	5.9e-03	246	3.5	2	
	465	34.157	108.240	2	135	40	8/8	-55.2	162.6	3.1e-02	142	4.7	2	
	127	32.806	107.521	15	175	30	8/8	-36.8	140.1	1.2e+00	177	4.2	1	Ac
	376	33.917	108.227	0	0	30	8/8	-31.5	153.7	1.8e-01	168	4.3	1	Ac
	498	32.887	108.291	30	204	30	8/8	-18.2	150.2	1.7e-01	464	2.6	1	Ac
	311	33.530	107.458	34	332	40	8/8	-75.7	138.9	1.2e-02	15	14.7	4	R
	384	33.995	108.172	0	0	30	8/8	41.3	297.7	3.1e-02	2	65.0	2	R
	412	33.271	107.629	8	194	40	4/8	66.5	29.3	8.9e-03	11	29.0	4	R
	413	33.271	107.629	8	194	40	4/8	-10.6	107.7	8.8e-04	2	36.3	2	R
* Stone House Ranch	mean						3/4	43.5	323.9		46	18.3		
(approx. 35.0 Ma)	177	33.382	107.712	10	130	30	8/8	52.2	325.1	1.6e-02	349	3.0	1	
	212	33.281	107.633	8	240	30	8/8	30.1	321.3	7.6e-02	64	7.0	1	

APPENDIX 2, continued.

Unit name (age)	site	lat [°N]	long [°W]	dip	strike	demag [mT]	n/nt	inc	dec	intensity [A/m]	k	α_{95}	type	
	213	33.284	107.635	8	240	30	7/8	48.1	326.2	3.7e-01	116	5.6	1	
	411	33.271	107.629	8	194	40	4/8	45.3	53.6	2.8e-02	12	28.1	2	R
Bell Top	mean						5/5	56.1	2.7		457	3.6		
tuff 4	125	32.508	107.145	8	285	40	8/8	54.4	5.9	2.0e+00	636	2.2	1	
(35.0 Ma)	206	32.532	107.106	3	280	100	5/8	58.9	5.3	3.9e-01	125	6.8	2	
	209	32.555	107.077	7	225	30	8/8	60.1	0.1	1.1e+00	970	1.8	1	
	211	33.280	107.633	8	240	PCA	7/9	55.4	1.8	2.1e-02	401	3.0	3	
	317	33.366	107.524	30	330	30	8/8	51.5	0.5	1.7e-01	618	2.2	2	
* Farr Ranch	mean						9/13	50.4	345.5		123	4.7		
(35.6 Ma)	065	33.767	107.436	15	162	30	6/8	50.0	347.7	5.4e-01	331	3.7	2	
	066	33.983	106.675	15	162	40	7/8	51.5	348.9	7.2e-01	482	2.8	2	
	071	33.998	106.654	43	175	40	8/8	52.8	354.0	4.5e-01	965	1.8	1	
	091	33.916	108.196	3	122	40	8/8	57.7	345.7	3.0e-01	423	2.7	2	
	308	33.499	107.418	19	293	30	8/8	43.7	337.9	1.4e-01	310	3.2	1	
	316	33.365	107.524	30	330	30	8/8	43.5	339.3	5.7e-01	302	3.2	1	
	388	33.492	107.409	10	0	30	8/8	60.7	347.6	9.2e-02	206	3.9	1	
	390	33.498	107.419	16	0	30	8/8	51.6	347.1	3.5e-01	410	2.7	1	
	437	33.974	108.213	0	0	40	7/8	41.1	344.7	5.9e-01	109	5.8	2	
	238	33.989	108.068	5	195	100	8/8	33.3	2.7	6.3e-02	39	8.9	2	Ae
	313	33.335	107.533	26	347	40	7/8	27.1	351.0	1.1e+00	157	4.8	1	Aa
	178	33.383	107.711	9	5	PCA	6/8	22.2	43.4	1.4e-02	28	12.8	3	R
	385	33.995	108.173	0	0	100	5/8	52.8	14.1	1.4e-01	11	24.3	2	R
Datil Well	mean						5/5	53.3	19.9		144	6.4		
(35.5 Ma)	085	34.160	107.845	7	152	40	7/8	49.4	15.5	8.3e-02	156	4.8	2	
	090	33.916	108.196	3	122	40	8/8	56.3	20.8	2.3e-01	647	2.2	2	
	237	33.989	108.067	5	195	35	7/8	45.6	15.1	8.9e-02	65	7.5	2	
	466	34.162	108.126	2	135	40	5/8	55.0	19.8	1.3e-01	488	3.5	2	
	481	33.307	107.021	9	272	100	8/8	59.6	31.3	6.9e-02	70	6.6	2	
Sugarlump tuffs	455	32.836	107.597	15	340	30	8/8	41.4	346.0	3.5e-01	338	3.0	1	
(approx. 35 Ma)	462	32.607	107.896	8	125	30	8/8	49.2	271.1	2.2e-01	250	3.5	2	E
	461	32.721	108.122	6	47	30	8/8	46.6	348.7	9.1e-01	1032	1.7	1	
	460	32.714	108.120	7	32	40	6/8	63.7	340.4	3.8e-02	166	5.2	2	
	509	32.482	108.464	28	315	30	7/8	60.9	335.2	1.2e-01	487	2.7	1	
Rubio Peak tuffs														
(approx. 35 Ma)	458	32.617	107.881	7	165	10	8/8	-40.1	166.5	6.9e-02	129	4.9	1	
	463	32.607	107.892	7	110	20	6/8	-63.8	152.6	2.2e-02	154	5.4	2	
* Steeple Rock tuffs	512	32.777	108.942	33	298	50	8/8	50.8	26.7	7.9e-03	141	4.7	2	
(approx. 35 Ma)	513	32.783	108.937	27	296	30	8/8	-62.1	159.9	1.4e-02	181	4.1	2	
Bell Top	mean						2/2	69.9	329.9		9000	1.6		
tuff 3	122	32.489	107.131	5	250	30	8/8	70.2	329.2	5.0e-02	123	5.0	2	
(35.7 Ma)	205	32.530	107.105	3	280	30	8/8	69.5	329.7	9.5e-02	302	3.2	2	
Bell Top	mean						2/2	39.7	350.0		210	17.3		
tuff 2	121	32.488	107.131	5	250	30	6/8	42.5	346.4	2.3e-01	61	8.6	2	
(>35.6 Ma)	204	32.529	107.105	3	280	30	8/8	36.7	353.4	7.0e-02	70	6.7	1	
Doña Ana	mean						2/2	54.4	155.3		29	48.5		
(35.5 Ma)	130	32.450	106.788	15	260	30	5/8	64.2	344.4	1.5e-02	146	6.4	1	
	203	32.437	106.838	19	165	30	8/8	44.4	329.7	1.2e+00	109	5.3	1	

APPENDIX 2, continued.

Unit name (age)	site	lat [°N]	long [°W]	dip	strike	demag [mT]	n/nt	inc	dec	intensity [A/m]	k	α_{95}	type
Squaw Mountain	mean						2/2	58.8	178.0		34	44.5	
(35.8 Ma)	417	32.289	106.598	46	158	30	7/8	66.9	10.5	1.4e-02	43	9.3	2
	529	32.295	106.607	44	162	30	9/9	49.9	350.4	1.6e-01	230	3.4	2
Achenback Park	mean						3/3	50.0	177.0		13	35.6	
(approx. 36 Ma)	418	32.284	106.594	44	170	30	7/9	47.0	321.6	7.2e-03	83	6.7	1
	419	32.285	106.584	43	162	30	9/9	51.3	0.1	6.7e-02	150	4.2	1
	484	32.235	106.602	26	215	40	8/8	42.1	26.1	1.1e-01	736	2.0	2
Cueva	mean						2/3	-53.4	220.3		4	67.8	
(36.2 Ma)	482	32.223	106.604	26	215	30	7/8	-67.1	208.4	6.1e-03	121	5.5	2
	485	32.223	106.600	26	215	30	8/8	-65.4	167.4	1.1e-02	99	5.6	1
	483	32.223	106.603	26	215	40	8/8	-12.2	245.2	2.9e-03	3	38.8	4 R
* local and/or	150	32.894	108.475	15	330	40	8/8	-43.1	134.8	1.5e-02	1	75.7	4 R
dome-related	151	32.896	108.473	15	330	30	8/8	-62.8	152.4	1.3e-01	538	2.4	2
units	152	32.898	108.471	15	330	30	8/8	-37.2	158.3	1.9e-01	148	4.6	2
(35 - 28 Ma)	174	33.947	107.675	14	197	40	6/9	28.2	320.8	3.2e-03	84	7.4	2
	214	33.274	107.673	14	155	30	8/8	-1.5	245.8	3.1e-03	1	76.9	4 R
	220	33.593	107.813	0	0	30	8/8	-55.4	146.6	1.2e-01	471	2.6	2
	221	33.590	107.845	0	0	30	8/8	-49.5	207.0	4.7e-02	1004	1.8	2
	222	33.571	107.838	15	182	30	8/8	-62.7	120.9	6.3e-02	417	2.7	1
	223	33.578	107.853	10	167	30	8/8	-52.5	184.0	9.2e-02	200	3.9	1
	224	33.583	107.858	10	187	30	6/8	-56.2	197.0	4.3e-02	238	4.4	1
	225	33.547	107.857	15	207	30	8/8	-44.8	177.5	6.0e-01	590	2.3	1
	264	32.651	108.893	18	320	40	8/8	-30.7	193.7	3.5e-02	221	3.7	2
	265	32.650	108.893	18	320	2	6/8	60.3	26.9	2.8e-02	52	9.4	1
	307	32.903	108.442	18	307	40	7/8	-67.9	155.3	9.8e-03	48	8.8	2
	309	33.514	107.459	20	208	30	2/4	33.8	20.5	2.4e-04	23	54.3	4 R
	320	33.525	107.422	18	305	40	6/8	-44.3	159.5	4.6e-01	70	8.1	2
	323	33.525	107.422	24	295	30	8/8	-30.8	160.3	7.8e-03	69	6.7	2
	327	33.903	108.228	2	90	40	8/8	-37.5	181.4	5.6e-01	334	3.0	2
	330	33.989	108.244	3	157	0	8/8	-68.2	50.1	8.0e-02	2	47.9	4 R
	340	33.869	107.202	43	342	35	4/4	-38.0	168.5	8.3e-03	121	8.5	2
	341	33.867	107.202	43	342	100	4/4	-53.2	52.6	1.9e-03	1	180.0	4 R
	342	33.866	107.202	43	342	60	4/4	-47.1	182.4	4.1e-04	8	35.4	4 R
	347	33.755	107.684	30	270	30	8/8	-34.4	175.1	5.3e+00	150	4.5	1
	360	33.556	107.406	0	0	40	8/8	-39.8	157.3	1.6e-02	17	13.7	2 R
	362	33.550	107.386	16	42	40	8/8	-34.9	153.1	1.9e+00	32	9.9	2
	365	33.942	107.644	18	260	35	6/4	-21.8	192.7	1.7e-03	7	27.3	4 R
	378	34.119	107.880	5	82	40	7/8	-47.9	182.3	1.5e+02	11	19.1	4 R
	382	34.125	107.926	4	40	40	2/8	-59.1	192.2	1.3e-02	23	55.4	4 R
	396	33.510	107.435	41	310	30	4/4	-59.5	69.6	2.1e-02	3	61.7	4 R
	398	33.509	107.436	41	310	40	6/8	56.7	328.2	4.7e-01	379	3.5	1
	425	33.859	107.305	13	42	30	4/4	19.0	200.6	1.3e-03	4	56.2	4 R
	427	33.853	107.297	13	42	2	4/4	-8.7	117.9	2.4e-01	15	24.8	4 R
	445	33.903	106.971	8	0	40	4/4	-4.5	302.1	1.1e-02	2	57.4	4 R
	448	33.908	106.958	0	0	40	4/4	-37.2	182.8	5.1e-02	8	34.5	4 R
	454	32.841	107.629	18	340	30	4/4	58.7	353.0	4.4e-01	1078	2.8	1
	457	32.673	107.840	5	343	30	8/8	40.6	67.8	3.0e-03	2	46.7	4 R
	475	33.142	108.439	24	276	50	4/4	-24.8	200.3	2.8e-01	494	4.1	2

APPENDIX 3—Site-mean paleomagnetic data from Mogollon–Datil lavas. Units are listed in order of increasing age.

Explanation: Second through fourth columns show age constraints provided by stratigraphically adjacent $^{40}Ar/^{39}Ar$-dated ignimbrites (abbreviations explained below); demag is alternating field demagnetization level for site-mean data; n/t denotes number of samples used in site mean/total samples; inc, dec, and int are site-mean inclination, declination, and intensity; k is Fisher's (1953) precision parameter; α_{95} is radius of cone of 95% confidence, type denotes demagnetization behavior: 1=TRM, 2=TRM+IRM; letter R following type number identifies sites with poor precision (α_{95}>15°).

Ignimbrite abbreviations: TS=Turkey Springs, SC=South Canyon, LM=Lemitar, VP=Vicks Peak, BG=Bloodgood Canyon, SP=Shelly Peak, LJ=La Jencia, LC=Little Mineral Creek, HM=Hells Mesa, SM=Squaw Mountain, BC=Blue Canyon, KN=Kneeling Nun, CB=Caballo Blanco, LP=Luna Park, DW=Datil Well.

Unit name	constrained age (Ma)	bracketing ignimbrites		site	lat [°N]	long [°W]	dip	strike	demag [mT]	n/t	inc	dec	intensity [A/m]	k	α_{95}	type
		under	over													
rhyolitic lavas																
unnamed	<24.3	TS		339	33.870	107.204	43	342	40	4/4	-43	179	0.09	839	3	2
unnamed	28.4–27.4	LM	SC	051	33.736	107.428	8	300	40	4/4	-30	181	0.05	513	4	2
unnamed	28.6–27.4	VP		249	33.746	107.885	0	0	40	4/4	46	348	0.20	185	7	2
unnamed	28.6–27.4	VP	SC	189	33.688	107.756	4	180	30	4/4	52	342	0.23	240	6	1
Rocky Canyon	<28.1	BG		474	33.112	108.006	15	270	30	4/4	38	11	0.07	770	3	1
Mojonera	<28.1	BG		442	33.332	107.762	10	180	40	3/4	43	250	0.05	611	5	2
unnamed	<28.1	BG		331	33.717	108.030	0	0	40	4/4	56	324	0.41	15	25	2 R
unnamed	<28.1	BG		489	33.273	108.407	0	0	50	4/4	64	289	0.06	121	8	2
Diablo Range	28.1	SP	BG	476	33.120	108.487	0	0	40	4/4	-47	172	0.10	697	3	2
Taylor Creek	28.1	LJ	SP	116	33.402	107.914	8	180	40	4/4	-58	151	0.92	175	7	1
Taylor Creek	28.1	LJ	SP	117	33.474	107.884	8	180	40	4/4	-44	159	0.04	2722	2	2
Taylor Creek	28.1	LJ	SP	336	33.623	107.990	0	0	40	4/4	-25	174	0.14	13	26	2 R
unnamed	28.9–28.1	LJ	SP	052	33.735	107.385	8	300	10	4/4	-28	174	0.04	472	4	2
unnamed	<28.6	VP		350	33.550	107.504	20	132	30	4/4	-52	135	0.09	890	3	1
unnamed	28.9–28.6	LJ	VP	241	33.945	107.665	0	0	40	4/4	11	165	0.03	2	77	4 R
unnamed	28.9–28.6	LJ	VP	245	33.904	107.686	15	145	30	4/4	-72	130	0.04	404	5	2
unnamed	28.9–28.6	LJ	VP	366	33.941	107.643	18	260	30	4/4	7	152	0.08	319	5	2
unnamed	28.9–28.6	LJ	VP	373	33.795	108.120	0	0	30	4/4	-46	169	0.17	65	11	2
unnamed	>28.6		VP	377	33.912	108.265	0	0	40	4/4	-24	172	0.32	7	39	2 R
Sawmill Pk.	29.0–28.9	LC	LJ	469	33.500	107.806	15	220	30	4/4	-24	221	0.01	6	40	2 R
Dolan Peak	29.0–28.9	LC	LJ	470	33.494	107.834	10	210	30	4/4	-41	197	0.10	838	3	2
unnamed	>29.0		LC	409	33.271	107.625	8	194	40	4/4	-54	180	0.05	38	15	2 R
Luis Lopez	32.1–28.9	HM	LJ	446	33.907	106.965	8	0	40	4/4	-67	102	0.11	186	7	1
Luis Lopez	32.1–28.9	HM	LJ	447	33.909	106.964	8	0	30	4/4	-74	127	0.19	62	12	1
Luis Lopez	32.1–28.9	HM	LJ	449	33.916	106.956	0	0	40	4/4	-30	165	0.18	11	29	2 R
Luis Lopez	32.1–28.9	HM	LJ	450	33.931	106.956	8	0	30	4/4	-57	108	0.04	188	7	1
unnamed	32.1–28.9	HM	LJ	072	33.701	107.280	15	300	20	4/4	-27	48	0.04	2	45	2 R
Western Lava	<35.8		SM	530	32.295	106.612	44	162	30	4/4	39	16	0.13	149	8	2
Hunt Mountain	>33.7		BC	357	33.509	107.430	26	315	40	6/6	-39	174	0.10	182	5	1
Mimbres Peak	34.9–31.6	KN	CB	452	32.917	107.651	17	10	30	4/4	71	358	0.11	275	6	1
Mimbres Peak	34.9–31.6	KN	CB	453	32.842	107.634	18	340	30	4/4	67	345	0.02	158	7	2
Mimbres Peak	34.9–31.6	KN	CB	459	32.992	107.888	25	170	40	4/4	2	205	0.67	436	4	1
Mimbres Peak	34.9–31.6	KN	CB	464	32.717	107.578	12	135	30	4/4	-61	169	0.01	438	4	2
Wildhorse	>34.9		KN	180	33.485	107.792	14	215	40	7/8	58	339	1.39	664	2	1
intermediate to mafic lavas																
Bearwallow	<24.3	TS		426	33.854	107.299	13	42	30	4/4	33	325	0.01	7	39	2 R
unnamed	27.3–24.3	SC	TS	363	33.869	107.688	6	145	40	4nd	59	328	0.06	9	32	2 R
La Jara Peak	28.0–27.3	LM	SC	035	34.156	106.825	67	180	40	6/8	66	324	0.81	48	10	2
unnamed	28.6–28.0	VP	BG	244	33.876	107.682	15	145	40	3/4	57	73	0.26	588	5	1
unnamed	28.6–27.3	VP	SC	326	33.878	108.263	0	0	40	4/4	-31	186	0.79	150	8	1
La Jara Peak	28.6–27.3	VP	SC	379	34.160	107.941	0	0	40	4/4	-34	174	0.14	41	15	2 R
unnamed	28.6–28.0	VP	BG	099	33.739	108.701	20	212	10	3/4	-56	151	0.65	276	7	1
La Jara Peak?	28.6	VP	VP	393	33.540	107.432	15	0	40	8/8	-59	207	2.71	6	25	2 R
La Jara Peak	<28.9	LJ		136	34.409	106.682	10	212	40	3/4	54	333	0.92	120	11	2 R
La Jara Peak	>28.9		LJ	353	33.543	107.459	36	325	30	4/4	44	354	0.13	47	14	1 R

APPENDIX 3, continued.

Unit name	constrained age (Ma)	bracketing ignimbrites		site	lat [°N]	long [°W]	dip	strike	demag [mT]	n/t	inc	dec	intensity [A/m]	k	α_{95}	type
		under	over													
Poverty Creek	31.6–29.0	CB	LC	440	33.462	107.845	10	180	40	4/4	74	340	1.03	1856	2	1
unnamed	32.1-28.8	HM	LJ	402	33.535	107.454	34	332	40	4/4	-46	172	0.09	194	7	2
Poverty Creek	31.6-29.0	CB	LC	410	33.271	107.630	8	194	30	4/4	-59	207	0.03	49	13	2 R
unnamed	32.1-28.8	HM	LJ	401	33.533	107.455	34	332	30	4/4	-72	157	1.02	116	9	2
Poverty Creek	31.6-29.0	CB	LC	407	33.435	107.828	13	160	40	3/4	-23	132	0.06	318	7	2
unnamed	32.1–28.8	HM	LJ	444	33.903	106.973	8	0	30	4/4	-38	146	0.20	587	4	2
unnamed	32.1–28.8	HM	LJ	400	33.531	107.457	34	332	40	4/4	67	24	4.11	1019	3	1
Poverty Creek	31.6–29.0	CB	LC	406	33.432	107.817	13	160	30	4/4	69	323	0.61	331	5	2
Spears	>32.0		HM	356	33.530	107.458	34	332	40	4/4	-66	173	0.79	165	7	2
Spears	<33.7	BC		043	34.162	106.811	52	207	10	4/4	-21	185	1.38	83	10	2
Spears	<33.7	BC		355	33.527	107.460	28	317	40	4/4	-56	157	3.73	146	8	2
Rock Springs	>33.7		BC	322	33.526	107.421	24	295	40	5/5	-30	103	0.23	9	27	2 R
Spears	>33.7		BC	044	34.162	106.810	52	207	30	6/4	-31	208	0.10	18	16	2 R
unnamed	>33.7		BC	310	33.524	107.463	25	267	40	4/4	-34	124	0.18	50	13	2 R
unnamed	>33.7		BC	358	33.510	107.430	26	315	40	3/4	-34	171	0.06	234	8	2
unnamed	35.6?–33.7	LP	BC	395	33.511	107.435	41	310	30	4/8	-1	148	2.90	2	87	2 R
unnamed	35.6?–33.7	LP	BC	359	33.504	107.429	15	25	40	3/4	60	293	0.25	26	25	3 R
unnamed	35.6?–33.7	LP	BC	397	33.510	107.436	41	310	40	3/4	30	333	0.12	38	20	2 R
unnamed	35.6?	LP	LP	391	33.497	107.420	16	0	30	4/4	74	184	4.44	1	180	3 R
unnamed	35.6?	LP	LP	392	33.498	107.420	15	0	40	4/4	74	307	2.16	5	45	3 R
Spears	>35.5		DW	087	34.155	107.847	7	152	40	4/4	71	313	0.07	4	50	2 R
unnamed	>35.6?		LP	399	33.493	107.451	34	332	30	4/4	42	20	0.06	13	26	2 R

References

Abitz, R. J., 1989, Geology and petrogenesis of the northern Emory Caldera, Sierra County, New Mexico: Unpublished PhD dissertation, University of New Mexico, Albuquerque, 174 pp.

Best, M. G., Shuey, R. T., Caskey, C. R., and Grant, S. K., 1973, Stratigraphic relations of members of the Needles Range Formation at type localities in southwestern Utah: Geological Society of America, Bulletin, v. 84, pp. 3269-3278.

Bogue, S. W., and Coe, R. S., 1981, Paleomagnetic correlation of Columbia River basalt flows using secular variation: Journal of Geophysical Research, v. 86, pp. 11883-11897.

Bornhorst, T. J., 1980, Major- and trace-element geochemistry and mineralogy of upper Eocene to Quaternary volcanic rocks of the Mogollon-Datil volcanic field, southwestern New Mexico: Unpublished PhD dissertation, University of New Mexico, Albuquerque, 1104 pp.

Bowring, S. A., 1980, The geology of the west-central Magdalena Mountains, Socorro County, New Mexico: New Mexico Bureau of Mines & Mineral Resources, Open-file Report 120, 135 pp., map, scale 1:24,000.

Cather, S. M., McIntosh, W. C., and Chapin, C. E., 1987, Stratigraphy, age, and rates of deposition of the Datil Group (Upper Eocene-Lower Oligocene), west-central New Mexico: New Mexico Geology, v. 9, pp. 50-54.

Chamberlin, R. M., 1983, Cenozoic domino-style crustal extension in the Lemitar Mountains, New Mexico: A summary: New Mexico Geological Society, Guidebook 34, pp. 111-118.

Chapin, C. E., and Seager, W. R., 1975, Evolution of the Rio Grande rift in the Socorro and Las Cruces areas: New Mexico Geological Society, Guidebook 26, pp. 297-322.

Chapin, C. E., Siemers, W. T., and Osburn, G. R., 1975, Summary of radiometric ages of New Mexico rocks: New Mexico Bureau of Mines & Mineral Resources, Open-file Report 60, ongoing data bank.

Clemons, R. E., 1976, Geology of the east half Corralitos Ranch quadrangle, New Mexico: New Mexico Bureau of Mines & Mineral Resources, Geologic Map 36, scale 1:24,000.

Dalrymple, B., Cox, A., and Doell, R. R., 1965, Potassium-argon age and paleomagnetism of the Bishop Tuff, California: Geological Society of America, Bulletin, v. 76, pp. 665-674.

Dalrymple, G. B., and Duffield, W. A., 1988, High-precision $^{40}Ar/^{39}Ar$ dating of Oligocene rhyolites from the Mogollon-Datil volcanic field using a continuous laser system: Geophysical Research Letters, v. 15, pp. 463-466.

Dalrymple, G. B., Alexander, E. C., Lanphere, M. A., et al., 1981, Irradiation of samples for $^{40}Ar/^{39}Ar$ dating using the Geological Survey, TRIGA reactor: U.S. Geological Survey, Professional Paper 1176, pp. 1-55.

Diehl, J. F., McClannahan, K. M., and Bornhorst, T. J., 1988, Paleomagnetic results from the Mogollon-Datil volcanic field, southwestern New Mexico, and a refined mid-Tertiary reference pole for North America: Journal of Geophysical Research, v. 93, pp. 4869-4879.

Donze, M. A., 1980, Geology of the Squaw Peak area, Magdalena Mountains, Socorro County, New Mexico (MS thesis): New Mexico Bureau of Mines & Mineral Resources, Open-file Report 123, 1-131 pp., map, scale 1:24,000.

Duffield, W. A., Richter, D. H., and Priest, S. S., 1987, Preliminary geologic map of the Taylor Creek Rhyolite, Catron and Sierra Counties, New Mexico: U.S. Geological Survey, Open-file Report 87-515, scale 1:50,000.

Eggleston, T. L., 1982, Geologic map of the Taylor Creek tin district, Black Range, New Mexico: New Mexico Bureau of Mines & Mineral Resources, Open-file Report Map 177, scale 1:24,000.

Elston, W. E., 1957, Geology and mineral resources of Dwyer quadrangle, Grant, Luna, and Sierra Counties, New Mexico:

New Mexico Bureau of Mines & Mineral Resources, Bulletin 37, 86 pp., map, scale 1:24,000.

Elston, W. E., 1984, Mid-Tertiary ash-flow tuff cauldrons, southwestern New Mexico: Journal of Geophysical Research, v. 89, pp. 8733-8750.

Elston, W. E., Damon, P. E., Coney, P. E., Rhodes, R. C., Smith, E. I., and Bikerman, M., 1973, Tertiary volcanic rocks, Mogollon-Datil province, and surrounding region: K-Ar dates, patterns of eruption, and periods of mineralization: Geological Society of America, Bulletin, v. 84, pp. 2259-2274.

Elston, W. E., Seager, W. R., and Clemons, R. E., 1975, Emory cauldron, Black Range, New Mexico: Source of the Kneeling Nun Tuff: New Mexico Geological Society, Guidebook 26, pp. 283-292.

Farkas, S. E., 1969, Geology of the southern San Mateo Mountains, Socorro and Sierra Counties, New Mexico: Unpublished PhD dissertation, University of New Mexico, Albuquerque, 137 pp.

Ferguson, C. A., 1986, Geology of the east-central San Mateo Mountains, Socorro County, New Mexico: New Mexico Bureau of Mines & Mineral Resources, Open-file Report 252, 1-135 pp., 4 maps, scale 1:24,000.

Finnell, T. L., 1976, Geologic map of the Twin Sisters quadrangle, Grant County, New Mexico: U.S. Geological Survey, Miscellaneous Field Studies Map MF-779, scale 1:24,000.

Finnell, T. L., 1982, Geologic map of the Dorsey Ranch quadrangle, Grant County, New Mexico: U.S. Geological Survey, Miscellaneous Field Studies Map MF-1431, scale 1:24,000.

Finnell, T. L., 1987, Geologic map of the Cliff quadrangle, Grant County, New Mexico: U.S. Geological Survey, Miscellaneous Investigations Map 1-1768, scale 1:24,000.

Fleck, R. J., Sutter, J. F., and Elliot, D. H., 1977, Interpretation of discordant $^{40}Ar/^{39}Ar$ age-spectra of Mesozoic tholeiites from Antarctica: Geochimica Cosmochimica Acta, v. 41, pp. 15-32.

Fodor, R. V., 1976, Volcanic geology of the northern Black Range, New Mexico: New Mexico Geological Society, Special Publication 5, pp. 68-70.

Grommé, C. S., McKee, E. H., and Blake, M. C., 1972, Paleomagnetic correlations and potassium-argon dating of middle Tertiary ash-flow sheets in eastern Great Basin, Nevada and Utah: Geological Society of America, Bulletin, v. 83, pp. 1619-1638.

Harrison, R. W., 1986, General geology of Chloride mining district, Sierra and Catron Counties, New Mexico: New Mexico Geological Society, Guidebook 37, pp. 265-272.

Harrison, R. W., 1990, Cenozoic stratigraphy, structure, and epithermal mineralization of north-central Black Range, New Mexico, in the regional framework of south-central New Mexico: Unpublished PhD dissertation, New Mexico Institute of Mining & Technology, Socorro, 386 pp., 7 plates.

Hedlund, D. C., 1978, Geologic map of the C-Bar Ranch quadrangle, Grant County, New Mexico: U.S. Geological Survey, Miscellaneous Field Studies Map MF-1039, scale 1:24,000.

Hedlund, D. C., 1990, Preliminary geologic map and sections of the Steeple Rock quadrangle, Grant and Hidalgo Counties, New Mexico: U.S. Geological Survey, Open-file Report, 90-0240, scale 1:24,000.

Hermann, M. L., 1986, Geology of the southwestern San Mateo Mountains, Socorro County, New Mexico: Unpublished MS thesis, New Mexico Institute of Mining & Technology, Socorro, 192 pp., map, scale 1:24,000.

Hildreth, W., and Mahood, G.,1985, Correlation of ash-flow tuffs: Geological Society of America, Bulletin, v. 96, pp. 968-974. Hoblitt, R. P., Reynolds, R. L., and Larson, E. E., 1985, Suitability of non-welded pyroclastic-flow deposits for studies of magnetic secular variation. A test based on deposits emplaced on Mount St. Helens, Washington, in 1980: Geology, v. 13, pp. 242-245. Holcomb, R., Champion, D., and McWilliams, M., 1986, Dating recent Hawaiian lava flows using paleomagnetic secular variation: Geological Society of America, Bulletin, v. 97, pp. 829-839.

Kedzie, L. L., 1984, High precision $^{40}Ar/39Ar$ dating of major ash-flow tuff sheets, Socorro, New Mexico: Unpublished MS thesis, New Mexico Institute of Mining & Technology, Socorro, 197 pp.

Krier, D. J., 1981, Geologic map of the southern part of the Gila Primitive Area, New Mexico: Unpublished MS thesis, University of New Mexico, Albuquerque, 58 pp., scale 1:24,000.

Kunk, M. J., Sutter, J. F., and Naeser, C. W., 1985, High-precision $^{40}Ar/39Ar$ ages of sanidine, biotite, hornblende, and plagioclase from the Fish Canyon Tuff, San Juan volcanic field, south-central Colorado: EOS, Transactions of the American Geophysical Union, v. 17, pp. 636.

Lopez, D. A., and Bornhorst, T. J., 1979, Geologic map of the Datil area, Catron County, New Mexico: U.S. Geological Survey, Miscellaneous Investigations Map 1-1098, scale 1:50,000.

Marvin, R. F., Naeser, C. W., Bikerman, M., Mehnert, H. H., and Raft& J. C., 1987, Isotopic ages of post-Paleocene igneous rocks within and bordering the Clifton 1° x 2° quadrangle, Arizona-New Mexico: New Mexico Bureau of Mines & Mineral Resources, Bulletin 118, 63 pp.

McIntosh, W. C., 1983, Preliminary results from a paleo- and rock-magnetic study of Oligocene ash-flow tuffs in Socorro County, New Mexico: New Mexico Geological Society, Guidebook 34, pp. 205-210.

McIntosh, W. C., 1989, Ages and distribution of ignimbrites in the Mogollon-Datil volcanic field: a stratigraphic framework using $^{40}Ar/^{39}Ar$ dating and paleomagnetism: Unpublished PhD dissertation, New Mexico Institute of Mining & Technology, Socorro, 311 pp.

McIntosh, W. C. (in press), Evaluation of paleomagnetism as a correlation criterion for Mogollon-Datil ignimbrites, southwestern New Mexico: Journal of Geophysical Research.

McIntosh, W. C., Sutter, J. F., Chapin, C. E., Osburn, G. R., and Ratté, J. C., 1986, A stratigraphic framework for the Mogollon-Datil volcanic field based on paleomagnetism and high-precision $^{40}Ar/^{39}Ar$ dating of ignimbrites - a progress report: New Mexico Geological Society, Guidebook 37, pp. 183-195.

McIntosh, W. C., Chapin, C. E., Ratté, J. C., and Sutter, J. F. (in press) Ages and distribution of ignimbrites in the Mogollon-Datil volcanic field, southwest New Mexico: a stratigraphic framework using $^{40}Ar/^{39}Ar$ dating and paleomagnetism: Geological Society of America, Bulletin.

McIntosh, W. C., Sutter, J. F., Chapin, C. E., and Kedzie, L. L., 1990, High-precision $^{40}Ar/^{39}Ar$ sanidine geochronology of ignimbrites in the Mogollon-Datil volcanic field, southwestern New Mexico: Bulletin of Volcanology, v.52, pp. 584-601.

Osburn, G. R., and Chapin, C. E., 1983a, Ash-flow tuffs and cauldrons in the northeast Mogollon-Datil volcanic field: a summary: New Mexico Geological Society, Guidebook 34, pp. 197-204.

Osburn, G. R., and Chapin, C. E., 1983b, Nomenclature for Cenozoic rocks of the northeast Mogollon-Datil volcanic field, New Mexico: New Mexico Bureau of Mines & Mineral Resources, Stratigraphic Chart 1, 7 pp., 1 sheet.

Ratté, J. C., 1989a, Direction-to-source indicators in Bloodgood Canyon Tuff and tuff of Triangle C Ranch at Coyote Well: New Mexico Bureau of Mines & Mineral Resources, Memoir 46, pp. 111-113.

Rate, J. C., 1989b, Geologic map of the Bull Basin quadrangle, Catron County, New Mexico: US. Geological Survey, Geologic Quadrangle Map GQ-1651, scale 1:24,000.

Raft& J. C., and Gaskill, D. L., 1975, Reconnaissance geologic map of the Gila Wilderness study area, southwestern New Mexico: U.S. Geologic Survey, Miscellaneous Investigations Map 1-886, scale 1:50,000.

Ratté, J. C., Marvin, R. F., and Naeser, C. W., 1984, Calderas and ash-flow tuffs of the Mogollon Mountains: Journal of Geophysical Research, v. 89, pp. 8713-8732.

Raft& J. C., McIntosh, W. C., and Houser, B. B., 1989, Geologic map of the Horse Springs West quadrangle: U.S. Geological

Survey, Open-file Report 89-210, scale 1:24,000.

Reynolds, R. L., 1977, Paleomagnetism of welded tuffs of the Yellowstone Group: Journal of Geophysical Research, v. 82, pp. 3677-3693.

Reynolds, R. L., Hudson, M. R., and Hon, K., 1986, Paleomagnetic evidence for the timing of collapse and resurgence of the Lake City Caldera, San Juan Mountains, Colorado: Journal of Geophysical Research, v. 91, pp. 9599-9613.

Rhodes, R. C., and Smith, E. I., 1976, Stratigraphy and structure of the northwestern part of the Mogollon Plateau volcanic province: New Mexico Geological Society, Special Publication 5, pp. 57-62.

Richter, D. H., 1978, Geologic map of the Spring Canyon quadrangle, Catron County, New Mexico: U.S. Geological Survey, Miscellaneous Field Studies Map MF-966, scale 1:24,000. Richter, D. H., Lawrence, V. A., Barton, H., Hanna, W., Duval, J. S., and Ryan, G. S., 1988, Mineral resources of the Gila Lower Box Wilderness study area, Grant and Hidalgo Counties, New Mexico: U.S. Geological Survey, Bulletin 1735-A, 13 pp. Rosenbaum, J. G., 1986, Paleomagnetic directional dispersion produced by plastic deformation ion a thick Miocene welded tuff, southern Nevada: Implications for welding temperatures: Journal of Geophysical Research, v. 91, pp. 12817-12834. Sampson, S. D., and Alexander, C. E., 1987, Calibration of the interlaboratory $^{40}Ar/^{39}Ar$ dating standard, Mmhb-1: Isotope Geoscience, v. 66, pp. 27-34.

Seager, W. R., 1981, Geology of the Organ Mountains and southern San Andes Mountains, New Mexico: New Mexico Bureau of Mines & Mineral Resources, Memoir 36, 97 pp., 4 sheets, scale 1:31,250.

Seager, W. R., and Mayer, W. R., 1988, Uplift, erosion, and burial of Laramide faults blocks, Salado Mountains, Sierra County, New Mexico: New Mexico Geology, v. 10, pp. 49-53.

Seager, W. R., and McCurry, M., 1988, The cogenetic Organ cauldron and batholith, south-central New Mexico: Evolution of a large-volume ash-flow cauldron and its source magma chamber: Journal of Geophysical Research, v. 93, pp. 4421-4433.

Seager, W. R., Kottlowski, F. E., and Hawley, J. W., 1976, Geology of the Doña Ana Mountains, New Mexico: New Mexico Bureau of Mines & Mineral Resources, Circular 147, 35 pp., 3 sheets, scale 1:24,000.

Seager, W. R., Clemons, R. E., Hawley, J. W., and Kelley, R. E., 1982, Geology of the northwest part of Las Cruces 1° x 2° sheet, New Mexico: New Mexico Bureau of Mines & Mineral Resources, Geologic Map GM-53, scale 1:125,000.

Strangway, D. E., Simpson, J., and York, D., 1976, Paleomagnetic studies of volcanic rocks from the Mogollon Plateau area of Arizona and New Mexico: New Mexico Geological Society, Special Publication 5, pp. 119-124.

Wahl, D. E., Jr., 1980, Mid-Tertiary volcanic geology in parts of Greenlee County, Arizona, Grant and Hidalgo Counties, New Mexico: Unpublished PhD dissertation, Arizona State University, Tempe, 149 p.

Walker, G. P. L., Heming, R. F., and Wilson, C. J. N., 1980, Low-aspect ratio ignimbrites: Nature, v. 283, pp. 286-287.

Weiss, S. J., Noble, D. C., and McKee, E. H., 1989, Paleomagnetic and cooling constraints on the duration of the Pahute Mesa-Trail Ridge eruptive event and associated magmatic evolution, Black Mountain volcanic center, southwestern Nevada: Journal of Geophysical Research, v. 94, pp. 6075-6084.

Wells, R. E., and Hillhouse, J. W., 1989, Paleomagnetism and tectonic rotation of the lower Miocene Peach Springs Tuff: Colorado Plateau, Arizona, to Barstow, California: Geological Society of America, Bulletin, v. 101, pp. 846-863.

Woodard, T. W., 1982, Geology of the Lookout Mountain area, Black Range, Sierra County, New Mexico: Unpublished MS thesis, University of New Mexico, Albuquerque, 95 pp., map, scale 1:24,000.

Selected conversion factors*

TO CONVERT	MULTIPLY BY	TO OBTAIN
Length		
inches, in	2.540	centimeters, cm
feet, ft	3.048×10^{-1}	meters, m
yards, yds	9.144×10^{-1}	m
statute miles, mi	1.609	kilometers, km
fathoms	1.829	m
angstroms, Å	1.0×10^{-8}	cm
Å	1.0×10^{-4}	micrometers, μm
Area		
in^2	6.452	cm^2
ft^2	9.29×10^{-2}	m^2
yds^2	8.361×10^{-1}	m^2
mi^2	2.590	km^2
acres	4.047×10^{3}	m^2
acres	4.047×10^{-1}	hectares, ha
Volume (wet and dry)		
in^3	1.639×10^{1}	cm^3
ft^3	2.832×10^{-2}	m^3
yds^3	7.646×10^{-1}	m^3
fluid ounces	2.957×10^{-2}	liters, l *or* L
quarts	9.463×10^{-1}	l
U.S. gallons, gal	3.785	l
U.S. gal	3.785×10^{-3}	m^3
acre-ft	1.234×10^{3}	m^3
barrels (oil), bbl	1.589×10^{-1}	m^3
Weight, mass		
ounces avoirdupois, avdp	2.8349×10^{1}	grams, gr
troy ounces, oz	3.1103×10^{1}	gr
pounds, lb	4.536×10^{-1}	kilograms, kg
long tons	1.016	metric tons, mt
short tons	9.078×10^{-1}	mt
oz mt^{-1}	3.43×10^{1}	parts per million, ppm
Velocity		
ft sec^{-1} (= ft/sec)	3.048×10^{-1}	m sec^{-1} (= m/sec)
mi hr^{-1}	1.6093	km hr^{-1}
mi hr^{-1}	4.470×10^{-1}	m sec^{-1}

TO CONVERT	MULTIPLY BY	TO OBTAIN
Pressure, stress		
lb in^{-2} (= lb/in^2), psi	7.03×10^{-2}	kg cm^{-2} (= kg/cm^2)
lb in^{-2}	6.804×10^{-2}	atmospheres, atm
lb in^{-2}	6.895×10^{3}	newtons (N)/m^2, N m^{-2}
atm	1.0333	kg cm^{-2}
atm	7.6×10^{2}	mm of Hg (at 0° C)
inches of Hg (at 0° C)	3.453×10^{-2}	kg cm^{-2}
bars, b	1.020	kg cm^{-2}
b	1.0×10^{6}	dynes cm^{-2}
b	9.869×10^{-1}	atm
b	1.0×10^{-1}	megapascals, MPa
Density		
lb in^{-3} (= lb/in^3)	2.768×10^{1}	gr cm^{-3} (= gr/cm^3)
Viscosity		
poises	1.0	gr cm^{-1} sec^{-1} *or* dynes cm^{-2}
Discharge		
U.S. gal min^{-1}, gpm	6.308×10^{-2}	l sec^{-1}
gpm	6.308×10^{-5}	m^3 sec^{-1}
ft^3 sec^{-1}	2.832×10^{-2}	m^3 sec^{-1}
Hydraulic conductivity		
U.S. gal day^{-1} ft^{-2}	4.720×10^{-7}	m sec^{-1}
Permeability		
darcies	9.870×10^{-13}	m^2
Transmissivity		
U.S. gal day^{-1} ft^{-1}	1.438×10^{-7}	m^2 sec^{-1}
U.S. gal min^{-1} ft^{-1}	2.072×10^{-1}	l sec^{-1} m^{-1}
Magnetic field intensity		
gausses	1.0×10^{5}	gammas
Energy, heat		
British thermal units, BTU	2.52×10^{-1}	calories, cal
BTU	1.0758×10^{2}	kilogram-meters, kgm
BTU lb^{-1}	5.56×10^{-1}	cal kg^{-1}
Temperature		
°C + 273	1.0	°K (Kelvin)
°C + 17.78	1.8	°F (Fahrenheit)
°F − 32	5/9	°C (Celsius)

Divide by the factor number to reverse conversions.
Exponents: for example 4.047×10^{3} (see acres) = 4,047; 9.29×10^{-2} (see ft^2) = 0.0929.

Editor: *Jiri Zidek*

Typeface: Palatino

Presswork: Miehle Single Color Offset
Harris Single Color Offset

Binding: Smyth sewn with softbound cover

Paper: Cover on 12-pt. Kivar
Text on 70-lb White Matte

Ink: Cover—4-color process and PMS 320
Text—Black

Quantity: 1,000